The Dynamics of death:

determining the relationship between within-host pathogen dynamics and host mortality

by

Tim O'Sullivan

In Partial Fulfillment

Of the Requirements for the Degree

Doctorate of Philosophy in the

School of Biology

The Dynamics of death:

determining the relationship between within-host pathogen dynamics and host mortality

Approved by:

Dr. Sam Brown, Adviser
School of Biology
Georgia Institute of Technology

Dr. Patrick McGrath
School of Biology
Georgia Institute of Technology

Dr. Kristofer Wollein Waldetoft
School of Biology
Georgia Institute of Technology

Dr. Nicole Vega
School of Biological Sciences
Emory University

Dr. Steve Diggle
School of Biology
Georgia Institute of Technology

Approved: 8/26/2021

Dedicated to June Hamel-Smith and Rita & Herbert O'Sullivan

AKNOWLEDGMENTS

I couldn’t have reached this stage without the support of my friends, family, and mentors both past and present. There are too many to count, but my advisers Drs. Sam Brown and Kristofer Wollein Waldetoft, my parents, Howard O’Sullivan and Simone Hamel-Smith, and my partner, Cristiana Giannini deserve special recognition.

Table of Contents

List of tables

List of figures

Summary

Infectious diseases remain a major cause of global mortality, yet basic questions concerning the relationship between within-host pathogen processes and epidemiological patterns of mortality remain obscure. Following an introductory chapter one, we lay out the conceptual challenge in chapter two – how do within-host pathogen dynamics (pathogen burden $p(t)$ as a function of time since infection t) link to changes in epidemiological risk of death, $m(t)$? We perform a structured literature review of the existing biomedical literature on controlled animal infections, and find consistent support across 28 experiments for an exponentially increasing risk of death $m(t)$ with time since infection. We then illustrate that survival data alone is insufficient to infer pathogen dynamics $p(t)$, with multiple models of pathogen growth and host-pathogen interactions consistent with observed survival data. In chapter three we develop an experimental *C. elegans / Pseudomonas aeruginosa* infection model platform to allow non-invasive tracking of $p(t)$, via fluorescence-tagged pathogen imaging. Our calibration results show that quantitative inference to pathogen density from fluorescence intensity is not reliable. As a result of this roadblock, in chapter four we turn to a destructive sampling approach, coupled to non-invasive imaging to identify live and dead worms. Estimating pathogen burden in both live and dead worms indicates that pathogen growth is approximately exponential across the transition from host life to death. Our control experiments indicate substantial background mortality in our experimental design, limiting our ability to map mortality onto pathogen dynamics. In chapter five we discuss methodological improvements to our platform, plus potential avenues for future research building on the results presented in this thesis.

Chapter one: Introduction

Tim O'Sullivan, Kristofer Wollein Waldetoft & Sam P. Brown

Abstract

In this PhD we address the relationship between within-host infection dynamics, and the fate of an infection. Each chapter is a self-contained presentation, focused on developing a conceptual framework and meta-analysis (chapter two), non-destructive experimental approaches (chapter three) and destructive experimental approaches (chapter four). Finally, chapter five offers a general discussion of the work, and outlines directions for future research. In the current chapter we provide an introduction to key concepts in the literature, building from an overview of host-parasite biology to a focus on bio-medical approaches (centered on physiology and dynamics within infected hosts) and then on to epidemiological approaches (centered on dynamics across populations of susceptible and infected individuals). Following this survey of relevant fields, we then review model host-parasite systems, ending with a focus on our model system of choice: the host organism *Caenorhabditis elegans* and the parasite organism *Pseudomonas aeruginosa.* we then conclude the chapter with a brief synopsis of the chapters to come.

Introduction

Infections and host-parasite biology

There has seldom been a more relevant time in modern history to assert that infectious disease is still an important source of morbidity and mortality globally. All living things suffer from infections. Humans face a daunting array of infecting agents, spanning most kingdoms of cellular life, plus viruses. Bacterial pathogens are themselves prone to infection by viral parasites (bacteriophages, and other mobile elements), reminiscent of Swift's 'little fleas have lesser fleas, and so *ad infinitum*' (Swift 1773).

The language we use to describe infecting agents varies across fields, with infecting agents variously described as 'pathogens' or 'parasites' (including micro- or macro-parasites) dependent on their size and natural history (Zelmer 1998). Here we take a more inclusive, ecologically inspired approach (Preston and Johnson 2010) and use the term 'parasite' to capture all infectious agents that are capable of inflicting harm during a symbiotic relationship with a larger host organism.

Another term that generates confusion due to variable definitions across fields is virulence. For evolutionary biologists, virulence is measured by the reduction in host fitness resulting from parasite infection due to mortality or loss of fecundity (Poulin and Combes 1999). For infectious disease epidemiologists, virulence is typically defined as the additional mortality imposed by an infection (van Seventer and Hochberg 2016). For plant pathologists, virulence is typically used as a synonym with infectivity (Shaner et al. 1992) – a virulent strain is able to infect a plant, where an avirulent strain cannot. Here

we use a broader and inclusive definition that is consistent with typical biomedical usage – defining virulence as harm to the host (Lipsitch and Moxon 1997).

Infectious disease research operates across multiple scales, from cell biologists studying the molecular interactions between parasite and host cells, through to epidemiologists studying the trajectories of infection case counts through populations of hosts. The breadth of infection research is a testament to the enduring importance of infections to humanity and provides an incredible resource to infection researchers working across these scales. Yet the specialization of research has led to a relative disconnect between the within-host focus of biomedical research and the population-scale focus of epidemiological research. In particular, we focus in this PhD on a disconnect over the analysis of a key infection outcome – life or death.

Biomedical infection research

The majority of research in infection biology focuses on the mechanisms of host exploitation using well defined laboratory model systems. Since the inception of the field of microbiology, animal infection experiments have been crucial to testing the underlying hypotheses for parasite-driven disease. Pasteur, already a renowned scientist and paragon in the burgeoning field of microbiology, engaged in animal experiments using common chickens and the zoonotic chicken cholera, *Pasteurella multocida* (Pasteur 1881). Pasteur found that when cultured under aerobic conditions, he could attenuate the virulence of *P. multocida*, and provide protection to subsequent infections by inoculating chickens with the attenuated strains. Robert Koch, another grandfather of microbiology, generated some of the key principles of the germ theory of disease primarily using animal infection experiments in a variety of mammals, especially rodents.

One of his first attempts included the isolation of blood from sheep killed by *Bacillus anthracis*, then subsequently reproducing the pathology and death in rodents upon inoculation (Blevins and Bronze 2010).

Generally, parasites are thought to reproduce inside their host while exploiting them for resources. The damage and taxation upon the host is thought to be proportionate to the burden, the number of the parasite or the growth rate of the pathogen at any given time (Gilchrist and Sasaki 2002; Alizon and van Baalen 2005). One of the most basic ways to determine parasite virulence (harm to the host) is by tests of lethal dose 50 (LD50), the amount of parasite needed to kill the host within a timeframe of interest (Sami et al. 2019). Yet this method is ultimately a crude way to examine host-parasite biology as at high doses, death can follow more from intense inflammatory and collateral immune damage (Borges et al. 2013; Wang et al. 2013; Vogel et al. 2014).

An addition complexity in the study of relationships between parasites and hosts is that virulence can be context-dependent. Many parasites exert complex regulatory control over their expression of virulence, through the context-dependent control of genes known as ‘virulence factors’ (Cross 2008; Brown, Cornforth, and Mideo 2012; Allen et al. 2014). Later in this chapter we will discuss specific mechanisms of virulence factor regulation. In addition, individual strains can gain or lose these virulence factors via processes of horizontal gene transfer, therefore modulating an organism’s ability to be virulent in the first place. Group A streptococcus (GAS) is an illustrative example of context dependency; normal colonization happens within the nasopharyngeal mucosa where it typically exists in a state of asymptomatic carriage. From this baseline, changes

in the environment can feedback with regulatory control of virulence factors, switching GAS from harmless commensal to an aggressive parasite generating symptomatic infection (e.g. strep throat), thought to facilitate transmission between hosts (Wollein Waldetoft and Råberg 2014). More rarely, this aggressive and symptomatic stage can spill over into the normally sterile blood compartment, triggering invasive – and life-threatening disease (Nelson et al. 2016).

Public health and epidemiological dynamics of infections

In contrast to the biomedical research focus on mechanisms of host exploitation, the central goal in epidemiological approaches to infectious diseases is to assess population scale impacts of infectious diseases, and their dynamics through time. From a methodological perspective, infectious diseases epidemiology combines extensive population scale data gathering in observational field settings (often led by national/international public health agencies such as the US and European Centers for Disease Control) with a long-standing tradition of mathematical modeling of infectious disease dynamics (Smith et al. 2012).

On an epidemiological scale, the standard model framework for 'microparasite' infections (viruses, bacteria, fungi, and protozoa) is known as 'compartmental' models, which structure host populations into compartments of 'susceptible' (S) and 'infected' (I) classes (Anderson and May 1979). Under these models, individuals in the S class can transition into the I class (following contact with an I individual), and then exit the I class following parasite clearance or death (Figure 1.1A). A key simplification in these models is that the mortality rate of an individual jumps from a baseline rate (while uninfected) to an elevated

rate while infected (capturing the additional parasite-induced mortality), and returning immediately to the baseline rate, when and if the infection is cleared (Figure 1.1B). A consequence of this modeling approach is that the probability of survival will follow an exponential decay through time since infection (Figure 1.1C), reflecting the constant and elevated risk posed by infection. This simplification of within-host dynamics has been flagged as problematic (Mideo, Alizon, and Day 2008; Gog et al. 2015; Handel and Rohani 2015) and is commonly relaxed in epidemiological models with very heterogeneous infection burdens, such as helminth infections (Pullan et al. 2014; Truscott et al. 2016). In this thesis we ask first what are the empirical patterns of mortality following experimentally induced infections, and then develop statistical, mathematical and experimental models of dynamical mortality in light of these data.

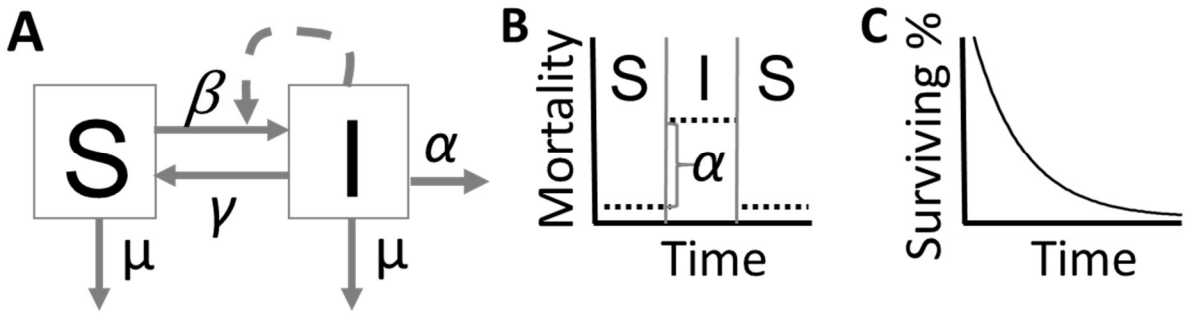

Figure 1.1. A schematic summary of mortality assumptions in a compartmental SIS epidemiological model. (A) An SIS compartmental model. Individuals are allocated to either the S or I class, dependent on whether susceptible or infected. Transitions among states are governed by coefficients capturing transmission (β), recovery (γ) and mortality (α). (B) The transitions between S and I states in model (a) imply instantaneous switches in mortality, between a background rate μ and an enhanced rate μ + α. (C) The constant (and elevated) rate of instantaneous mortality during infection implies that among the infected class, survivors (in the absence of subsequent infections or recoveries) will decay exponentially with time since infection.

Infection model systems

Since Koch and Pasteur, there have been a number of well-established animal models for infectious disease and host-parasite interactions. All have their distinct advantages and disadvantages, with mammalian model organisms being generally preferred for generalizability to humans.

Vertebrate experimental models

Among vertebrates, mammals present the most common choices for animal models, due to our shared ancestry. Rodents take up the bulk of this focus, being relatively easy to breed and therefore control host genotypes (Sarkar and Heise 2019). Indeed, many important genetic mutants exists for mice, including a variety of immune deficient mice which allows us to better understand mechanisms of host defense in response to infection. With few exceptions, many human parasites can infect mice with broadly similar pathogenic systems. In cases where infections cannot happen readily, researchers have used natural rodent parasites that are taxonomically similar to human ones, such as in the case of rodent malaria *Plasmodium chabaudi* (Stephens, Culleton, and Lamb 2012).

However, there are some parasites (predominately viruses), where the only suitable animal models are non-human primates (Estes, Wong, and Brenchley 2018). Several species fit this role, including chimpanzees, sooty mangabeys, and macaques (Ghosh and Das 2020). Due to a number of ethical concerns, as well as the high costs to perform these experiments, nonhuman primates are used as animal model exceedingly sparingly when compared to mice (Carvalho et al. 2019).

Invertebrate experimental models

Invertebrate animals have also been a workhorse in the field of infection biology. Though lacking an adaptive immune system like vertebrates, several species share a number of innate immune factors with humans. In general, these models do not include the considerable overhead required for vertebrate species, while the relative lack of ethical concerns allows experimenters to be more agile when designing projects, in particular opening the potential for larger scale epidemiological experiments.

One broadly used experimental host is the waxmoth larva *Galleria mellonella,* which can be readily infected with clinically relevant bacterial and fungal species. Host mortality be can estimated on short timescales, and can be demonstrably improved via antibiotics, anti-virulence drugs, and even bacteriophage (Ross-Gillespie et al. 2014; Thomas et al. 2013; Gurney et al. 2020). Versus other invertebrate models, *G. mellonella* falls short in other ways. The genotype of the host is usually poorly controlled, and it lacks strain libraries that other potential hosts have. Though this may soon change, as molecular work using the larvae has gained traction in recent years (Pereira et al. 2018).

Probably the oldest invertebrate animal model still in use, the fruit fly *Drosophila melanogaster* (and related species) has been used in a number of infection experiments, with a primary focus on bacterial parasites (Dionne and Schneider 2008). Infections can be performed with either ingestion or injection, which serves as chronic or acute models of infection, respectively (Nehme et al. 2007; Dionne and Schneider 2008). Years as an

animal model for classical genetics has yielded a robust strain library for flies, allowing investigators to test a number of genotype-by-genotype interactions.

The last arthropod model worth noting is *Daphnia magna*, infected by its natural bacterial parasite, *Pasteuria ramosa*. This model allows researchers to ask interesting questions about natural parasite-host coevolution in an experimentally tractable system (Decaestecker et al. 2007). Both of these species are amenable to culturing in the lab, and the natural diapause the *Daphnia* undergo allow for co-evolutionary 'time-shift' experiments, in which experimenters can mix and match coevolving hosts and parasites from different points in time (Ebert 2008). Since the inception of this model host-parasite system, additional natural parasites have been classified, including fungal, microsporidian, and nematode parasites (Ebert 2005).

Finally, *Caenorhabditis elegans* has long served as model system for classical genetics. The field of *C. elegans* infection research is still developing, but is attractive due to the vast genetic library, the small and tractable host scale and the bacterivorous lifestyle of the worms. To tackle questions related to infection and death on a broader population scale, we aimed to use a model that was highly tractable, and after review we concluded that *C. elegans* is the optimal choice to address our research agenda.

C elegans as a model host system

Caenorhabditis elegans is a free-living soil nematode that can be found globally and has been used extensively across multiple fields since first use a model organism by Sydney

Brenner (Calahorro and Ruiz-Rubio 2011; Zhang et al. 2017; Markaki and Tavernarakis 2020). As a self-fertile hermaphrodite, the nematode has historically been a very tractable model for classical geneticists, with the ability to generate double mutants and heterozygotes with relative ease. Worms can be evolved experimentally, transformed via CRISPR and other modern techniques, and mutagenized to generate variation. Resulting worm strains can then be easily stored at 80°C for further studies (Stiernagle 2006; Dickinson and Goldstein 2016).

With the discovery of the *daf-2* mutants, which extend lifespan by approximately 3 fold, *C. elegans* has in addition become a major animal model of mortality and aging (Kimura et al. 1997). Even *daf-2* mutants have a relatively tractable lifespan, and the different biotic and abiotic stressors involved in shifts of nematode lifespan are now well characterized. As a result, there are many existing tools and techniques to accurately describe worm aging and senescence (Roussel et al. 2014; Stroustrup et al. 2016; Le et al. 2020).

In the wild, *C. elegans* can often be found in rotting fruit, where the nematode feeds on the bacterial saprophytes involved in breaking down plant matter. Wild *C. elegans* tend to consume a variety of different bacterial species. Given their pan-prokaryotic diet, it is no surprise that laboratory *C. elegans* can be easily coaxed into consuming a bacterial species of choice. Although originally used as an animal model for classical genetics, many have highlighted the strength of *C. elegans* as a host to various microbial taxa; including bacteria, viruses, microsporidia, and fungi (Darby 2005). *C. elegans* is emerging not only as a model host for pathogenic infection, but also for microbiome

assembly and host-microbiome relationships (Kurz and Ewbank 2000; Mallo et al. 2002; Gammon 2017; Zhang et al. 2017; Vega and Gore 2017).

Though *C. elegans* are not indiscriminate in their consumption of bacterial cells, it has been shown to be relatively easy to induce feeding on bacterial species to which the worm is naïve. It is in this context that *C. elegans* has been pioneered as a model for enteric infections. Many common parasites can be consumed by *C. elegans* to then induce pathogenic infection, including major human bacterial pathogens. Though worms lack a vertebrate immunity that includes an adaptive response, there are a few conserved pathways of the innate immunity that are shared with humans and other mammals (Millet and Ewbank 2004).

Despite the phylogenetic distance between nematode and mammalian hosts, the pathogenicity of virulence factors are broadly conserved between mammalian and nematode hosts (Mahajan-Miklos et al. 1999; Kurz et al. 2003; Bae et al. 2004). Together, these features make *C. elegans* a robust, tractable and relevant model for examining host-parasite interactions.

Pseudomonas aeruginosa as a model parasite

Pseudomonas aeruginosa is a Gram-negative bacterium that can be found worldwide in diverse habitats including soils, water bodies and in particular in human associated environments, including plumbing drains (Diggle and Whiteley 2020). Initially identified infecting wounds, *P. aeruginosa* is known as an opportunistic parasite in human

infections, in which it takes of advantage of prior tissue damage or compromised immune responses (Gross et al. 2013). In addition to humans, *P. aeruginosa* demonstrates a broad ability to exploit and kill vertebrates, invertebrates, and plants (Gross et al. 2013). In a laboratory setting, the species is readily culturable. It is a facultative anaerobe, and can grow on a variety of media and in a wide range of temperatures (LaBauve and Wargo 2012).

Epidemiologically, *P. aeruginosa* infections are widespread, and a major source of healthcare burden worldwide, responsible for approximately 15% of severe infections in hospitals (Horcajada et al. 2019). In a particularly well-studied example, *P. aeruginosa* is a frequent pathogen of the cystic fibrosis lung, in which the parasite can establish chronic, years-long infections (Davies 2002; Høiby, Ciofu, and Bjarnsholt 2010). Both acute and chronic infections are often worsened by *P. aeruginosa*'s robust capacity for antibiotic resistance, which includes efflux pumps, beta-lactamases, and target modifications, among others (Lister, Wolter, and Hanson 2009). Approximately 13% of *P. aeruginosa* infections demonstrate some form of multidrug resistance, which often leads to lethal infections (Horcajada et al. 2019). The frequency of these types of infections has led *P. aeruginosa* to be an important model system on researching strategies to combat and circumvent antibiotic resistance.

In addition to antibiotic resistance, *P. aeruginosa* includes other mechanisms in its toolbox that are relevant to infection outcomes. Up to 10% of the 6 Mbp genome are regulated via quorum sensing, a cell-cell communication system which connects the expression of multiple virulence factors to increases in bacterial cell density (Darch et al.

2012; Rumbaugh et al. 2012). The *P. aeruginosa* genome has 3 major and inter-linked quorum sensing circuits (*las, rhl* and *pqs* systems) (Schuster and Greenberg 2006; Wilder, Diggle, and Schuster 2011) which provide the parasite with a complex repertoire of regulatory responses to changes in both the social environment (density and genotypic composition) (Darch et al. 2012; Allen et al. 2016), and the physical environment (Redfield 2002; Cornforth et al. 2014).

C. elegans and Pseudomonas aeruginosa as a model host-parasite system

Initially established by Man-Wah Tan et al (1999), the *C. elegans – P. aeruginosa* system was one of the first models of infection in the nematode. The system was noted for the relative ease of infecting worms, and the easy integration of the host system into existing microbiological laboratories. These experiments described two types of death due to infection—slow killing and fast killing. At an overview level, slow killing is thought to be driven primarily by parasite burden, and fast killing is thought to be mediated by virulence factor (specifically, toxin) production (Mahajan-Miklos et al. 1999; Ruiz-Díez et al. 2003).

Variable virulence mechanisms

The choice of bacterial culture media is key when studying this host-parasite interaction, due to the fast/slow killing dichotomy. The use of high osmolarity media induces phenazine production in *P. aeruginosa* PA14 that leads to “fast-killing” in worms (Mahajan-Miklos et al. 1999). In our experiments, we used the minimal media “slow-killing” method, in which death is driven primarily by accumulation of bacteria in the lumen (Tan, Mahajan-Miklos, and Ausubel 1999). Note that subsequent studies have

shed additional light on connections between specific bacterial media conditions, *P. aeruginosa* virulence factor expression, and the rate of *C. elegans* killing (Ruiz-Díez et al. 2003; Zaborin et al. 2009).

Natural history

While the *P. aeruginosa / C. elegans* infection model was initially developed in light of the practicality of combining two model organisms, there is mounting biological evidence that *C. elegans* and *Pseudomonas aeruginosa* (and other members of the *Pseudomonas* genus) could interact outside of laboratory settings, as described below.

One of the first clues was the relative attraction that *C. elegans* has to common *P. aeruginosa* quorum-sensing molecules. Lab reared worms that were naïve to *Pseudomonas* exposure showed positive chemotaxis to several autoinducers (signal molecules) produced by *P. aeruginosa* (Beale et al. 2006). Normally, when *C. elegans* is exposed to parasitic bacteria, worms can learn to subsequently avoid the bacteria after clearing the infection (Anderson and McMullan 2018). Despite this, mucoid *P. aeruginosa* can induce *C. elegans* feeding by suppressing the expression of the npr-1 gene which regulates this type of behavioral avoidance (Martin, Singh, and Aballay 2017). Additionally, *P. aeruginosa* strain PA14 can suppress the expression of the *daf-2* signaling pathway in worms, reducing the nematode's immune response and enhancing virulence (Garsin et al. 2001).

From a field survey perspective, *Pseudomonas* species (including *P. aeruginosa*) have been found in wild-caught *C. elegans* isolates (Berg et al. 2016; Dirksen et al. 2016; Zimmermann et al. 2020). Isolated *Pseudomonas* species showed a range of interactions with their nematode hosts, from positive, neutral, and negative effects on fitness (Samuel et al. 2016). Work is still emerging on the frequency of these types of interactions in nature.

Summary

In this introductory chapter we briefly review the different academic traditions of the study of infectious diseases, from molecular biology to infectious disease epidemiology. We then review some of the most commonly used infection models in laboratory biology, before we turn to our focal system – the *P. aeruginosa* – *C. elegans* model. This host-parasite system is a robust, well-established system to address questions on the interface of pathogen within-host dynamics and host population dynamics. Below, we end this introductory chapter with a brief synopsis of the chapters to come.

In chapter two we introduce the conceptual challenge of the entire thesis – how do the dynamics of host death map onto the within-host dynamics of pathogen expansion? To begin to address this question I leverage the extensive published biomedical data generated by controlled animal infections to assess what are the dynamics of experimentally-induced death due to acute infection. We find that across diverse infection models, the risk of death accelerates in time since infection. We further show that this pattern of accelerating risk is consistent with multiple alternate mechanisms of pathogen growth (static, linear or exponential) and host interaction, underlining the

limitations of current experimental approaches to connect within-host processes to epidemiological patterns.

In chapter three we develop experimental methodologies to address the questions posed in chapter two. We address the methodological challenge of directly and non-invasively tracking pathogen burden $p(t)$ and time of death t^* across cohorts of individual infected animals, using a fluorescently tagged *P. aeruginosa*. Attempts at calibration suggested that fluorescence was only weakly correlated to the worm burden measured by colony counting (colony forming units, CFUs), though there was a discernable signal. Experimental results indicate an absence of within-host pathogen growth, and an absence of relationship between individual time of death and pathogen burden (as estimated from fluorescence). Given the problematic calibration results for our non-invasive methods, we decided to switch in our final data chapter (chapter four) to a destructive approach to estimate the pathogen burden in our model system.

In chapter four, we combine well-established destructive sampling methods for pathogen burden, with non-invasive live/dead activity tracking. Our results demonstrate pathogen growth and a positive relationship between pathogen burden and worm death. Our analysis also illustrates the problem of survival bias in estimating within-host pathogen growth from destructive sampling data, which we overcome by sampling both live and dead worms.

Finally, in chapter five we review limitations and next steps in our experimental design. Building on this review, we outline a series of future experimental avenues that are

opened by our conceptual and methodological work. These future avenues include (1) using expression reporters to assess the role of virulence factor induction in determining the outcome of infection; (2) using lower infective doses to further assess the role of pathogen expansion in determining outcomes; (3) using different pathogen and host strains to assess the role of host / pathogen genetics; (4) introducing treatment interventions (antibiotics, anti-virulence drugs, anti-inflammatories, etc.) to assess the time-dependency of treatment success.

Chapter two: Risk of death during acute infection is accelerating across diverse host-pathogen systems, and consistent with multiple models of host-pathogen interaction

Tim O'Sullivan, Kristofer Wollein Waldetoft & Sam P. Brown

Abstract

Infectious diseases remain a major cause of global mortality, yet basic questions concerning the relationship between within-host processes governing pathogen burden (pathogen replication, immune responses) and population-scale (epidemiological) patterns of mortality remain obscure. We use a structured literature review to leverage the extensive biomedical data generated by controlled animal infections to address the epidemiological question of whether infection-induced mortality is constant, accelerating or follows some other pattern of change, and to infer the within-host mechanistic basis of this pattern. We show that across diverse animal infection models, the risk of death increases exponentially in time since infection, in a manner phenomenologically similar to the dynamics of all-causes death. We further show that this pattern of accelerating risk is consistent with multiple alternate mechanisms of pathogen growth (static, linear, or exponential) and host-pathogen interaction, underlining the limitations of current experimental approaches to connect within-host processes to epidemiological patterns. We review critical experimental questions that our work highlights, requiring additional non-invasive data on pathogen burden throughout the course of infection, and end with a discussion on the unpicking of the mechanistic and dynamical basis of accelerating mortality risk during the course of human infections.

Introduction

Infectious disease research operates across multiple scales, from cell biologists studying the molecular interactions between pathogen and host cells, through to

epidemiologists studying the trajectories of infection case counts through populations of hosts. The breadth of infection research is a testament to the enduring importance of infections to humanity and provides an incredible resource to infection researchers working across these scales. Yet the specialization of research has led to a relative disconnect between the within-host focus of biomedical research and the among-host focus of epidemiological research. In particular, we focus in this PhD on a disconnect over the analysis of a key infection outcome – life or death.

In the biomedical tradition, the study of mortality focusses on establishing pathogen causal mechanisms of host damage, and methods to control infection. A primary strategy to identify mechanisms of host damage ('virulence factors'; non-essential molecular determinants of harm to the host , (Allen et al. 2014)) or therapeutics is to conduct infection screens using well-controlled experimental infections of animal models. These screens are typically conducted across genetic knockout and/or chemical libraries to identify genes (virulence factors) or compounds (antimicrobials) of interest. Thanks to this thriving tradition, we now have extensive databases on pathogen virulence factors (Goll et al. 2008; Liu et al. 2019; Sayers et al. 2019) and chemical interactions, accompanied in many cases with detailed molecular mechanisms underpinning their mode of action on host cells or tissues, their regulatory control, delivery, host immune responses, etc.

In contrast, the epidemiological approach focusses on describing, interpreting and predicting the trajectory of infections on the host population scale. A critical focus in this work is on how processes of pathogen transmission, host recovery and infection-induced mortality combine to govern whether an infection expands or contracts on a population scale. Infectious disease epidemiology is characterized by a strong

mathematical modeling tradition applied to clinical case-report data on human infections (R. M. Anderson and May 1992). (The dominant modeling traditions treat pathogen-induced mortality as a constant (elevated above background mortality) throughout the duration of infection. Yet, in the few contexts where high-resolution temporal data on infection-induced human mortality is available on a population scale (notably for sepsis), there is evidence that the risk of death is increasing with time (Kumar et al. 2006; D. Zhang, Micek, and Kollef 2015; Way 2017).

In this paper we seek to leverage the extensive published biomedical data generated by controlled animal infections to address the epidemiological question of whether infection-induced mortality is constant, accelerating or follows some other pattern of change, and to infer the mechanistic basis of this pattern. We find that across diverse infection models, the risk of death accelerates in time since infection. We further show that this pattern of accelerating risk is consistent with multiple alternate mechanisms of pathogen growth (static, linear, or exponential) and host interaction, underlining the limitations of current experimental approaches to connect within-host processes to epidemiological patterns.

Results

To assess the dynamics of infection-induced mortality across experimental host-pathogen systems, we performed a structured literature search of the EBSCO Medline database, with the following search term applied to the MeSH Major Heading (Exact Match) search field: (infection OR pathogen OR virulence) AND (survival analysis) AND ((animal models, disease OR (animals AND disease)). Applying this search term on March 13th,

2021 over the years 1991 – 2019 resulted in 335 papers. We then applied the following exclusions via manual review: host population size < 20, raw survival data not available, non-wildtype host (*e.g.* immune-compromised), non-wildtype pathogen (e.g. virulence factor knock-out strain), infection treatment (e.g. antibiotics), no defined pathogen infection dose or exposure, no un-infected control treatment, mortality in uninfected control treatment > 20%. For each qualifying paper we separately recorded all individual qualifying experiments, extracting data from tables or graphs (using WebPlotDigitizer (Rohatgi 2021)). This process resulted in survival data for 28 experiments from 10 papers (Chamilos et al. 2008; Chao et al. 2010; Day et al. 2012; de Souza et al. 2019; Kim et al. 2015; Kong et al. 2014; Lutter et al. 2008; Ortega-Riveros et al. 2017; Vergunst et al. 2010).

Our structured literature review returned a phylogenetically diverse range of hosts and pathogens. Our experimental hosts spanned vertebrates (zebrafish), nematodes (*C. elegans*) and insects (fruit flies). Our pathogens spanned 3 species of gram-negative bacteria, 4 species of gram-positive bacteria, and 9 species of eukaryotes. Collectively, these infection models represent many different mechanisms of host immunity and pathogen virulence.

Prior to surveying all of the data together, we begin with an illustrative example to orient our subsequent analyses (Figure 2.1.), featuring the proportion of surviving nematodes at time t since experimental infection with *Staphylococcus aureus* (data from Kong et al. 2014).

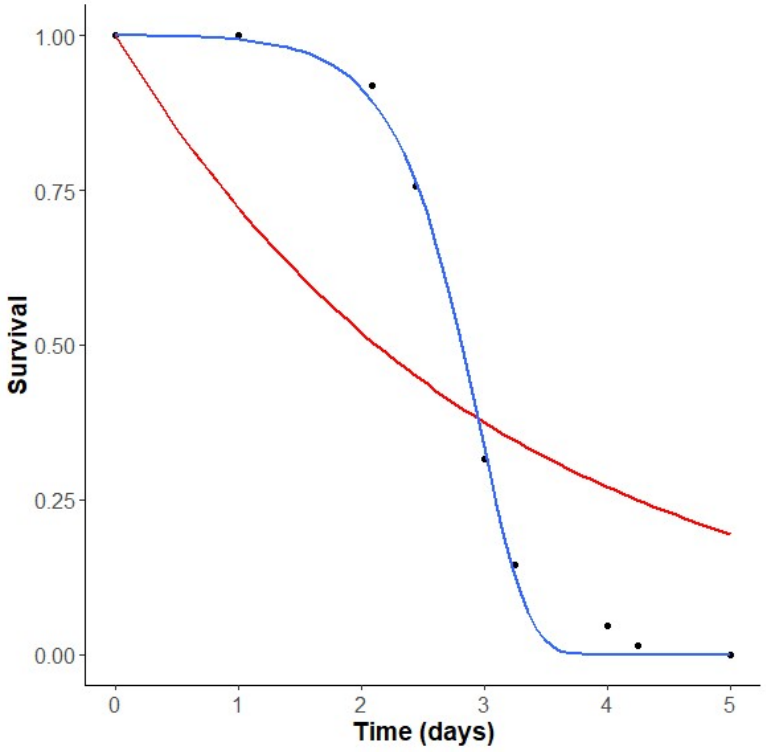

Figure 2.1. Survival data for a nematode – *S. aureus* model system indicates the failure of a constant mortality assumption. Black dots represent experimental data from a nematode/*S. aureus* model (N=120, (Kong et al. 2014)). The red lines represent exponential model fits (constant mortality rate), the blue lines represent a Gompertz model fit, which allows for accelerating mortality in time. Model fits were made using a nonlinear least squares method in R (Wu, Hung, and Tsai 2004). Parameter estimates and model comparisons are in Table A2.

To begin our assessment of whether we see accelerating risk of death through time since infection, we first fit an exponential model to capture the null hypothesis of constant risk (Figure 2.1. red line). On even a cursory examination, the data are not consistent with the constant risk (exponential) model. The survivorship data systematically deviate from the best fit exponential with higher survivorship early in the infection, and lower survivorship late in the infection. In other words, the data support an increasing risk of death as the infection proceeds.

Pathogen-induced death as a process of accelerated aging

This pattern of increasing instantaneous mortality or 'hazard' through time is familiar from the aging literature. In a human context, the instantaneous risk of death increases approximately exponentially, doubling approximately every 7 years (Kochanek et al. 2019). In controlled animal aging experiments, the same statistical patterns are observed, with the absolute rates varying with the animal (Economos 1979; Austad 2005; Boiko, Labas, and Gordeeva 2011), their genetics (Petralia, Mattson, and Yao 2014), and the environment (Stroustrup et al. 2016; Thanos et al. 2016). Working from this connection, we decided to test one of the most common models from the aging literature, the Gompertz (Gavrilov and Gavrilova 2019; Sasson 2021). Briefly, the two parameter Gompertz mortality function defines the instantaneous rate of mortality $m(t)$ as:

$$m(t) = a * e^{b*t}. \qquad \text{[Equation 1]}$$

When $b = 0$, the Gompertz recovers the exponential distribution with a constant mortality rate a. Increasing b leads to an increasing acceleration of instantaneous mortality with time (El-Gohary, Alshamrani, and Al-Otaibi 2013; Missov et al. 2015). We used a nonlinear least squares method (Wu, Hung, and Tsai 2004) in the statistical software R (R Development Core Team 2020) to fit these distributions to the experimental data, and observe in our focal example (Figure 2.1) that the model of accelerated mortality (akin to aging) fits the survival data better than the exponential model (Figure 2.1), but at the expense of an additional parameter. To assess model fit while accounting for parameter number, we used an information criterion approach, with Akaike Information Criterion (corrected for small samples sizes; AICc) values favoring the Gompertz model (lower AICc value, see appendix table A2.2).

The use of an information criterion approach to separate the exponential and Gompertz model fits to the data in Figure 2.1. is arguably an overkill given the striking difference in model fit. Yet it provides us with a currency to further interrogate comparative model performance across the multiple datasets in our structured literature review (Figure 2.2). Figure 2.2. illustrates survival data along with exponential (blue) and Gompertz (red) model fits for all 28 experimental infection datasets from our structured literature review. Using AICc as a yardstick, we find that the more complex (two parameter) Gompertz model produces a lower AICc score in all models (model fit and AICc data in table A2.2).

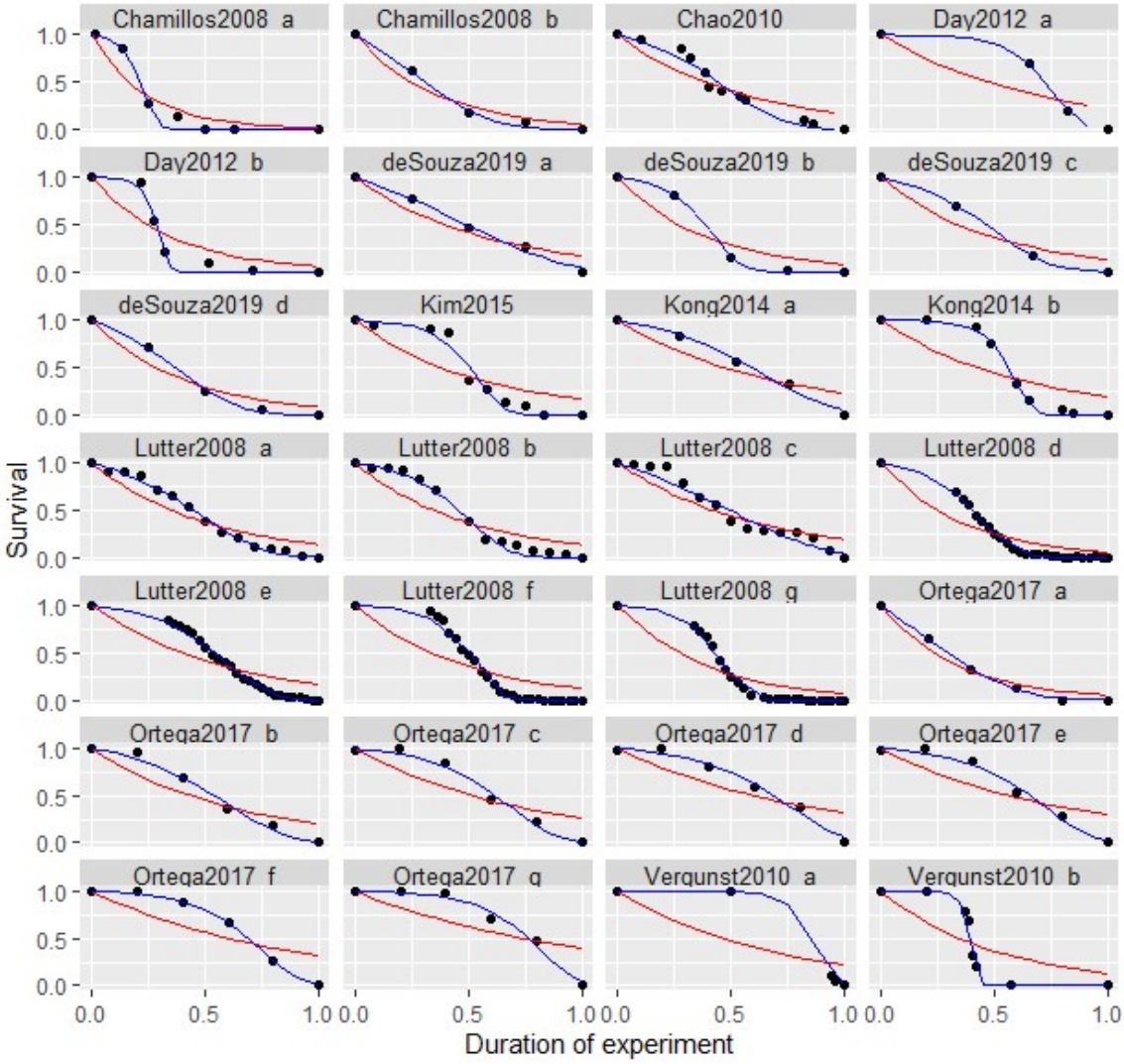

Figure 2.2. Survival data for 28 host pathogen model systems indicates the general failure of a constant mortality assumption. Black dots represent experimental data from 28 studies, with duration of experiment normalized to 1, and total mortality normalized to 1 (see appendix table A1. for more study details). The red lines represent exponential model fits (constant mortality rate), the blue lines represent a Gompertz model fit, which allows for accelerating mortality in time. Model fits were made using a nonlinear least squares method in R (Wu, Hung, and Tsai 2004). Parameter estimates and model comparisons are in appendix table A2.2, and diagnostic plots of the residuals are shown in A2.1-A2.4.

Figure 2.2. illustrates that the studies vary considerably in the number of observed timepoints (from 4 to 24), and it is plausible that an additional shape parameter is better justified when there are more timepoints to reveal changes in risk through time. To assess this effect, we plot Δ AICc as a function of the number of timepoints (Figure 2.4A), and we find support for this conjecture ($\beta = 4.23$, $p = 5.59 \times 10^{-9}$). The experimental studies also vary tenfold in host population size N, ranging from 20 (our lower limit on inclusion) to 120. Plotting Δ AICc on N (Figure 2.4B) we find no significant trend between host population size and support for the accelerating risk model ($\beta = 0.16$, $p = 0.63$).

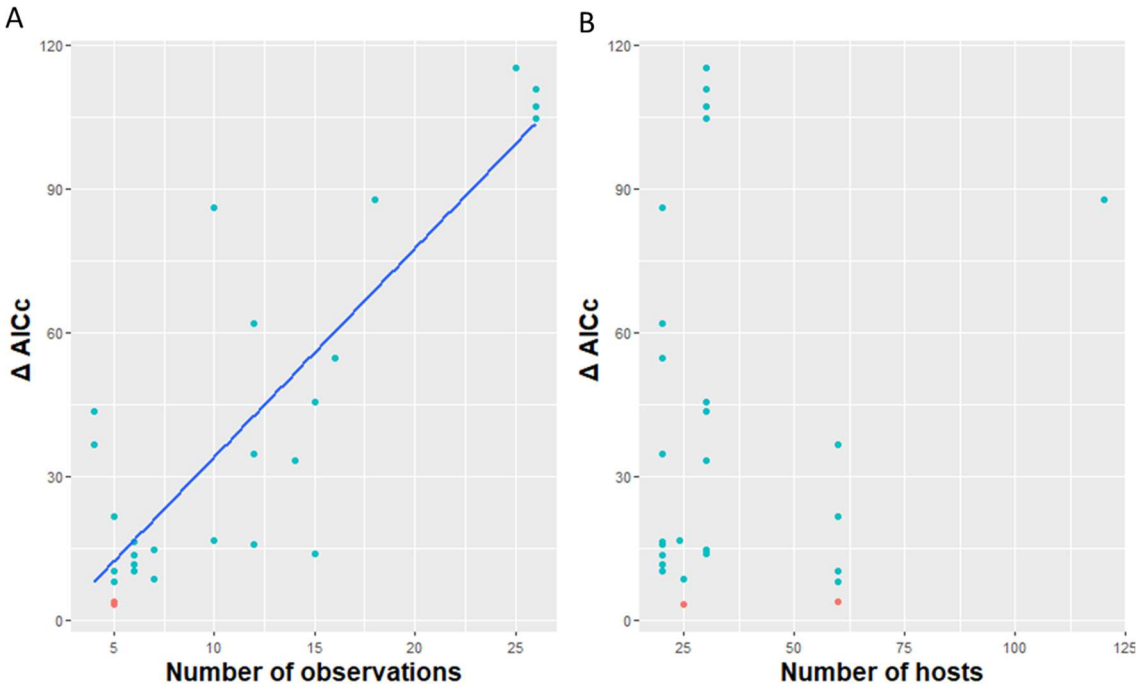

Figure 2.3. The number of time points and host cohort size do not correlate with support for the accelerating risk model. Each dot represents an individual data set and the ΔAIC (exponential model AICc – Gompertz model AICc) as an indicator of support for the accelerating risk model. Dots in pink denote studies where ΔAICc is non-significant (controlling for false discovery rate = 5%). A linear regression of ΔAICc on timepoints revealed a significant relationship ($\beta = 4.23$, $p = 5.59 \times 10^{-9}$). A linear regression ΔAIC on number of hosts also revealed no significant relationship ($\beta = 0.16$, $p = 0.63$).

Finally, we assess whether differential model performance (Δ AICc) varies with the taxonomic assignment of host (Figure 2.4A) or pathogen (Figure 2.4B), and again we find that support for the accelerating risk model is robust across the diversity of our experimental studies.

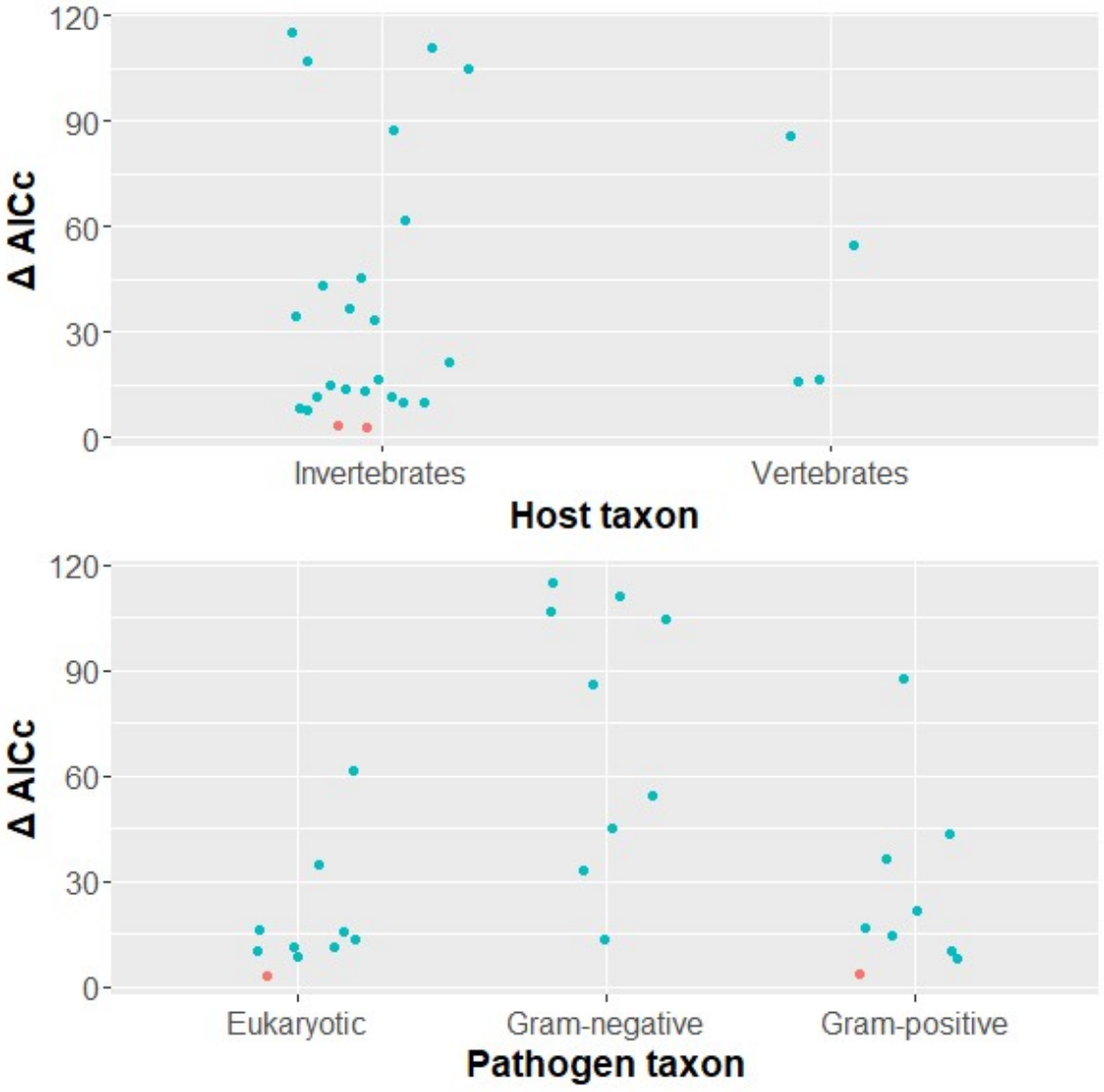

Figure 2.4. The accelerating risk model is supported across broad host and pathogen taxonomic contrasts. Invertebrate hosts (n = 24) and vertebrate hosts (n=4) showed no statistical difference in Δ AICc, (Welch's t-test, t = -0.25, p=0.82). Pathogen taxa also showed no difference (ANOVA, F=10.53, p= 0.0005). Dots in pink denote studies where ΔAIC is non-significant (controlling for false discovery rate = 5%).

To summarize our data collection, we see broad support for a model of accelerating risk across taxa (Figure 2.5) and study dimensions (Figure 2.4).

Connecting mortality to pathogen dynamics and mechanisms of host death.

The results in Figures 2.1. – 2.5 show the extra parameter in the Gompertz model is well justified across a diverse range of experimental infection studies, supporting the conclusion that the risk of death is accelerating following the initiation of infection – analogous to the acceleration in mortality across entire lifespans, known as aging.

While experimental infection and aging give rise to similar patterns of survival, there is a difference in underlying process. In the case of the experimental infection models illustrated above, we have a clear experimental cause of death – the pathogen (background mortality was minimal by our study inclusion criteria; see Appendix figure 2.4. for similar patterns including studies without effective controls for background mortality). This causal clarity offers a window into the study of mortality, as we have a potential internal currency (pathogen dynamics) to map onto the changing risk of death. In the following sections we evaluate three qualitatively distinct alternate models for the underlying processes of pathogen growth and host/pathogen interaction.

Model 1: exponential pathogen growth, with linear mapping to host mortality.

The observation of an approximately exponential increase in risk (*i.e.*, a Gompertz function) suggests one simple mechanistic model: the instantaneous mortality is linearly proportional to the instantaneous burden of an exponentially expanding pathogen population. We can break this down into two sets of assumptions. First, we assume that within-host pathogen density $p(t)$ is growing exponentially, $p(t) = p_0 e^{rt}$, with dynamics governed by initial inoculum p_0 and an exponential pathogen growth rate r. Given an acute

infection, this is a plausible assumption and commonly made in 'nested' epidemiological models (Mideo, Alizon, and Day 2008). Next, we assume that instantaneous mortality $m(t)$ is linearly proportional to bacterial burden, with mortality coefficient *v,* that is $m(t) = v * p(t)$. This again is a plausible assumption, capturing the notion that higher pathogen burdens are more dangerous. Putting these pieces together, we arrive at an instantaneous mortality function that is driven by pathogen demography, and is identical to the Gompertz function (given $a = v * p0$ and $b = r$);

$$m(t) = v * p_0 e^{rt} . \qquad \text{[Equation 2]}$$

We can provide an initial plausibility test of this mechanistic model (equation 2) by examining the implied range of pathogen growth rates r, given that under this model, $r = a$ from our earlier Gompertz model fits (Figure 2.2). In Figure 2.6 we plot fitted values for r, which fall within plausible bounds set by maximal pathogen growth rates. Using *E. coli* as a benchmark, typical lab doubling times are 20 minutes, implying a growth rate per day of 72. Figure 2.6 also illustrates that in some instances inferred growth rate is negative, which is again biologically plausible (implying a degree of host clearance of the infecting pathogen) and translates to a *decelerating* risk of death through time since infection.

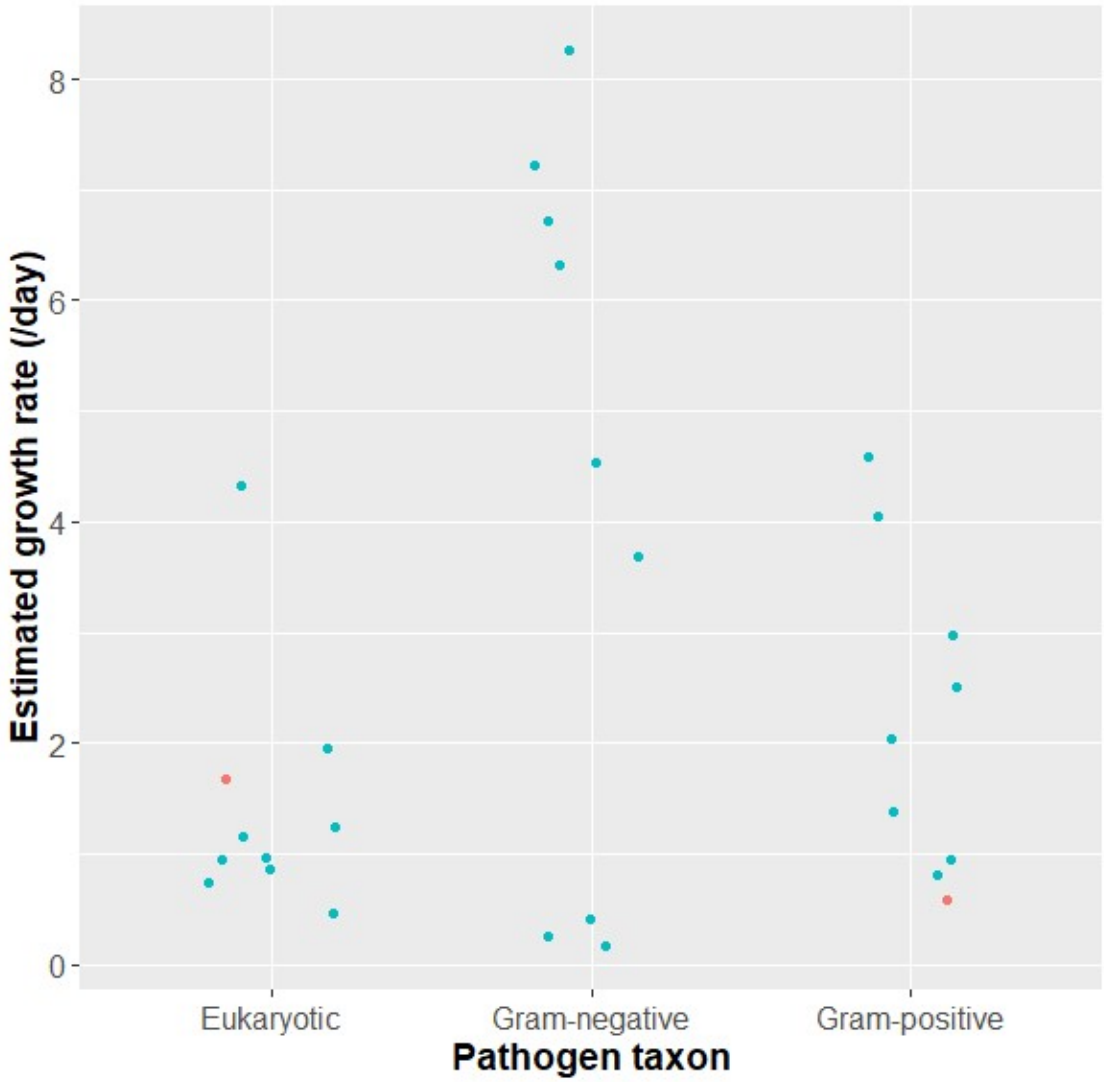

Figure 2.5. Implied pathogen exponential growth rates r (/day), inferred from survival data (Figure 2.1) under the assumption of model equation 2. Given equation 2 holds, the b parameter from the Gompertz fits to Figure 2.1. data translates to exponential growth rate r of the infecting pathogen. Dots in pink denote studies where ΔAICc is non-significant (controlling for false discovery rate = 5%).

While the model assumptions of exponential growth and a linear mapping appear plausible, and the resulting Gompertz equation fits the data above, we must heed the caution that multiple mechanistic processes can be consistent with a single statistical pattern (Frank 2009) In the following sections we explore two alternate scenarios that are

consistent with plausible within-host processes of pathogen growth and host impact and also generate the observed acceleration in risk during the course of infection.

Model 2: linear pathogen growth, exponential mapping of pathogen density to host mortality.

In a second avenue of approach, we assume a linear expansion of the pathogen following infection at rate g, $(p(t) = p_0 + gt)$. In this case, we can again return to a Gompertz function in the limit of $p_0 -> 0$, given that mortality is an exponential function of pathogen density $m(t) = v * e^{p(t)}$. This mapping of instantaneous mortality onto pathogen density implies that larger pathogen densities are disproportionately harmful, which is consistent with a pathogen regulatory shift model (positive density-dependent virulence expression due to quorum-sensing control,(Rumbaugh et al. 2012)), and/or with density-dependent loss of host defenses. By substitution, we can now connect within-host pathogen growth to population mortality by $m(t) = v * e^{gt}$. Fitting this model to our survival data ($g = a$), we find poor quantitative support as the model fits imply very low rates of linear growth (less than 10 cells per day) from a zero inoculum.

Model 3: Constant pathogen density, density independent acceleration in mortality.

Data on the within-host dynamics of infection are sadly limited, but in some studies there is little change through time in pathogen density (Pletzer et al. 2017), and in some cases there are even appreciable declines – albeit from deliberately high inocula (Kamada et al. 2012). In light of these data, we could conservatively assume that within-host dynamics are relatively constant, *i.e.*, $p(t) = p_0$. From this standpoint, we can still return to a Gompertz mortality function by assuming $m(t) = a * e^{b*t}$, *i.e.*, the acceleration in risk is independent of the demography of the pathogen. These assumptions leave open the

question of mechanism, and here we note two broad avenues. First, an increase in instantaneous mortality from a static pathogen population could result in regulatory shifts in the pathogen towards virulence at later time points. Second, a similar pattern of increasing mortality could result from a model of cumulative damage, where the same population of pathogens exerting the same pattern of virulence expression through time leads to a cumulative degradation of host function, and rising risk of death.

The ability of three distinct math models to produce logically consistent accounts of within-host infection processes $p(t)$ and $m(p)$ demonstrates that inferring within-host behavior purely from mortality trajectories is an under-determined problem. In short, we need to look inside hosts to directly observe pathogen dynamics.

Discussion

Our data analysis shows that the instantaneous rate of mortality increases exponentially during the course of infection, in diverse experimental models of infection (Figure 2.1-2.5). This exponential increase in risk is a hallmark of aging in humans (Gavrilov and Gavrilova 2019) and other organisms (Cole et al. 2017), and is phenomenologically described by the two parameter Gompertz equation (equation 1). Unlike the aging literature, however, we have in the case of acute lethal infections a clear causal currency – the bacterial or protozoan pathogen. Building on this causal connection, we next outline potential mechanistic paths between the within-host dynamics of the pathogen and the observed acceleration in mortality. Our analysis demonstrates that multiple causal processes are consistent with the observed survival data, illustrating that the observation of accelerating mortality alone is insufficient to infer the underlying process of mortality.

Our mechanistic model analyses highlight two sets of assumptions that together combine to define instantaneous mortality, $m(t)$, in terms of pathogen dynamics $p(t)$. First, we need to define the nature of pathogen growth $p(t)$. Across our math models we consider exponential, linear or no growth. Other reasonable choices include logistic growth (Biancalani and Gore 2019), or even declines from a high inoculum, as observed in some experimental models with large challenge inoculations (Pletzer et al. 2017). Second, we need to define how pathogen dynamics $p(t)$ shape instantaneous mortality $m(t)$. Here we consider a linear mapping, exponential mapping or $m(t)$ independent of p. Again, other choices could be made, for instance a mapping incorporating infection history, $m(t) \sim \int p(t)\, dt$. For each of these sets of assumptions on the form of $p(t)$ and $m(t)$, we next review possible data sources to constrain and inform our model assumptions.

To address the challenge of measuring within-host pathogen dynamics $p(t)$, broadly two paths are available. The first and simplest path is destructive sampling, where a large cohort is tracked during the course of infection, and sample individuals are taken at intervals and sacrificed to estimate pathogen burden at time t, *e.g.* by grinding up the entire host or a sample of host tissue and plating on selective media for a defined bacterial pathogen (Biancalani and Gore 2019). Biancalani & Gore used this method to characterize the dynamics of pathogen growth within cohorts of infected nematodes and reported support for a model of logistic growth. Yet their protocols illustrate a potential limitation with destructive sampling, namely the introduction of a selection bias into the data, given the measurement of infection burdens from live worms only. If worms tend to die at high infection burdens, then the apparent plateau in reported bacterial densities could result from the selective removal of worms with high infections due to death.

A second path is to track infection burden non-destructively via repeat measures from the same population of hosts. While requiring fewer hosts to produce workable data (by allowing repeat observations from the same individuals), the requirement to minimize invasive observational effects can become a limitation (Ahmed et al. 2019). Fluorescent microscopy is an attractive route, though in practice, most existing methods are more concerned with pathogen localization and describing disease severity, rather than attempting to estimate absolute counts (White et al. 2010; Pletzer et al. 2017).

Turning to the mapping function, $m(t) = f(p(t))$, some evidence can be gleaned from experiments varying inocula (Aaberge et al. 1995; Barnes et al. 2006; Borges et al. 2013), but without tracking subsequent dynamics of the pathogen within the host, this approach is limited to defining initial conditions. To empirically estimate mapping functions will require empirical measures through time of instantaneous mortality $m(t)$ (from survival data, e.g., Figure 3), together with measures of pathogen density, $p(t)$, as outlined in the previous paragraph. In subsequent chapters, we pursue this agenda using an experimental *C. elegans* infection system.

In the current chapter, we focused on diverse experimental infection models, with divergent modes of pathogen replication and host immune control. Despite this biological diversity, we witnessed a similar phenomenological pattern of accelerating risk. Our approach raises the potential for incorporating age of infection (t) and pathogen dynamics $p(t)$ into epidemiological analyses, a topic which has been pursued under the banner of 'nested' epidemiological models (Grenfell and Harwood 1997; Grant et al. 2008). While

previous work on nested epidemiology has relied on 'plausible' models of $p(t)$, e.g., (Antia, Levin, and May 1994; Gilchrist and Sasaki 2002), we caution that multiple within-host processes can be consistent with epidemiological data (Figure 2.3). What we now require are studies to empirically determine the within-host dynamics of infection and their mapping to mortality. With this data we will be able to further constrain models and explore new avenues for intervention strategies that are conditioned on the progressive state of infectious disease.

Chapter three: Non-destructive assessment of pathogen burden and host survival in a model infection system

Tim O'Sullivan, Yifei Wang, Kristofer Wollein Waldetoft, Sam P. Brown

Abstract

In this chapter we develop and assess multiple platforms to assay survival and pathogen dynamics non-invasively across a cohort of worms. Using fluorescently tagged pathogens and light/fluorescence microscopy, we investigated both 'open-field' and individually-housed worm platforms, ultimately opting for a 96-well plate method of individual worm tracking. We developed multiple bioinformatic platforms in the attempt to overcome image processing issues, and here report data showing that pathogen dynamics (measured by infection fluorescence scores) do not predict time of death. Calibration data underscored multiple issues with fluorescence data processing, revealing an absence of sufficiently reliable association between our fluorescence scores and 'gold-standard' (CFU) measures of pathogen density. As a result of these persistent challenges, we conclude that our best approach in the context of this thesis is to switch to a destructive-sampling / CFU counting approach to infection tracking, which we develop in chapter four.

Introduction

Estimating pathogen burden, p, in animal infection experiments is conventionally done by destructive sampling from a large cohort of infected animals. Individuals are taken at intervals (or simply at the endpoint) and sacrificed to estimate pathogen burden at time t since infection, e.g. by grinding up the host or host tissue and plating on selective media for a defined bacterial pathogen (N. Wang et al. 2011; Palominos and Calixto 2020). Estimating $p(t)$, the pathogen burden over time since infection t, is often done using this

destructive sampling approach (Lindberg et al. 2018; Biancalani and Gore 2019). However, one of the key weaknesses of destructive sampling is the inability to measure pathogen burden in a single individual at multiple timepoints, making longitudinal analysis impossible on an individual host scale.

In comparison to destructive approaches, *non-destructive* sampling of infected hosts confers key advantages, in particular the ability to connect pathogen density to infection outcome on an individual host scale. Yet the requirement to minimize invasive observational effects can become a limitation (Ahmed et al. 2019). One attractive route is to use fluorescent or luminescent reporter strains, that can be imaged within a host non-invasively (Ohlsen and Hertlein 2018). This path has been taken in diverse animal models, from mice (Leevy, Serazin, and Smith 2007) to nematodes (Vega and Gore 2017). Typically, these methods are used to describe the location and intensity of infection, yet can't always be translated into a quantitative pathogen burden once inside the host (White et al. 2010; Pletzer et al. 2017). In the absence of light-based reporters, other routes are possible via the sampling of peripheral fluids, e.g. for malaria (Armah et al. 2007; Buppan et al. 2010). However the risk of observer effects are higher in these cases, as attempting to sample from moribund hosts, one may inadvertently accelerate mortality, thereby warping the relationship between pathogen burden and death (Fink 2014; Lewis, Seymour, and Rosengart 2016). In a nematode context, survival assays are common (for example in the assessment of anti-infectives (Kong et al. 2014; Conery et al. 2014)), but standard survival assays lack single worm tracking.

C. elegans – P. aeruginosa model system

In light of the pros and cons of alternate approaches outlined above, we focus on a nematode model, infected with the tractable model pathogen *Pseudomonas aeruginosa* (Diggle and Whiteley 2020). This specific infection model has been developed previously by several other groups (M. W. Tan, Mahajan-Miklos, and Ausubel 1999). *C. elegans* is readily infected by multiple strains of *P. aeruginosa* and infection under appropriate conditions produces reliable host mortality (Ruiz-Díez et al. 2003). The standard infection route is via a defined oral exposure window, where the pathogen then establishes in the nematodes' gut lumen. Leveraging the nematode's translucent body, many scientists have used fluorescence microscopy to measure a number of different in vivo dynamics including gene expression, cell development, and microbial interactions within the worm. In principle, such a tool could allow us to track pathogen growth dynamics non-invasively (albeit with some minimal background effects, De Magalhaes Filho et al. 2018). While lacking a vertebrate immune system, the *C. elegans* model offers a multitude of advantages that are not available with mammalian host systems. Principally, the nematode system can be used for high-throughput experiments on scales far beyond typical vertebrate systems, is easily culturable, and offers a vast genetic library to explore more genotype-by-genotype interactions in a host-pathogen system.

Methods

Bacterial strains and culturing

We used the *Pseudomonas aeruginosa* strain PAO1 from the Nottingham collection. PAO1 serves as the canonical strain of *P. aeruginosa*, and much work has been done on the interactions between PAO1 and nematode hosts (see first chapter). *Escherichia coli* OP50 is a non-pathogenic strain that is used to rear worms (Brenner 1974).

For all bacterial strains, single colonies were inoculated in Luria-Bertani (LB, Sigma Aldrich) broth overnight in a shaking incubator at 37°C, atmospheric conditions. Overnight cultures were then standardized to 0.8 $OD_{600,}$ pathlength 10mm. Then, 750µL of the overnight culture was plated on nematode growth medium (NGM) (US Biological) plates in order to create lawns of bacteria. Plates were incubated overnight at 37°C. Bacterial lawns were allowed to acclimate to room temperature before introduction of worms.

Nematode strains

We used the self-incompatible mutant SS104 for our experiments (Beanan and Strome 1992). Due to the classical problems with progeny for nematodes during long-term infections (Kirienko et al. 2014), this strain is widely used to produce worm cultures with experimental control of reproduction. Strain SS104 possess the *glp-4* mutation that prevents self-fertilization at specific temperatures. Previous work has shown that *glp-4* mutants have enhanced resistance to *P. aeruginosa*, as well as other pathogens relative to wild-type N2 worms, though the observed survival dynamics show broadly similar dynamics as discussed in chapter 2 (Tekippe and Aballay 2010).The germline is arrested at temperatures >15°C, while it is permitted at 15°C. During rearing, worms are kept inside a temperature controlled (15°C) environmental growth chamber until reaching adulthood, with minimal exposure to light. To produce an age-controlled cohort of worms, gravid hermaphrodites are isolated from plates and then destroyed with a hypochlorite bleach solution to liberate eggs and destroy adult worm tissue (Stiernagle 2006).

Nematode infection

Adult worms were transferred to lawns of either PAO1 or OP50. Exposure to the bacterial lawns lasted for 16 hours, in which time infection occurs though consumption of the pathogen (PAO1) or control (*E. coli* OP50). Worms were then washed off of their respective bacterial lawns using M9 buffer (Stiernagle 2006) and captured into 1.5mL microcentrifuge tubes for washing. Initially, worms are chilled for 7 minutes at 5°C in order to reduce pharyngeal pumping. Once pumping slowed, a dilute bleach solution (0.1%) was used to wash the worms. Washing consisted of gently centrifuging worms to the bottom of the microcentrifuge tube (2500 rpm, 45 seconds) and discarding supernatant (while being careful not to accidentally remove live worms from the tube). After the initial bleach wash, a dilute detergent solution (0.01% Triton) was used to remove any remaining bacterial particles, which was then followed by three more washes of sterile M9 buffer. Finally, worms were transferred to a platform to monitor survival (as described below; either NGM plates, microfluidic chip, or finally the half-area 96 well plate.

Existing platforms for high throughput worm-tracking following infection.

C. elegans is a well-studied organism in both the field of aging and host-pathogen research, so we searched for existing tools and methods that would suit our purposes to test our hypotheses. Here, we quickly give an overview of the methods we tried to adapt to for our own experimental designs.

The C. elegans Lifespan Machine

Our first solution to the challenge of tracking individual infected worms through their remaining lifespans was to use the established *C. elegans* Lifespan Machine (LSM) (Stroustrup et al. 2013). Stroustrup et al. developed the LSM to track individual worm

activity (including death) through time, resolving individual worm trajectories from visual data on multiple worms co-housed in petri dishes. The LSM combines hardware and software components. The LSM hardware is a modified Epson v800 office scanner, engineered to run continuously, gathering images every hour on populations of worms housed in 16 agar plates on the scanner bed. After the assay is complete, the image data are analyzed through an analysis pipeline that tracks individual worms and can bin nematodes in healthy, morbid, or dead states. In an infection context, we aimed to use the LSM to generate high resolution individual morbidity and mortality data, and merge with less frequent fluorescence microscopy imaging of the same plates to generate periodic infection burden estimates.

Over the course of our experiments, we noticed a consistent difficulty to identify infected worms, potentially due distinct and idiosyncratic shapes that worms are prone to during infection. These match poorly with the existing data that the LSM was trained on, cohorts of worms that were monitored in a more classical ageing context. Our initial pilot experiments involved a small (~100) cohort of N2 worms exposed to PAO1 for a period of 24 hours, similar to the description of *Nematode infection*, above. After this period of time, worms were washed and placed on NGM dishes containing FUDR (5-fluorodeoxyuridine) to halt egg production. Figure 3.1 provides a vignette of the image analysis challenge, presenting a representative sample of 25 worms imaged 1 hour after the start of the survival experiment. Although we attempted additional training for the LSM software, we encountered technical difficulties that were outside the range of our current expertise for the project. Though not continuing with the LSM seemed like an unfortunate trade-off, considering the potential for very large cohort sizes, lack of an

effective way to sample bacterial burden was enough of a drawback that we considered other avenues of work.

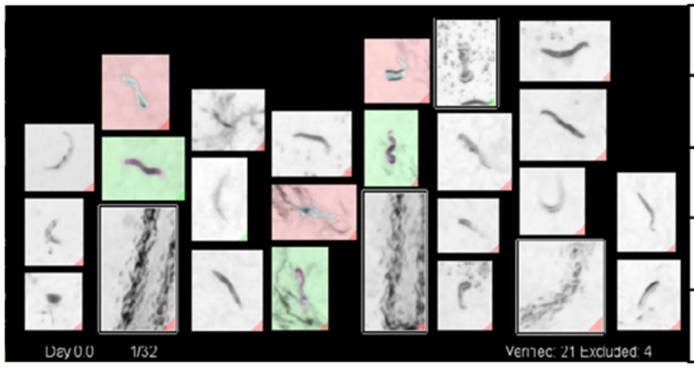

Category	Count
Correctly identified	3 (12%)
Correctly excluded	3 (12%)
Failure to bin	19 (76%)
Total	25

Figure 3.1. Difficulty in worm identification using the Lifespan Machine. Worms that are properly screened are highlighted in green, whereas "dead" worms are highlighted in red. The normal, brightfield images failed to be detected by the model, evidenced by the number of worms that have failed to be identified (white background, no green) and instances where artifacts are misidentified as worms

Health And Lifespan Testing Hub (HeALTH)

Our experiences with the LSM point to the difficulty in bioinformatically identifying infected worms in 'open field' experimental designs. To address this difficulty we turned towards platforms that would allow individual housing of large cohorts of worms, making the computational step of tracking individual worms straightforward. Le et al. (2020) recently developed a microfluidic device designed specifically for individual worm tracking over time, termed the Health and Lifespan Testing Hub (HeALTH). We sought to use the HeALTH platform to separately house and track multiple worms from infection through to death, via repeated imaging of individual worms through both brightfield and fluorescence channels.

Within the Brown lab, we lacked the finesse necessary to capture loading as seen in Le et al. (2020). This does not mean there was anything wrong with the original microfluidic design, merely that operator error led to chips being destroyed due to pressure, to

improper loading, or shearing of worms forced through inlets that were already pressurized. Other than user observation from failed attempts of these loadings (numbering 12 instances in total), there are no other accompanying data. Despite our best efforts to make this protocol work within our setting, we did not have the manual dexterity to establish it in the lab. We mention this attempt here solely as an accounting for the time spent during the PhD. In response to these difficulties, we sought an approach that would leverage a microtiter method that might be more suited to my own skills, and a more general approach that might be available to existing microbiology labs.

Developing a new platform: using florescence to estimate burden in microtiter arenas

In our next round of experimental method development, we turned to a simple 96-well plate design, where we aimed to separate worms into individual wells. This experimental design broadly reflects protocols for testing anti-infectives in worms (Conery et al. 2014). We experimented with liquid inoculation of wells (varying worm density in liquid, and volume of liquid per well), tuning the loading parameters to maximize the count of singleton-worm wells. This design is simple to conduct, but ran into image focus problems due to the 3D experimental volume.

We next attempted a 2D surface scenario where each well contained 120 µl agarose pad and worms were inoculated by picking (Tritech research). This method was ultimately imperfect due to the introduction of bubbles into the agarose pads. Bubbles present an imaging problem, and also provide opportunity for worm burrowing, making imaging even more difficult. In our final design, we continued with worm picking from solid plates, but now delivered the worms into small (150 µL) liquid volumes of M9 buffer

that formed shallow pools for the worms and therefore allowed reliable image focus. We used the Cytation 5 (BioTek Instruments) microplate reader and microscope to image worms over time. Note that in chapter four we switch to a pipetting method of worm delivery.

Nematode imaging

Nematode imaging was performed using a Cytation 5 microplate reader (BioTek). We used the tractable magnification of 1.25x, which captures the whole well in a single field of view (so no image stitching required). We captured bright field and GFP (excitation: 459, emission: 525). Camera settings for brightfield images were set to an LED intensity of 3, integration time of 123 ms, and gain of 10. Images were captured for each nematode once every hour. The time between each imaging for each well was approximately 30 seconds. Data was monitored regularly approximately every 12 hours to ensure that the full survival dynamics (as defined below) were captured. The captured 16-bit TIFF files were then uploaded to the Georgia Tech high-performance computing cluster for analysis.

Bioinformatic methods to process data from 96-well plate experiments

Our first challenge was to identify mortality events from the brightfield image data, for each worm. Though easy to track manually by eye, preexisting automated approaches proved to be difficult to adapt given the needed microscopy settings—the resultant haloing present in the wells worked poorly for established pipelines such as CellProfiler (Carpenter et al. 2006). In response to this limitation, we opted for a manual

identification of time of death. For each tracked worm, we inspect the image series (~180 time-points for each worm) in reverse chronological order (working back from established death) and identify time-of-death as the timestep after the final worm movement. Using this simple approach, we can rapidly and reliably determine time-of-death, and fit statistical models as described in the previous chapter.

Infection burden: whole well fluorescence

To estimate pathogen burden (per worm) from fluorescence data, we begin with a 'whole well' approach. In principle, the dominant fluorescence signal per well should come from the infected worm. As a first pass, we took whole well reads of the fluorescence data, yet ran into difficulties due to large and variable background fluorescent objects. We explored sources of background fluorescence variation and identified well debris (microfibers or partial cadavers introduced during worm picking and transfer) as a source of variation. To address this limitation, we next sought bioinformatic methods that could extract the worm body and then correctly draw the fluorescence intensity from the defined worm object.

Infection burden: worm object fluorescence

To remove problematic background fluorescence, we turn to the brightfield image channel to identify a worm binary (the spatial extent of the worm, at time t) which we can then use to filter the fluorescence data to produce a 'whole worm' fluorescence score. Figure 3.2 illustrates the key steps in our worm binary identification. Figure 3.2A illustrates a typical brightfield image of a single-worm well, highlighting the challenge of a substantial halo effect due to the 3D structure of the well. To maximize the worm object against the variably lit background of the well, we attempted to accentuate the

appearance of the worm using a contrast stretching method (Yang 2006). From there, we reduced image noise by using a Gaussian filter to smooth the image. Using our pre-processed set of images, we applied a Sobel filter (Mohan, Vijayarani, and Vinupriya 2013) in order to detect gradients within the image, specifically the outline of the worm of interest. As seen in figure 3.2B, the Sobel filter eases worm identification against a somewhat dark background. At this point in the process, we attempted to transform the image into a binary to facilitate analysis. Due to the uneven distribution of light in our brightfield images, we opted for an adaptive thresholding method using the *opencv* package in Python to detect pixel intensities (Bradley and Roth 2007). The method automatically weights thresholding across the image space in order to extract objects from the image background. As can be seen in Figure 3.2C, the package extracted the worm along with additional noise around the "halo" of the well. Finally, we used an additional filter to remove small objects (< 255 pixels, Figure 3.2D).

As discussed earlier in the chapter, identification of infected worms is problematic in an open plate arena. In the 96-well plate format, we face additional challenges due to the halo effect at well edges. We explored methods to correct for edge effects However, analysis became problematic when the worm is found within this signature 'haloing' observed in the brightfield image – as commonly occurs if worms move towards the periphery of well space. Figure 3.2 highlights a successful application of our pipeline to-a worm that is partially within the halo zone, yet in many cases the same pipeline resulted in biologically unreasonable worm shapes and sizes.

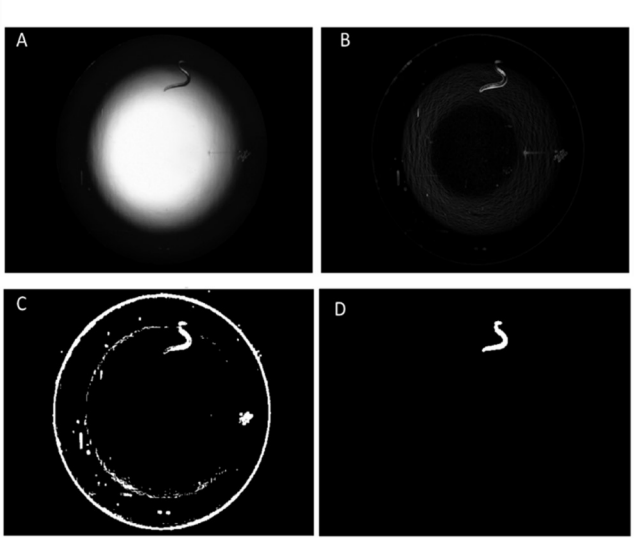

Figure 3.2. Brightfield image processing to identify whole-worm binaries. (A) raw unprocessed brightfield image of a single worm well. (B) – Sobel filter to accentuate the worm object on a dark background – (C) binary image with typical noise, (D) Binary image with small objects filtered out using adaptive thresholding.

As a result of these multiple difficulties, application of the worm identification pipeline outlined in Figure 3.2 resulted in highly noisy data, characterized by temporal fluctuations in worm binary size and frequent identification of unfeasibly large worm objects (10x the size of typical worm objects). We explored censoring worm data by defining minimum and maximum object sizes (3000 pixels and 4500 pixels, respectively), designed to capture worms against illumination noise. Though we used an isogenic and identically reared population of worms, which would suggest a small variation in worm size and morphology, our thresholding parameters had to be lenient enough to detect worms in various conformations—especially due to signature “coiling” that occurs over the course of infection experiments. While data censoring removed outliers in the worm object binary, we ran into additional challenges when overlaying the brightfield derived worm object binary and the fluorescence data. The worm object binary is identified in order to extract fluorescence data for the worm only, however there is a 10 second mechanical delay

between brightfield image capture and fluorescence capture, leading to a potential processing disconnect if the worm is moving at this time. This was of particular difficulty in the early stages of the experiment as healthier worms show more displacement in the 10s between brightfield and fluorescence imaging.

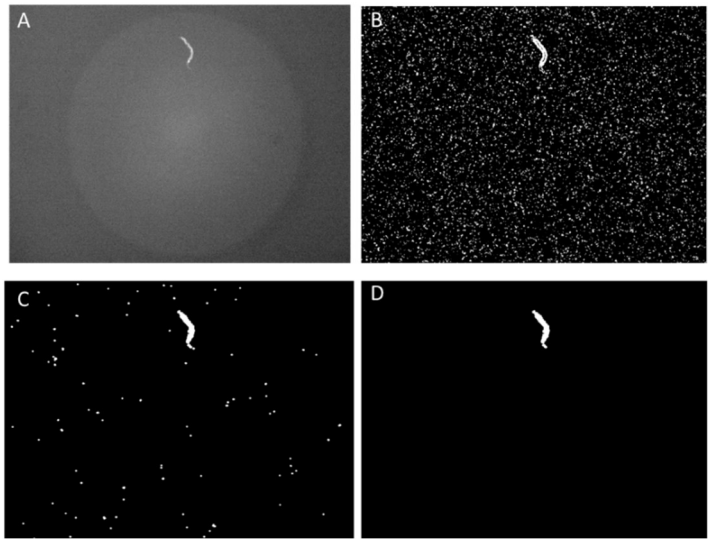

Figure 3.3 Identification of infection object. (A) the unprocessed GFP image from a single worm timepoint. (B) After the using smoothing and background removal, we then used line thresholding in order to detect objects within the well. (C) Transformed image after line thresholding, Though worm detection is clear, many small autofluorescent "objects" have been captured. (D) Final image filtering out small objects.

Infection burden: infection object fluorescence

To address the object identification challenges and temporal delays inherent to our worm object identification, we next turned to an alternate strategy focused on the fluorescence channel alone. Our goal was to identify an 'infection object' (the spatial location and extent of the site of infection within a worm) from the fluorescence data and use this 'infection object' as a binary to extract only the fluorescence data from within this location. This process effectively deals with the halo and time-delay issues mentioned above.

Again, we used the *opencv* package from Python to transform fluorescent images to binaries (Figure 3.3). First, we applied a background correction and smoothing parameter to reduce potential noise in the fluorescent field image. From there, we attempt to find the infection object using line thresholding (Figure 3.3B). Similar to our pipeline from before, we used filters to remove lingering noise (Figure 3.3C), removing objects with < 255 pixels (Figure 3.3D).

We applied some quality control measures for extracted objects, to ensure confidence in our following data analysis. Our first step was to account for instances where the pipeline performed poorly when extracting worms from the edges of the well, which consisted of an observer manually verifying that the extraction only contained pixels contained within the nematode image. After censoring these images from our dataset, we performed a final quality control measure for data completeness—we only included worms that had reasonable automated extraction for at least 50% of the time points ($\geq$ 93 of the 185 timepoints).

Applying the infection object binaries (Figure 3.6) as a filter to the whole well fluorescence data (Figure 3.5), we can now estimate per worm trajectories *of P. aeruginosa* fluorescence (Figure 3.7). Figure 3.7 indicates that for the bulk of the worms, the infection burden (as indicated by infection site fluorescence) is high and stable. However, some worms show greater variation, which in some cases clearly indicates problems with our data analysis.

We then performed an additional screening in two steps; first we chose to only include wells that had a high level of completeness (≥ 135 of the 185 timepoints). Then, we performed a manual screening process, checking that the pipeline did not add objects that were clearly not worms (as checked by a corresponding brightfield image). We removed all wells that had at least one instance of worm misidentification.

After screening for completeness, we then wanted to control for the potential of debris and non-worm objects being inadvertently maintained. This required a manual curation step, in which we culled any well that captured non-worm objects during the extraction step. Applying these filters results in our final fluorescence data set (Figure 3.10, also indicating time-of-death data).

Calibrating fluorescence to pathogen burden

To validate our assumption that our fluorescence scores reflect underlying pathogen burden, we next performed calibration experiments, using destructive sampling and Colony Forming Unit (CFU) counting as our gold-standard estimate of pathogen burden. We calibrated for both fluorescent PAO1 and OP50.

Worms were prepared in the same manner as described in *Nematode infection*, above. Washed worms are then transferred to an NGM plate for ultimate transfer to a half-area 96 well plate (Greiner BioOne). Wells were prepped with 170 µL of M9 buffer before transfer, leaving worms floating in wells for imaging. In order to assay burden before microbial density becomes saturated within the lumen, we sampled at multiple time points after exposure. For our OP50 GFP experiments, worms were sampled at 2.5 hours, 6 hours, 10 hours, and 14 hours. We also sampled controls, exposed to live

OP50. For our PAO1 GFP experiments, we followed a similar design, sampling worms at 2 hours, 4 hours, 8 hours, and 12 hours. For florescence measurements, we used the same pipeline described above to extract RFU values, with the exception of manually defining worm object instead of using the automated aspects of our pipeline—to ensure high fidelity extraction of worm objects.

Results

Validation of bioinformatic pipeline

We first analyzed the survival dynamics of our initial cohort of 92 worms to confirm that mortality dynamics accelerate per our *a priori* assumptions (Figure 3.4). Note that in Chapter 4 we repeat this experiment with the addition of non-infected controls, confirming that mortality is primarily due to infection.

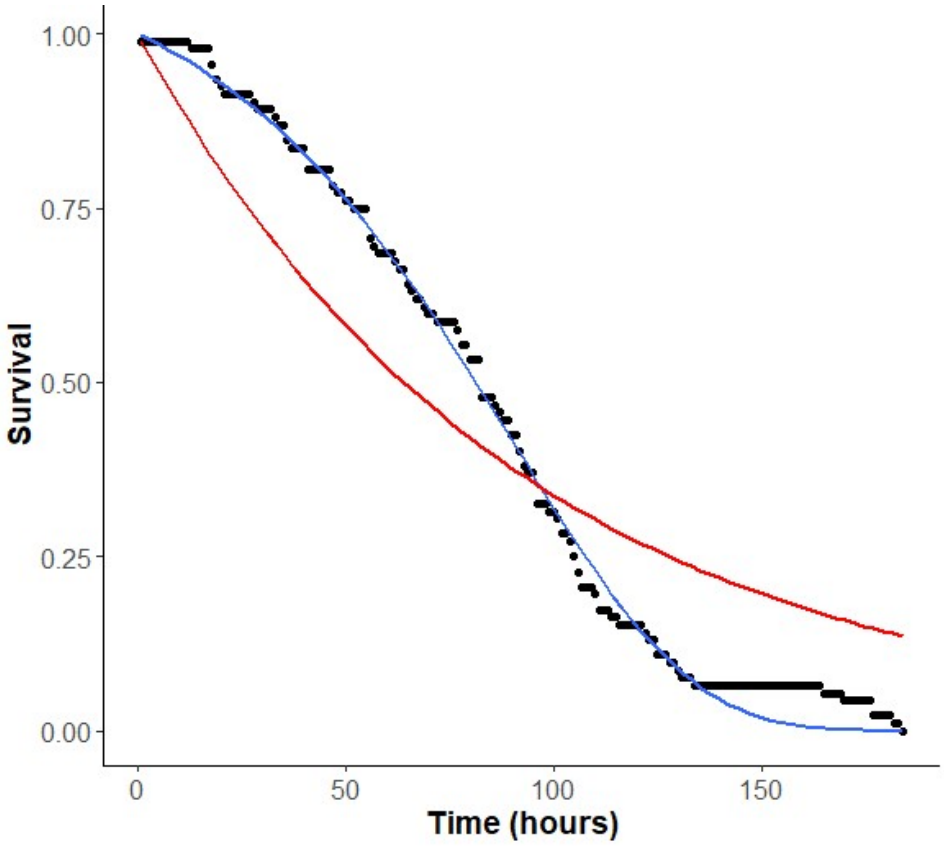

Figure 3.4 Survival data for *C. elegans* / *P. aeruginosa* infections indicate accelerating mortality. Black dots represent experimental survival data (*N* = 92); the blue line represents a Gompertz model fit ($m(t) = b * e^{a*t}$), *b* = 0.003/hr, ***a*** = 0.023 and the red line represent an exponential model ($m(t) = \lambda$), λ = 0.011/hr.

Our first pass at tracking worm florescence in wells proved difficult, as the effect of background fluorescence within the wells made it difficult to distinguish empty wells from those that house worms. To assess background signal, we simultaneously analyzed wells with zero, one or greater than 1 worm per well (Figure 3.5). Figure 3.5 clearly illustrates that the background fluorescence is variable (across empty wells) and overwhelms signal from infected worms.

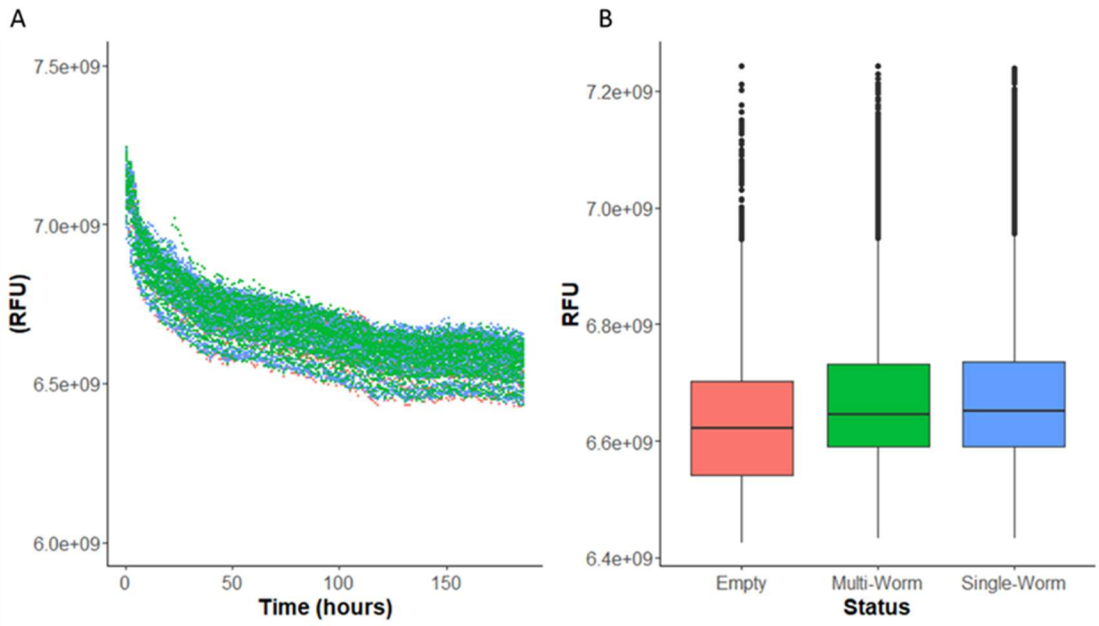

Figure 3.5. Background well fluorescence overwhelms worm fluorescence. (A) The total (summed) fluorescence per well, through time, across all wells. Empty wells (peach), multi-worm wells (green) and single-worm wells (blue). (B) The mean fluorescence intensity averaged across time for empty, multi-worm and single-worm wells. RFU = relative fluorescence units, capturing total (summed) fluorescence across entire well, at time.

In the prior section we identified a preferable method to produce sequential fluorescence and light images of individually identified wells. We then analyzed our brightfield images underneath our “infection object” guidelines, as stated above. After screening for completeness (again, images where there were ≥50% of objects extracted from fluorescent images), we end up with a cohort of 52 worms. Below is a distribution of pixel intensities for this cohort.

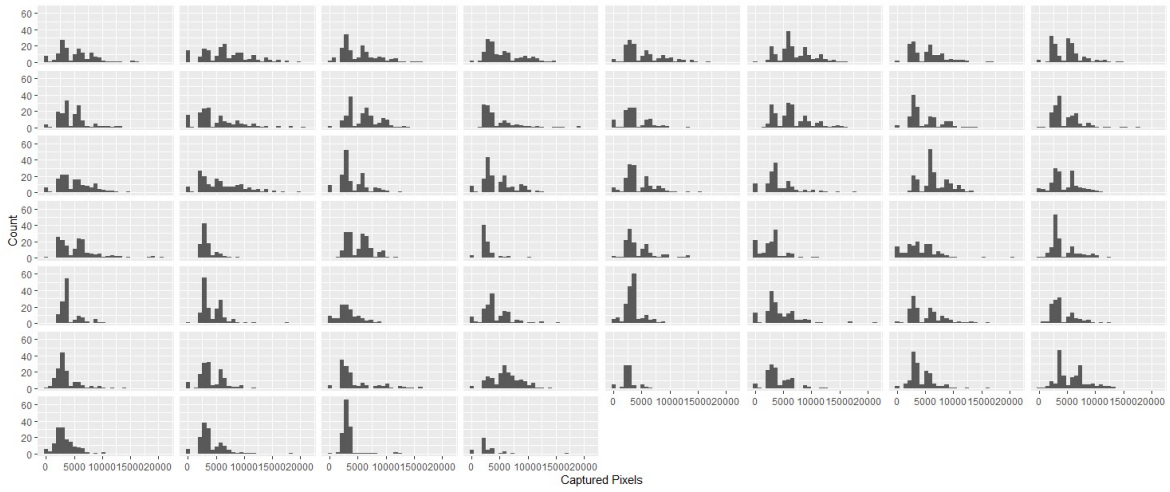

Figure 3.6. Distribution of infection object sizes, per worm. Histograms of multiple observations through time for each single worm well (each panel represents an individual singleton-well worm).

From here, we plot the relative fluorescence units (RFU) as defined by the infection binaries shown in Figure 3.6. In Figure 3.7, we plot these interpretated RFU values over time. Overall, RFU is shown to be stable for most worms, but there are outliers that show dramatic changes in RFU that suggest some occasional error with our pipeline. In Figure 3.7, we show an individual worm, which shows changes that don't seem biologically plausible (jumps from 2 x 10^7 and 4 x 10^7 within two days). We performed the additional selection criteria (explained above) that leads to our final data set of 46 worms.

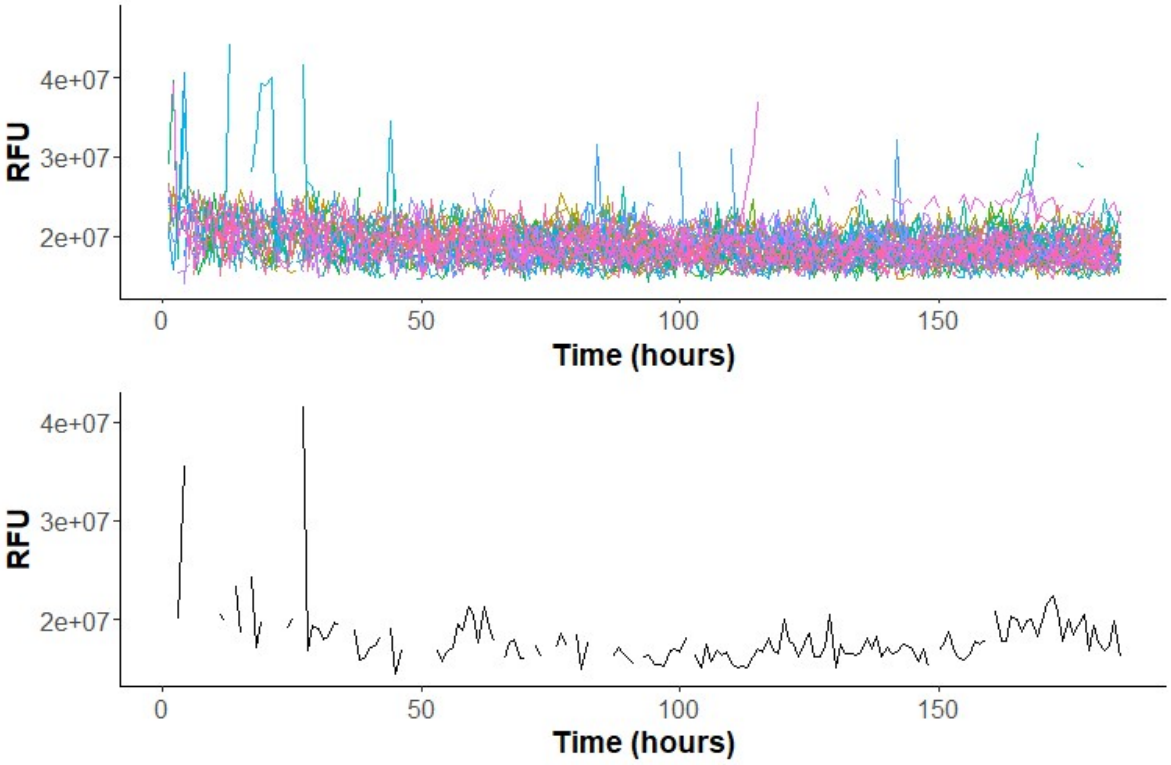

Figure 3.7. Total fluorescence per infection object. Total (summed) fluorescence per infection binary, through time. Some values are clearly unreasonable from biological context. Each color represents a different well (N=52 singleton worm wells). Well F10_2 is shown in greater detail at the bottom, the dynamics do not follow a biologically plausible pattern.

This final dataset serves as the basis for analysis for Figures 3.8-3.12. We broadly summarize the trajectories for our final cohort in Figure 3.8. For each worm (1 to 46), we attempt to estimate pathogen burden, $p(t)$ as RFU, and indicate time of death by color change (black=living, red=dead). For each worm, we also add a linear regression fit: $(p(t) = p(0) + \beta t)$. In general, RFU seems to be stable and consistent as interpreted from our bioinformatic pipeline.

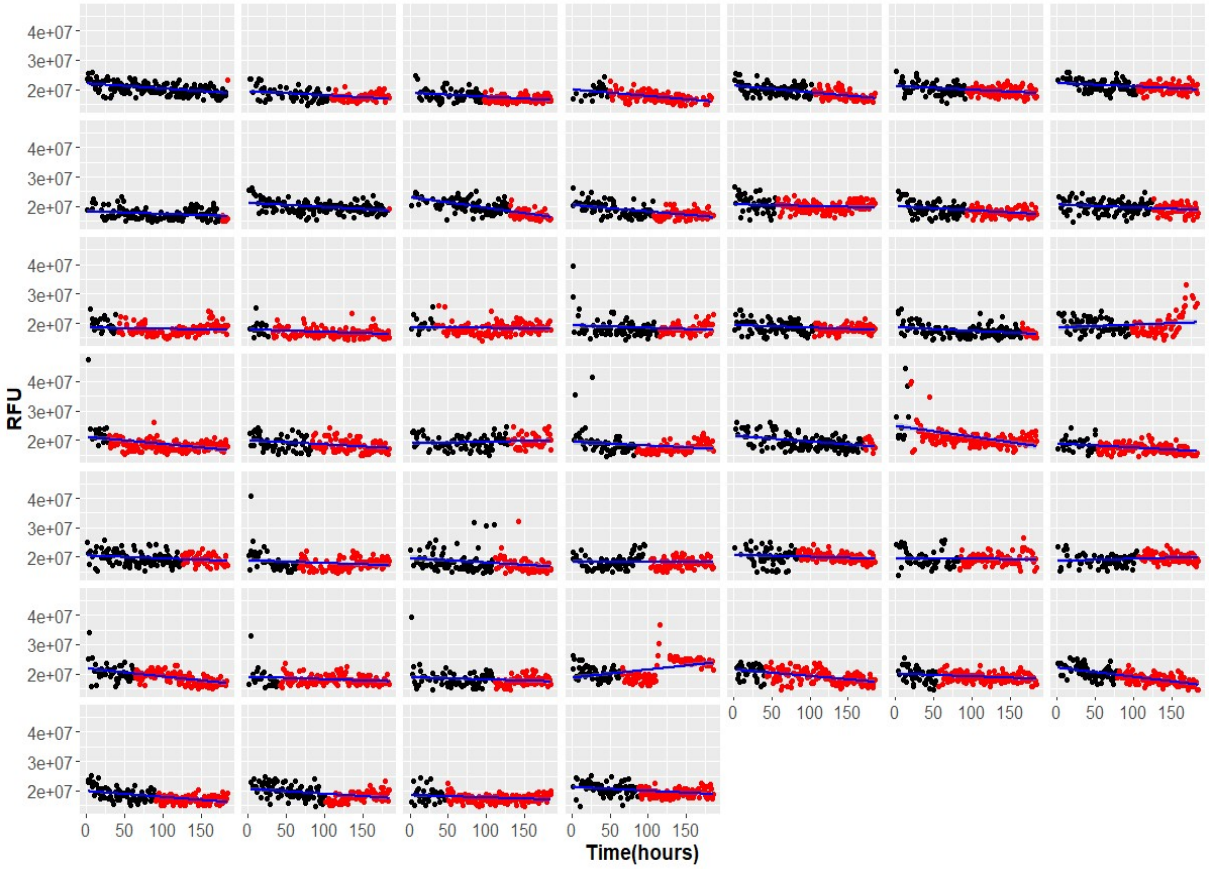

Figure 3.8. Dynamics of pathogen burden *p*(*t*) and time of death t^* across 46 worms. Total (summed) pathogen burden $p(t)$ estimated by fluorescence per infection binary, through time. Data from Figure 3.8, censored for quality control measures. Wells were censored by having low level of capture (binary extraction < 70%) and manually curated for binary extractions that included non-worm objects. Red indicates dead worms. Blue lines are individual regression lines per worm through time.

Aggregating times of death t^* across worms, we next illustrate survival curves and fit survival models as described in chapter two. Figure 3.9 illustrates the survival data for the retained 46 worms (similar to the 'all worms' analysis in Figure 3.4). The constant risk (exponential model) fit clearly shows that as in our chapter two examples, the instantaneous risk of death $m(t)$ is accelerating in time, captured by the exponential model first over- then under-representing the risk of death in time. In agreement with this qualitative diagnosis, the Gompertz model again provides a superior model fit, while accounting for the additional model parameter (AIC=-37.50 and -128.7, respectively).

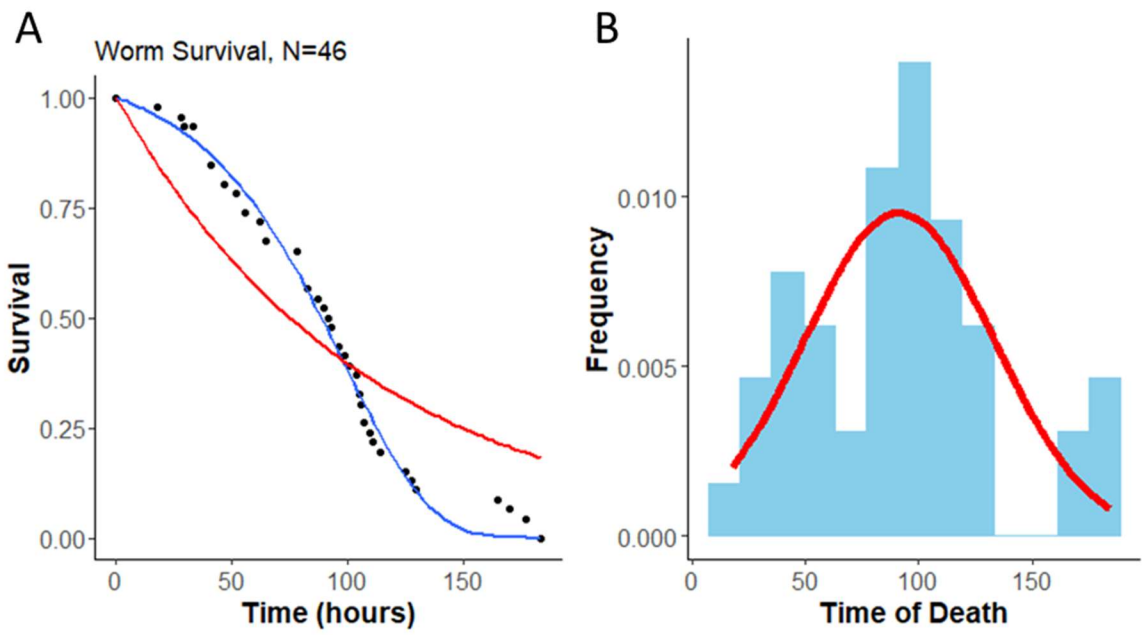

Figure 3.9. Survival data for C. elegans / P. aeruginosa infections indicate accelerating mortality. Black dots represent experimental survival data (N = 46), the blue line represents a Gompertz model fit ($m(t) = b * e^{a*t}$), b = 0.003, a = 0.023, (AIC = -128.7), and the red line represent an exponential model ($m(t) = \lambda$), λ = 0.01/hr, (AIC= -37.50). (B) Distribution of the time of death is broadly normal (mean = 91.35, standard deviation =41.87 hours.

Linking mortality to pathogen dynamics

In chapter two we discussed three alternate models of within host pathogen expansion that were each consistent with a commonly observed survivorship pattern of exponentially increasing risk of death (Figure 2.2, Figure 3.9A). Two of these models featured an expanding pathogen burden (either exponential or linear expansion), and so at first glance, our data reject these hypotheses (Figure 3.9). Aggregating burdens across worms, we also see a modest yet highly significant negative relationship between time since infection and average fluorescence intensity (Figure 3.10).

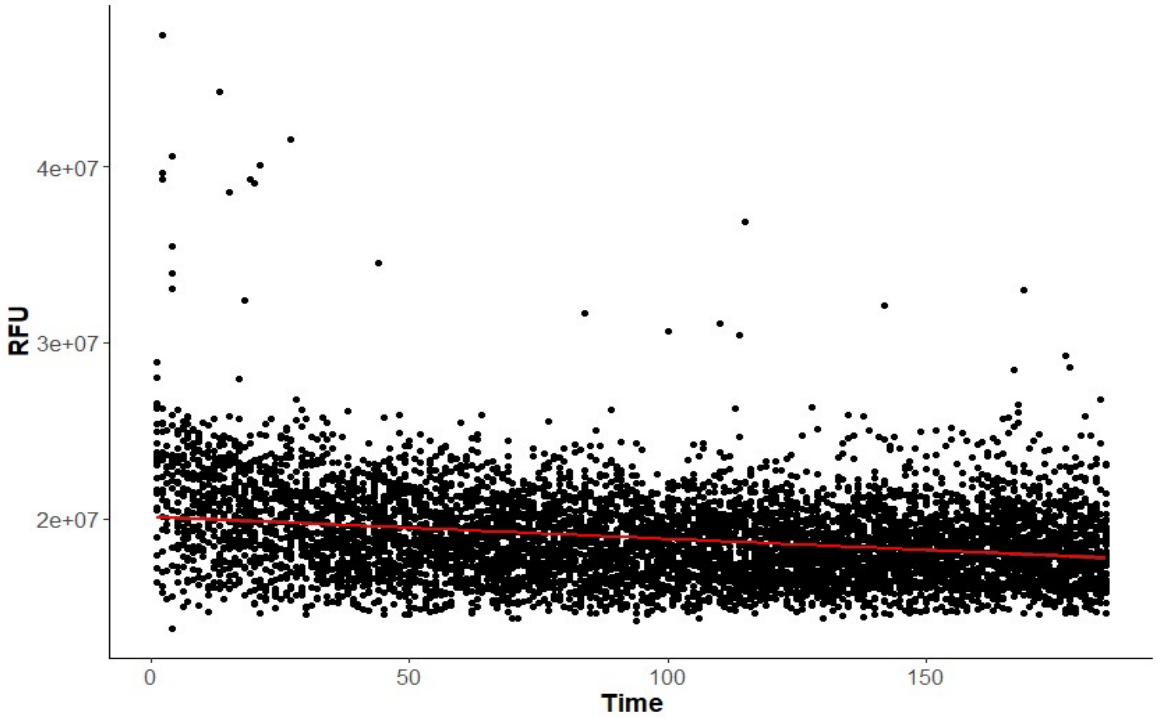

Figure 3.10. Average pathogen burden is high and stable across time. Fluorescence data for 46 worms (black dots) is superimposed on a single figure. Fitting a linear regression to this data (red line) reveals a high and relatively stable average worm burden through time (intercept $p(0)$ = 2.01 x 10^7, β= 1.81 x 10^{-11} / hr).

Given the variation across worms in time of death t^*, initial inoculum p_0 and decline in burden β (Figures 3.8, 3.9) we next hypothesized that worms with larger initial inocula and/or weaker declines in burden were more likely to die sooner. To test this hypothesis we ran a series of regression analyses across worms, with the structure time of death t^* ~ measures of initial burden and change in burden through time.

In a first linear regression model, we recognized that pathogen burden is relatively invariant and so we asked whether the time-average fluorescence per worm is a significant determinant of time-of-death. Figure 3.12A shows that there is no significant relationship (β0= 3 x 10^{-6}, p-value=0.623). We repeated our analysis using median

fluorescence to limit the impact of outlier values, and found qualitatively the same result ($\beta 0 = 5.24 \times 10^{-6}$, p-value = 0.385, Figure 3.12B).

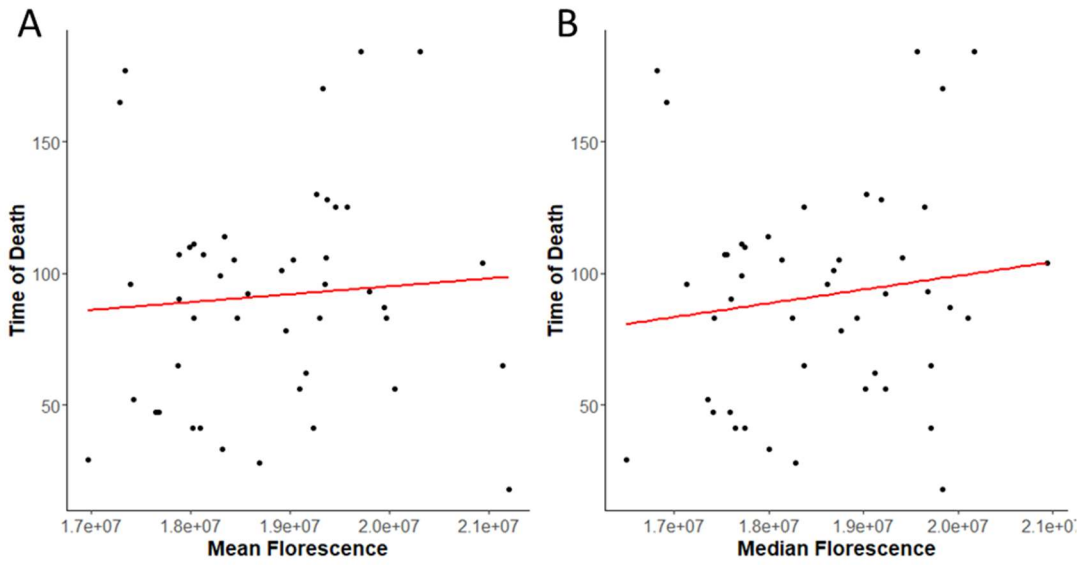

Figure 3.11. Neither mean nor median pathogen burden is predictive of time-of-death. Each dot corresponds to an individual worm, characterized by (A) mean fluorescence through time, (B) median fluorescence through time, and time-of-death. (A), Intercept = 34.86, slope = 3×10^{-6}, slope p-value = 0.623. (B), Intercept = -5.73, slope = 5.24×10^{-6}, slope p-value = 0.385.

We next turned to predictors that capture the temporal dynamics per worm (Figure 3.9). Specifically, we used the linear regression parameters for each worm regression model (intercept – capturing the initial inoculum burden; slope – capturing the rate of decline in burden). Analyzing these predictors separately, we found that neither predictor was significantly associated with time of death (Figure 3.13).

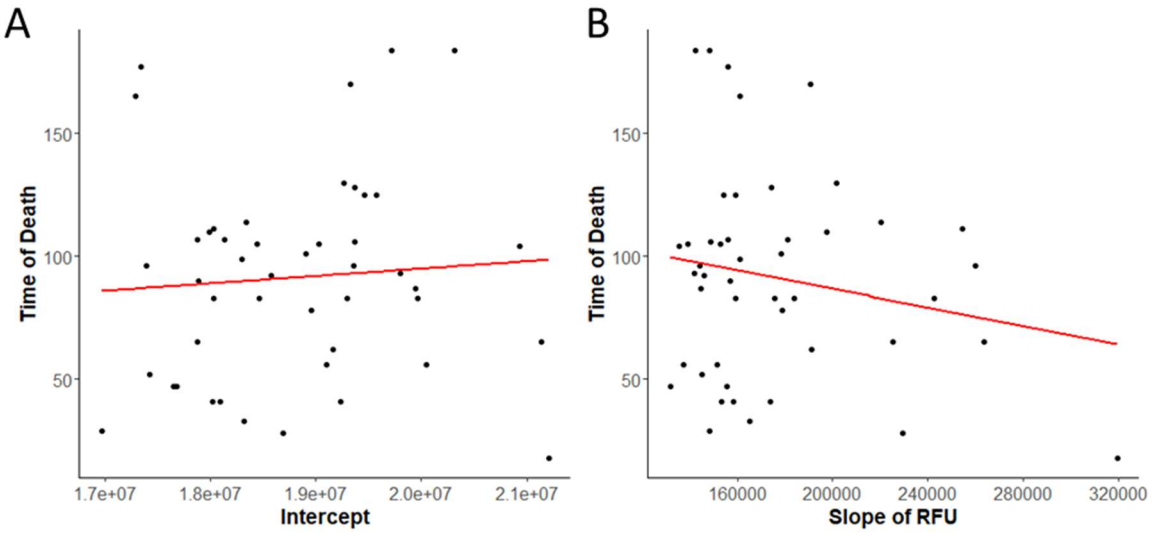

Figure 3.12. Neither intercept nor rate of decline in pathogen burden is predictive of time-of-death. Each dot corresponds to an individual worm, characterized by (A) intercept of per-worm regression model, (B) rate of decline in per-worm regression model, and time-of-death. (A), intercept = 33.32, slope = 3.099×10^{-6}, slope p-value=0.305 (B), intercept= 124.6, slope = -1.889×10^{-4}, slope p-value = 0.221.

Finally, we ran multiple regressions to assess all predictors in Figure 3.12 and 3.13 simultaneously, and again we found no evidence for a significant relationship between metrics of pathogen dynamics, initial inoculum, rate of decline, mean or median fluorescence, and time of death.

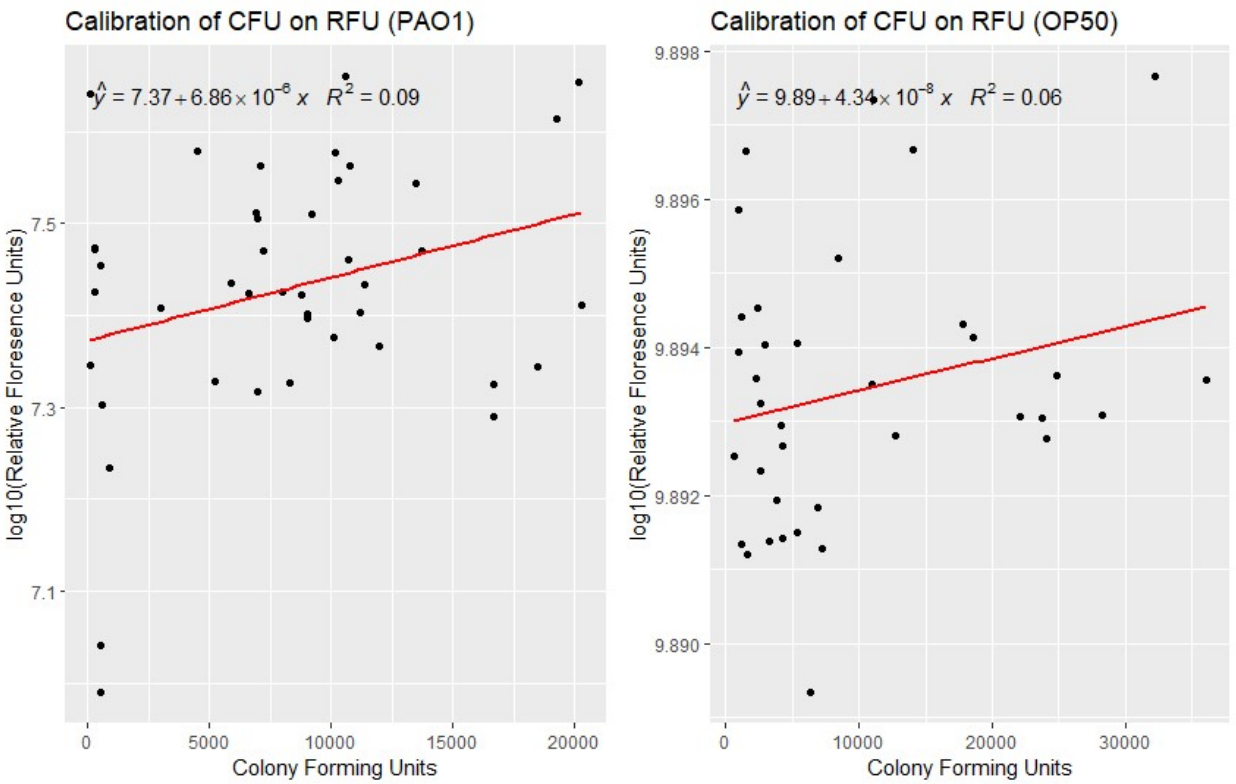

Figure 3.13. No correlation between fluorescence intensity and burden in both OP50-GFP and PAO1-GFP. For both PAO1 and OP50, there was no correlation between the detected burden and the detected RFU. In both cases, there was no discernable correlation (R^2=0.09 PAO1, R^2=0.06 OP50).

Although we could clearly distinguish worms that were exposed to OP50 GFP+ and those that were the control, there was no correlation between CFU and relative fluorescence units. These results draw significant doubt as to the link between burden and fluorescence detected within the worm gut. We posited that using a pathogen might contribute to different dynamics in important ways: most notably, the ability for the pathogen to colonize within the worm and establish an infection, rather than the passive grazing of OP50 that occurs in the typical laboratory context. Using similar experimental parameters described above, we designed an experiment instead using our PAO1 GFP+ strain from before.

Discussion

In this chapter we report on a range of methods to non-invasively estimate pathogen burden in hosts over time using a fluorescent reporter design. A consistent challenge throughout method development was the fragility and irregular shape of heavily infected worms, leading to poor worm identification in ‘open field’ platforms such as the Lifespan Machine (Figure 3.1), handling challenges with the HeALTH microfluidic platform and finally to challenging worm object identification in our final 96-well plate method of choice.

Our final design attempted to balance high-quality brightfield data for survival analysis, with the ability to visualize bacterially-driven fluorescence within the worms. We developed a bioinformatic pipeline that helped distinguish nematodes from difficult brightfield contrasts, as well as a pipeline to track relative fluorescence units in the worm over time. Despite our best efforts, the results were ultimately difficult to interpret. Key challenges include the unrealistically high temporal variability in infection object size likely reflecting changes in worm shape and position within the well, along with interference from overlapping background fluorescence. The ultimate failure of this approach is most clearly captured by our calibration data, which shows that variation in ‘ground truth’ bacterial density (measured by CFU) accounts for less than 10% of the variation in our fluorescence scores of density (Figure 3.13). In light of these challenges, the reported analysis results based on fluorescence score data (Figures 3.8) cannot be trusted as reflecting the underlying biology of pathogen expansion and pathogen impact on host mortality through time. Additionally, work that was previously unknown to us support this conclusion. Hsiao et al. (2013), show that live bacterial cells cannot be easily distinguished from fluorescent bacterial debris within the worm lumen.

With these caveats in mind, in the following chapter we move towards a destructive sampling design, that partially retains aspects developed in this chapter, in particular the censusing of both live and dead worms. We encourage future researchers to learn from the method development in this chapter, as the development of an effective, non-destructive method to track infection dynamics across large populations of nematodes remains – in our view – a reasonable and attainable goal.

Chapter four: *Pseudomonas aeruginosa* grows exponentially within infected nematodes, before and after death

Tim O'Sullivan, James Gurney, Kristofer Wollein Waldetoft, Sam P. Brown.

Abstract

In chapter three we reported an exponential increase in instantaneous mortality in our *C. elegans* – *P. aeruginosa* infection model, but due to a number of technical issues we failed to reliably estimate concurrent pathogen dynamics using non-invasive methods. As a result of these challenges, we move in chapter four to develop and evaluate destructive sampling techniques to assess mortality and pathogen dynamics in separate, parallel cohorts of worms. We find that instantaneous mortality $m(t)$ increases approximately exponentially in time t since infection, with a significant increase in mortality compared to non-infected controls. From destructive sampling data, we estimate that pathogen density $p(t)$ also increases exponentially, when we census pathogen density across both live and dead worms. Our data supports a model where pathogen density is the primary driver of pathogen-induced mortality, but we note that the substantial background mortality under the experimental conditions limits our ability to parse the mapping between pathogen dynamics and risk of host death.

Introduction

In the introduction to chapter three we discussed the merits of non-invasive observations of infection dynamics, yet our methods ultimately failed to deliver reliable data. As a result of this limitation, we move in chapter four to a more conventional destructive technique.

Our specific methodology is detailed below, but in outline it largely follows the example of Biancalani and Gore 2019. This important paper destructively sampled groups of 36 live worms to produce pooled (multi-worm) estimates of pathogen burden at defined time points since infection. Using this data, the authors concluded that the within-host growth of multiple pathogens is approximately logistic, with a clear plateau at a defined density. For *P. aeruginosa*, bacterial density plateaued around 10^5CFU per ml.

The observed plateaus in bacterial density indicate that pathogens reach a stationary state due to limitations of space and/or nutrients within the host. However another interpretation follows from the possibility of a statistical selection bias (McElreath 2018) due to the analysis of pathogen density in surviving worms only. Consider an alternate model where pathogens grow exponentially without limit, and worms die once some threshold pathogen density k is met. Under this model, if we only census live worms, then we will infer that pathogen growth is logistic with a carrying capacity *k* (as we will never observe the higher densities in dead worms). To address this potential statistical bias, we propose here to measure pathogen density through time in both live and dead worms, with worm live/dead status assessed from real-time image analysis of worm activity. Using this modified methodology, we find support for a model of exponential pathogen growth, continuing through death.

Methods

The basic methodology of worm culture and pathogen exposure builds on our previous methods detailed in chapter 3. Briefly, an age-controlled cohort of SS104 worms were reared on live OP50, until adulthood. Afterwards, worms were allowed to feed on heat-killed OP50 over the course of 24 hours in order to clear live bacterial cells from the lumen. From this plate, worms were transferred either to a PAO1 (infection) plate or

OP50 (control) plate for exposure over the next 16 hours. The following day, worms were washed of their respective exposure plates using M9. Worms were then transferred to a bed of ice and washed with an antibiotic-levamisole-M9 solution. Antibiotics (200 µg/ml gentamicin and 200 µg/mL carbenicillin) were used to sterilize the outside of the worm, and 50µM levamisole was used to inhibit pharyngeal pumping. We replaced the media every 20 minutes over the next hour for this sterilization period. We then washed the worms 4 times with sterile M9 to remove any remaining antibiotic in the tube. Throughout the experimental setup, control and infected worms were reared, handled and washed separately from one another, to minimize the risk of pathogen contamination..

After this washing period, worms were transferred to a Petri dish containing 10mL M9 Triton 0.01%. Worms were then individually transferred using a p20 micropipette (volume set to 10 µL) and added to a well containing 90µL M9 across three 96-well plates. To estimate the burden at the start of the experiment ($t(0)$), 20 worms were sampled immediately from the Petri dish. Our experimental design for the worm survival experiment comprised of 264 PAO1-exposed worms (the infection treatment) and 24 OP50-exposed worms (the control treatment). The infection treatment further divided into a destructive sampling arm (180 worms) and a survival assay arm (84 worms). Plates were loaded into a Cytation 5 microplate reader (BioTek ™) and all worms were imaged in the brightfield channel every hour for 5 days, to allow tracking of activity and live/dead assignation (time of death defined as 3 hours without movement, as described in chapter three). Every 24 hours, 36 worms from the infection treatment arm were randomly selected for destructive CFU plating. Worms were chosen from a randomly generated list of all available PAO1 wells. Live/dead status for each of the 36 worms was assigned following manual inspection of the preceding 3 hours of image data for the

corresponding well, and pooled groups of live-only and dead-only worms (maximum 12 worms per group) were then formed using a contingency table for group formation dependent on the number of live and dead worms (appendix table A4.1). We repeated the washing steps with our antibiotic-levamisole-M9 solution as described above.After washing, worm groups were transferred to a microcentrifuge tube containing 1% SDS PAGE and 3-4 sterile 3mm microbeads. Worms were then disrupted using a TissueLyser II ™, run at 30,000 rpm for 30 seconds, repeated twice. After disruption, worms were plated on NGM plates over a series of dilutions in order to estimate CFU.

The control treatment and the survival arm of the infection treatment were not destructively sampled for pathogen burden, and resulted in 23 control animals and 72 infected animals tracked hourly for survival over 5 days. From the destructive sampling arm, 12 worms (a single pooled sample) from day 4 were excluded from analysis due to mishandling during sampling, leading to a total of 188 worms total (20 at $t(0)$, 168 over the course of the 5 days). No data was recorded from 23 wells due to failure to load a worm, or loading of multiple worms, or loading of debris that interfered with image analysis.

Results

Dynamics of infection-induced mortality

Figure 4.1. illustrates the results of the survival analysis arm of our experiment, presenting hourly tracking of the proportion of surviving worms, following exposure to PAO1 (*N* = 72, black data points) or to OP50 (*N* = 23 grey data points).

Consistent with our earlier structured literature review of experimental infection data (chapter 2), we find support for accelerating mortality during the time-course of our

PAO1 infection (Gompertz model AIC = -524.88; exponential model AIC = -140.55). In our control arm, we also witness substantial mortality, likely reflecting the starvation conditions of the survival assay. Mortality in our control arm was also accelerating (see legend for statistical details), consistent with the widespread observation that all-causes morality is accelerating with time (Stroustrup et al. 2016). Comparing experimental versus control survival data, we see evidence that PAO1 caused a significant increase in mortality (log-rank test, X^2=3.95, p=0.047).

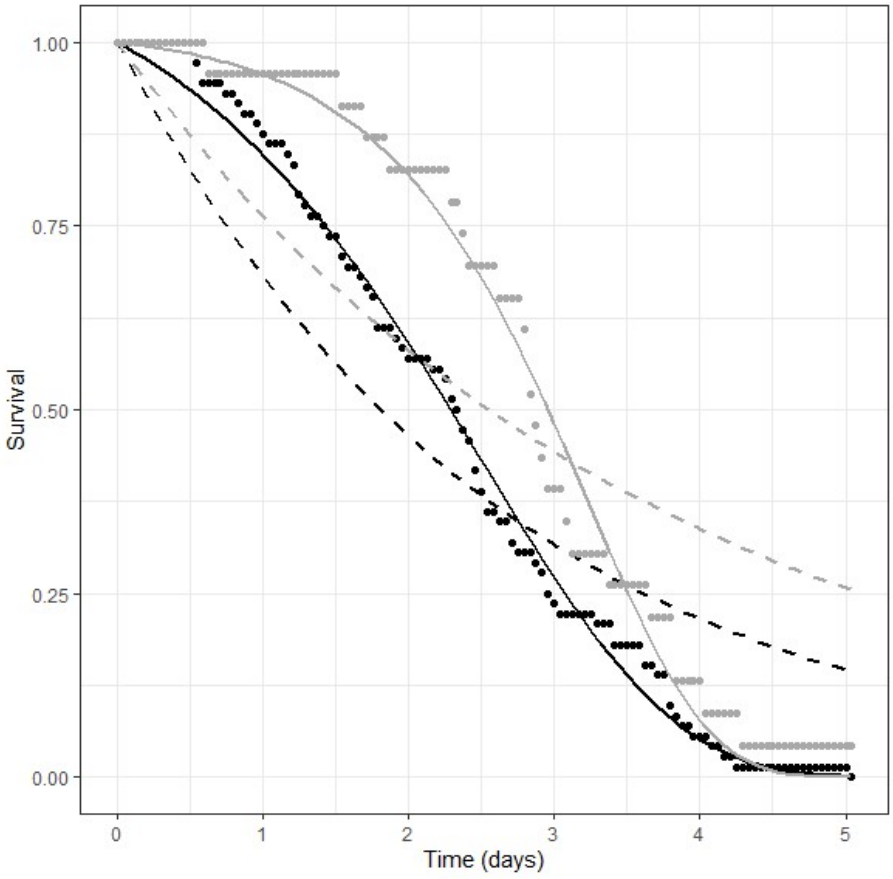

Figure 4.1. PAO1 infection causes increased mortality, compared to non-pathogen (OP50) control exposure. Black circles: proportion surviving among PAO1 exposed worms (*N* = 72). Solid black line: Gompertz model fit to PAO1 exposure data (a=0.11, b = 0.78, AIC = -524.88). dashed black line: Exponential model fit to PAO1 exposure data (λ= 0.38, AIC= -140.55). Grey circles: proportion surviving among OP50-exposed worms (controls, *N* = 23). Solid grey line: Gompertz model fit to control data (a=0.023, b = 1.23, AIC = -432.61). Dashed grey line: Exponential model fit to control data (λ=0.27, AIC = -46.39) The difference between infected and control worms was significant (log-rank test, X^2=3.95, p < 0.05).

Dynamics of pathogen density p(t)

Figure 4.1 establishes that PAO1 infection is a causal driver of death, significantly reducing life expectancy. We now turn to assessing the dynamics of pathogen growth during the course of infection, from the destructive sampling arm of the experiment.

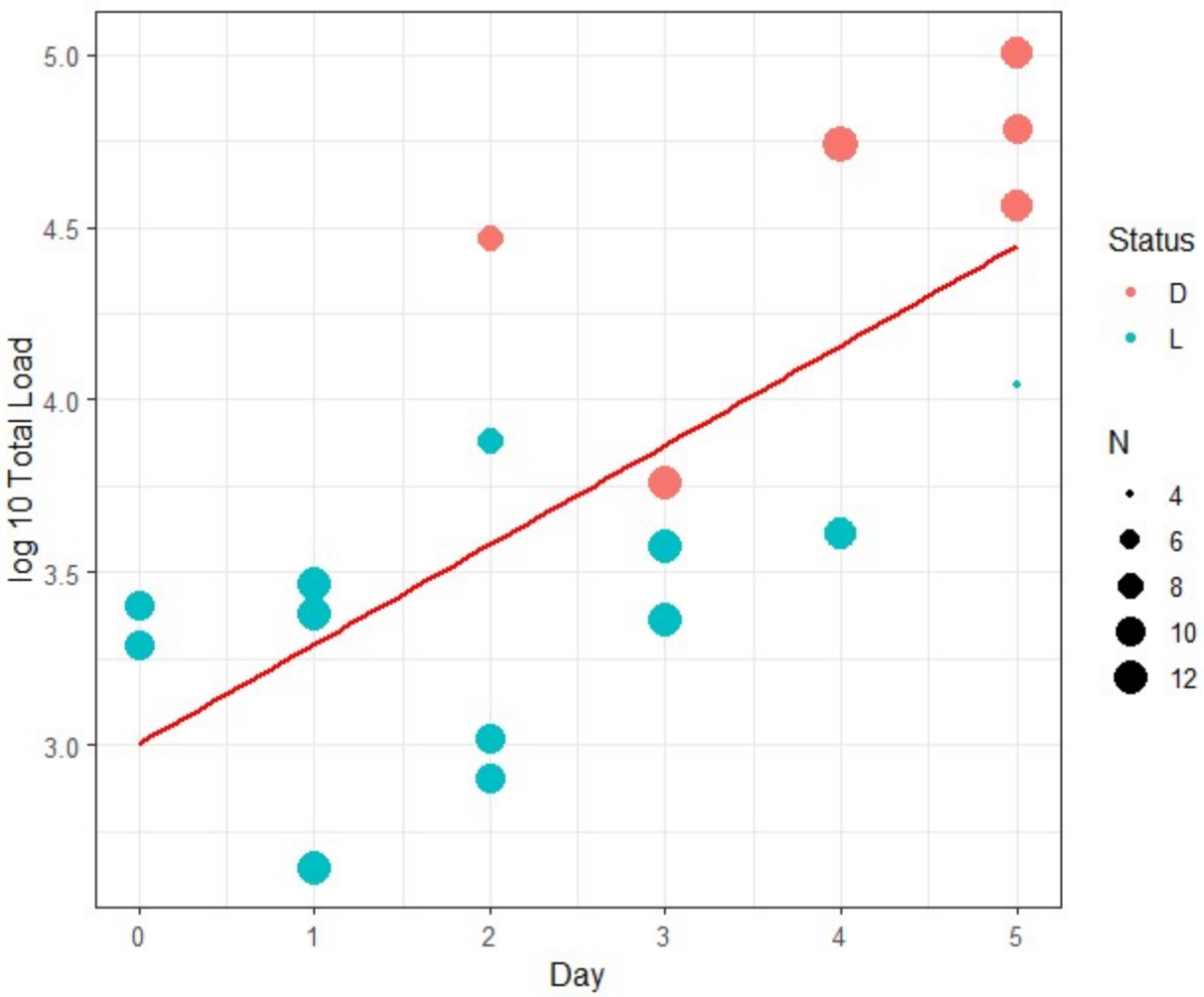

Figure 4.2. Pathogen density increases approximately exponentially in time. Worm live/dead status is indicated by color (red = dead, blue = live). The sample size of each data point (the number of worms per CFU estimation tube) is captured by dot size (scale to right). Regressing log10(pathogen burden) on time (days) demonstrates a significant log-linear relationship between pathogen burden and time, represented by the red line (log($p(t)$ = 3.0 + 2.9 x days) (see appendix A.4.2 model 1 for model details).

Looking across both worms that were identified as live (blue dots) or dead (red dots) at the point of CFU estimation, the data in Figure 4.2 indicates a clear increase in pathogen burden through time. An initial inspection of the data supports our concerns over the impact of censoring by live / dead, as all pathogen counts above 10^4 CFU per worm were in dead worms only. The presence of a plateau in pathogen density among live worms is in qualitative agreement with Biancalani & Gore (2019), although the level of this plateau is approximately 10-fold higher in this earlier study, potentially reflecting differences of pathogen strain and experimental conditions.

Analyzing all worms – live and dead – together (fitting a linear model for $\log_{10}$(pathogen density) ~ time) , we find support for an exponential increase in pathogen density through time, with an initial density of approximately 10^3 CFU per worm, and a significant 10-fold increase approximately every 3 days (time coefficient 2.9/day, p = 0.008; see appendix A4.2 model 1 for statistical tables). In contrast, if we analyze live worm data only, we do not find support for exponential growth (see appendix A4.2 model 2). Together, these analyses indicate that *P. aeruginosa* does not experience a plateau in pathogen growth. By looking beyond the point of death, we see evidence for ongoing pathogen expansion.

Determinants of host death

In our earlier theoretical work (chapter 2), we set out a simple causal cascade where time influences pathogen density (for example, via exponential growth in time), and pathogen density in turn influences host mortality (for example, via a linear mapping function to the instantaneous rate of death). To begin to frame our statistical analysis of

mortality events (Figure 4.2), we formalize this causal framework as a directed acyclic graph (DAG). In light of Figure 4.1 evidence of substantial background mortality, we also include an additional causal path where time directly impacts risk of death due to background mortality. Capturing our model as a DAG allows use of established causal inference logic to guide how to conduct appropriate statistical controls (Pearl 2009; McElreath 2018)

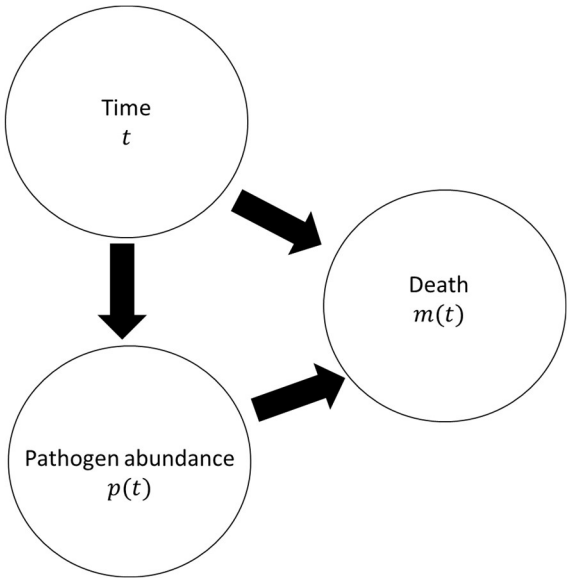

Figure 4.3. Potential causal relationships in our experimental model system. Arrows represent causal influence (positive or negative impacts) in the direction of the arrowhead. Capturing a causal hypothesis as a directed acyclic graph provides guidance on appropriate statistical controls, but does not rule out other potential causal processes not captured by the graph above. In the discussion we address alternate causal pathways, in particular the potential for a causal influence of death on the rate of pathogen growth.

Figure 4.3 illustrates that a univariate regression of live/dead status on pathogen density $p(t)$ will capture the total effect of two causal paths: the direct path ($p(t)$-> death) and an indirect path ($p(t)$<- t -> death). This indirect path is known in the causal analysis field as a fork (McElreath 2018), which can be closed in this context by controlling for time. Similarly, Figure 4.3 also illustrates that a univariate regression of live/dead status on

time will capture the total effect of time via two paths: the direct path (t -> death) and an indirect path (t -> $p(t)$-> death). This indirect path is known in the causal analysis field as a pipe (McElreath 2018), which can be closed in this context by controlling for pathogen density.

Conversely, Figure 4.3 illustrates that regressing pathogen density on time (Figure 4.2) does not require statistical control via live/dead status. The indirect path t -> death < - $p(t)$ is known as a collider (Sauer and VanderWeele 2013), and a collider path is closed unless the collider variable is entered into the statistical model as a predictor (Pearce and Lawlor 2016; Vandenbroucke, Broadbent, and Pearce 2016). This result presents the same message as the earlier discussion of 'selection bias' – to gain a full picture of pathogen dynamics it is critical to analyze the pathogen abundance data independently of the host live/dead status (Figure 4.2). Following this statistical detour, we can begin with the univariate analysis of live/dead status on pathogen load and on time, keeping in mind that these analyses will capture the total effects by both direct and indirect causal pathways in Figure 4.3

In Figure 4.4 we first re-plot the data highlighting live/dead status (y-axis) as a function of bacterial density $p(t)$ (x-axis). This figure illustrates a separation of live/dead status by bacterial density, with a threshold CFU around 10^4. To analyze the dependency of live/dead status on pathogen density, we fit a statistical model for live status ~ log($p(t)$), using a generalized linear model (GLM) with logit link function. The model supports a significant negative impact of (log-transformed) pathogen density on the probability of being alive (pathogen coefficient= -6.03, p=0.049, see appendix A4.2 model 3).

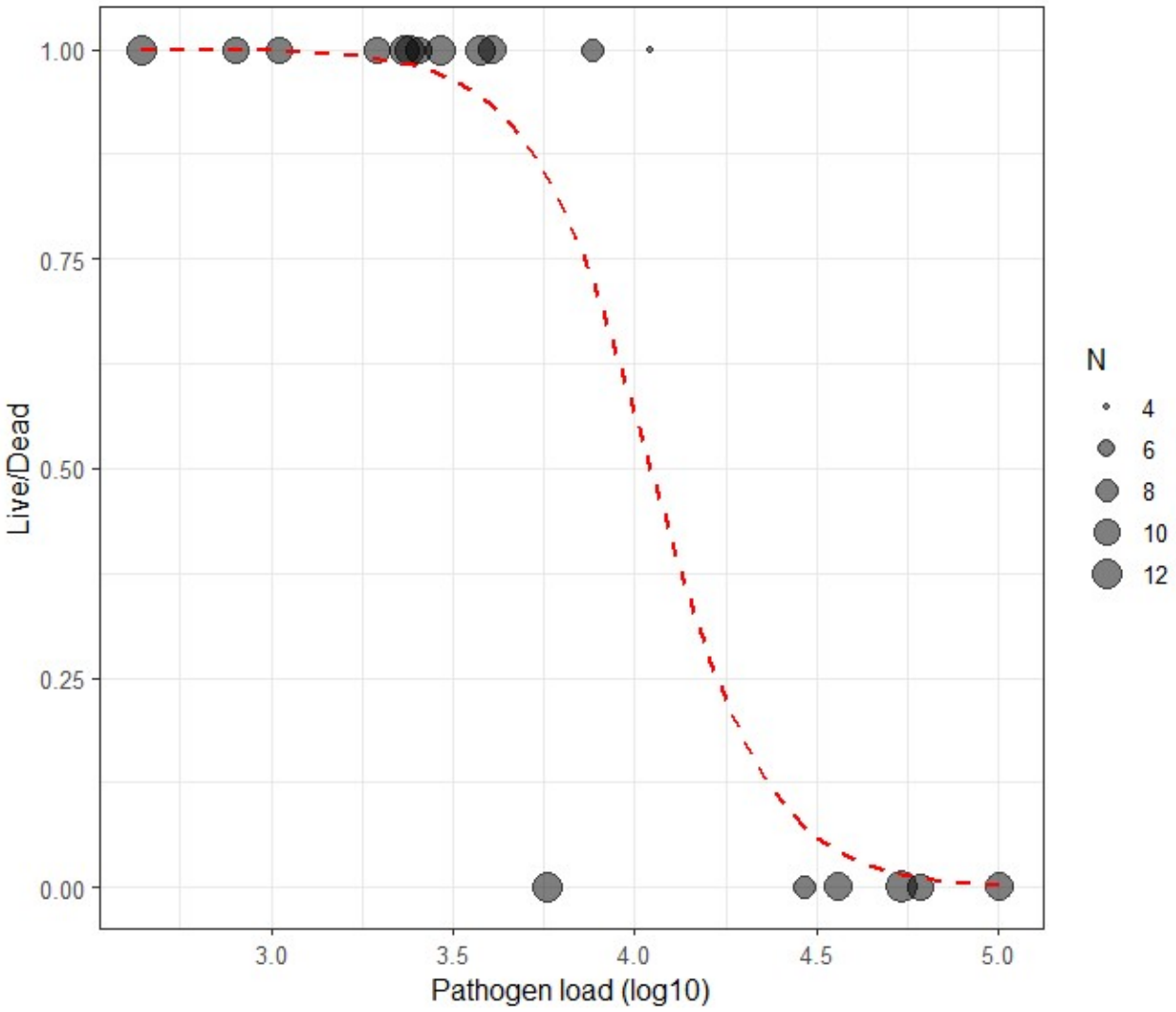

Figure 4.4. Pathogen density is a negative predictor live status. Data redrawn from Figure 4.2., bubble size again reports number of worms per data point (see sidebar). Red line illustrates GLM fit: log odds of survival = 24.4 - 6.03 * pathogen load, (predicted survival probability converted from the log odds of the model). Pathogen load is a significant predictor in this model (p = 0.049). For parameter details, see appendix A4.2, model 4.

Before turning to multivariate models, we next turn to the impact of time on live/dead status, in isolation (Figure 4.5). Figure 4.5 illustrates that later time points are associated with greater prevalence of dead worms. Accordingly, a GLM model for live status ~ time reports a significant negative impact of time (time coefficient = - 0.95 , p=0.04, see

appendix A4.2, model 4), where status denotes the live/dead status of the binned worms, shown in the dots of figure 4.1.

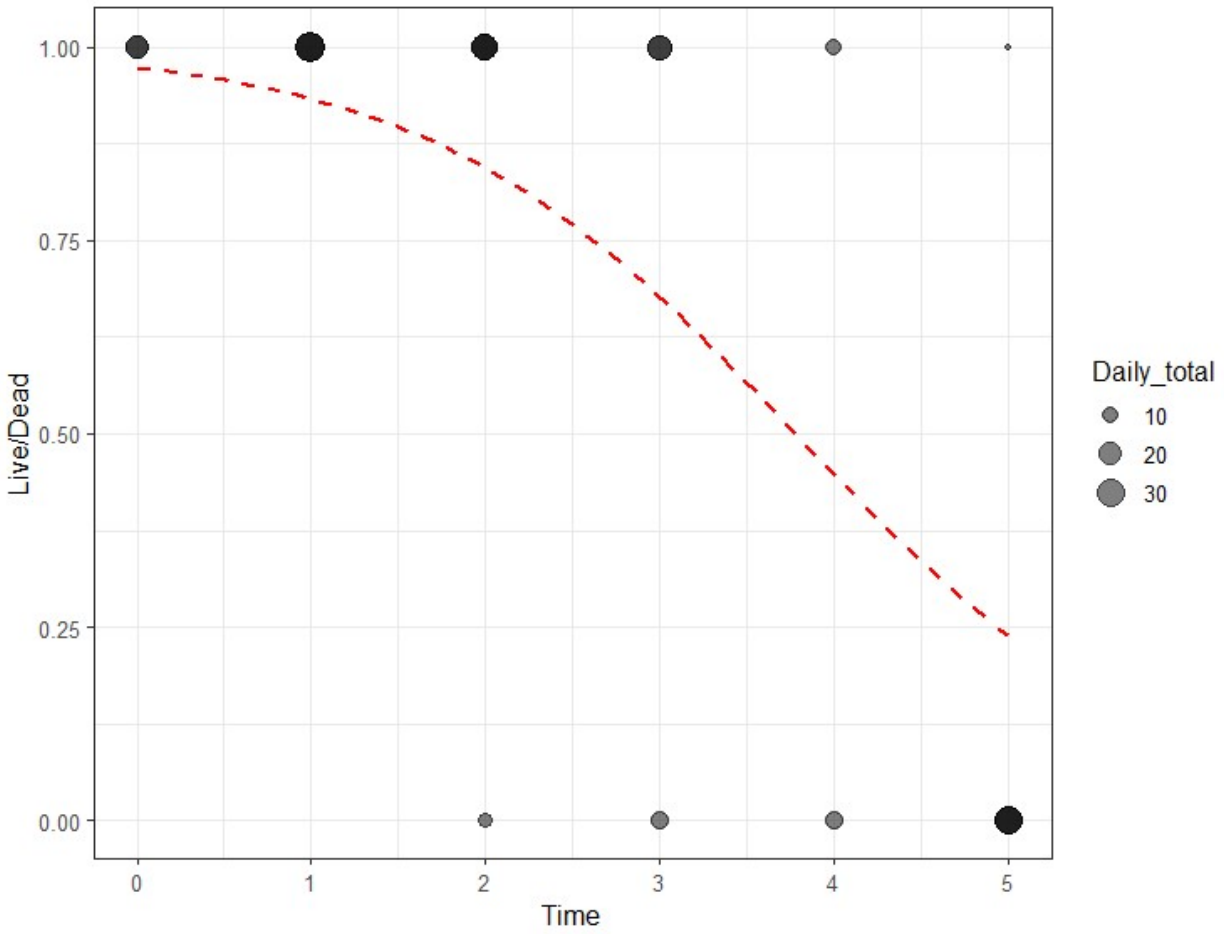

Figure 4.5. Time is a negative predictor live status. Data redrawn from Figure 4.2. Bubble sizes now reflect potentially multiple grouped observations for the same timepoint and live/dead status. Red line illustrates GLM fit: Log odds survival = 3.6 - 0.95 * time. Predicted survival probability converted from the log odds coefficient. Time is a significant predictor in this model, *p*=0.037. For parameter details, see appendix A4.2, model 4.

Figures 4.4 and 4.5 indicate that both time and density are correlated with mortality, yet we know from Figure 4.2 that pathogen density is in turn dependent on time t since infection. Our causal analysis approach (Figure 4.3) indicates that we must add

appropriate statistical controls to close the indirect paths in our univariate analyses. This can be achieved by a single multi-variate model, a GLM of live/dead status ~ time + log($p(t)$). This model (see appendix A4.2, model 5) retains pathogen density as a negative predictor with similar magnitude of effect as in the univariate model, but is no longer significant at the 5% level (p = 0.09). Conversely, the effect of time changes sign and is not close to significance (p = 0.67). Together these results indicate that pathogen density is the primary causal driver of live/dead status in the infection treatment arm of the experiment, although questions remain about the significance of the effect, which we discuss below.

Discussion

In chapter four we provide an analysis of pathogen dynamics and host survival across a population of worms. On the aggregate worm population scale, we recover the same pattern that we observed across the majority of studies in chapter two – early in the course of infection, individuals have a low instantaneous mortality rate, which then grows exponentially (Figure 4.1). In addition, we complement the controlled survival experiments with simultaneous destructive sampling experiments to track the dynamics of the experimentally introduced cause of death – an oral inoculation with a lethal dose of the pathogen *P. aeruginosa.* Looking across live and dead worm individuals, we find evidence that the pathogen population expands exponentially (Figure 4.2), with death associated with increased pathogen density (Figures 4.2, 4.4).

Our experiment was designed in part to assess the alternate mechanistic models presented in chapter 2, measuring pathogen dynamics $p(t)$, instantaneous mortality $m(t)$ and the link between mortality and pathogen dynamics $m(p,t)$. While our data can

give us reasonable confidence in pathogen exponential growth in time (figure 4.2), the extent of death in control worms (grey dots, Figure 4.1) makes the mapping of mortality onto pathogen dynamics $m(p,t)$ harder to parse. In our chapter 2 theory we treated background mortality as negligible, and in our structured literature review we added a requirement for non-pathogen control survival to be at least 80% over the course of experimental observation. We note that our experimental data would clearly fail this inclusion criteria, with near-100% mortality in our control worms over the course of our experiment.

In light of this challenge, we next review why background mortality was so high in our experimental design. Typical *C. elegans* experimental infection experiments (e.g. Ortega-Riveros et al. 2017; de Souza et al. 2019) use continuous exposure of the nematode to a pathogen or control organism, producing a simple experimental design and minimal mortality in the control arm due to the ability to continuously feed. We opted to change this design to an initial exposure followed by a sterile buffer environment, in order to minimize ongoing pathogen colonization dynamics. While excluding continuous colonization, we introduced additional complexities due to the introduction of a starvation phase. *C. elegans* mortality responses to starvation are complex, and dependent on environment and timing of starvation (Kang, You, and Avery 2007; Angelo and Gilst 2009; Baugh and Hu 2020). A common behavioral response to starvation is a sustained reduction in movement (Wu et al. 2018), which when combined with our activity definition of death, could have led to the mis-assignment of starving and lethargic worms as dead. Our experimental design ensured that infected and control worms were handled separately, but we note that we cannot rule out the possibility that mortality was accelerated in the control arm due to pathogen contamination. Finally, we note that additional mortality could also follow due to extensive worm handling throughout our

protocol, as observed with levamisole exposure (Manjarrez and Mailler 2020). We further review and discuss these limitations in chapter five.

Our results indicate that by reducing the complexities of dueling colonization and growth dynamics (discussed in Biancalani and Gore 2019), we introduced new complexities due to substantial background mortality. Moving forward, one option would be to use a continuous exposure experiment as a parallel approach, and leveraging analysis tools developed by Biancalani and Gore 2019 to partition colonization versus growth. An alternate solution would be to augment the sterile buffer solution with heat-killed OP50 to provide ongoing caloric support and therefore maintain live worm activity levels

While our conclusion that pathogens are growing approximately exponentially through the transition from live to dead is supported by our data (Figure 4.2) it also has scope for further refinement. In particular, we note that our statistical approach is premised on a particular causal diagram (Figure 4.3) which is certainly not the last word in the relationship between life, death and pathogen burden. Specifically, our causal network ignores the potential for the event of death to be a positive causal factor promoting pathogen growth, introducing a reciprocal causality between pathogen growth and death. In the particular case of *P. aeruginosa*, this additional causal effect is highly plausible, given *P. aeruginosa's* established functional role as a saprophyte (Moradali, Ghods, and Rehm 2017; Diggle and Whiteley 2020). Our interim conclusion on this point is that once an infection is established, *P. aeruginosa* doesn't 'notice' whether its host is alive or dead – in future work it would be intriguing to dive more deeply into this question to assess pathogen kinetics across this transition with greater resolution.

Our analysis of the determinants of death indicated pathogen density as a positive predictor of death, with similar effect sizes in both the univariate and multivariate regressions. Yet, when controlling for time we found the effect of pathogen was no longer significant at the 5% level ($p = 0.09$). We note that our analysis used pooled worm CFU estimates, which arguably reduces the statistical power of our analyses below the potential of our experimental design. For each of the 188 individual worms in our destructive sampling experiment (20 at time zero plus 168 sampled over 5 days), we have data on their live/dead status at the time of destructive observation, the time of observation, and a pooled estimate of their pathogen density (CFU). Our analyses above were performed on pooled data for groups of worms from the same CFU estimation tubes (the 18 data points in Figures 4.2, 4.4, 4.5), reducing the effective statistical population size down from 188 individual worms to 18 CFU estimations. In this light we view our analyses as conservative, and note that there is a potential avenue to leverage our data through the lens of a 'missing data' problem, leveraging information on the variation in CFUs (Figure 4.2) to interpolate individual CFU values for all 188 individual worms. At this point we opted to not pursue this statistical approach in light of our basic caution in interpreting mortality results from an experiment with substantial background mortality.

To conclude, chapter four provides evidence in favor of exponential pathogen growth during the course of experimental nematode infection, but fails to fully tackle our remaining question of how pathogen dynamics map onto the risk of death. In a final discussion chapter five, we outline potential future research avenues building on the findings of this thesis.

Chapter five: Discussion of future research avenues

Tim O'Sullivan, Kristofer Wollein Waldetoft & Sam P. Brown

Abstract

In this final chapter we offer a brief summary of the principal goals and findings from this PhD; spanning structured literature review, mathematical modeling and experimental infections using a *C. elegans – P. aeruginosa* model system. From the ensemble of these approaches we are able to reach the firm conclusion that the risk of death during acute, lethal infections is increasing exponentially in time since infection, and we also find support in our model system that concurrent pathogen density is also increasing exponentially, through the transition from live to dead host. We outline potential mapping functions to link pathogen dynamics with instantaneous mortality, and note that these functions remain under-determined, with multiple alternate mapping functions consistent with the data assembled to date. We end with an outline road-map of potential future research avenues that are opened by this work, spanning behavioral, ecological/demographic, genetic and intervention avenues of research.

Summary of results

The core conceptual challenge of this thesis is to connect the epidemiological dynamics of infection-induced death onto the within-host dynamics of the causal factor – the pathogen. To do this requires assessment of three key components: (1) the dynamics of host death, captured by instantaneous mortality $m(t)$ in time since infection t; (2) the

dynamics of pathogen density, $p(t)$; and (3) the mapping function linking mortality to pathogen density $m(t) = f(p(t))$.

Following an introductory chapter one, we turn in chapter two to the published biomedical data on survival curves during acute, lethal infections. Using a structured literature review, we find evidence for an accelerating risk of death $m(t)$ during the course of infection across 28 diverse animal and pathogen study systems, including in our focal host, *C. elegans*. We then ask what functions of $p(t)$ and $m(p,t)$ are consistent with this data, and show that this pattern of accelerating risk is consistent with multiple alternate mechanisms of pathogen growth (static, linear or exponential) and host interaction, underlining the limitations of current experimental approaches to connect within-host processes to epidemiological patterns.

In chapters three and four we develop experimental methodologies to directly assess pathogen dynamics and mapping of pathogen expansion to host risk of death. Chapter three focuses on non-invasive tracking methods, following worm death via worm motion time-series, and pathogen density via fluorescence imaging of GFP-tagged *P. aeruginosa* within each worm. Ultimately this approach did not produce sufficiently robust results, exemplified by poor calibration between fluorescence measures (after various bio-informatic image processing steps) and the basic gold-standard of pathogen density estimation via destructive sampling and colony forming unit (CFU) counting. Unknown to us at the time, other groups have also encountered problems when estimating live pathogen burden in nematode-bacterial systems (Hsiao et al. 2013).

In chapter four, we combine well-established destructive sampling methods for pathogen burden, with non-invasive live/dead activity tracking. Our analysis illustrates the problem of survival bias in estimating within-host pathogen growth from destructive sampling data, which we overcome by sampling both live and dead worms. The results support a model of exponential pathogen growth across the transition from live to dead host, and also indicate a positive relationship between pathogen burden and worm death. A limitation of this final experiment was the substantial degree of mortality in our control worms, discussed below.

Lessons from our microtiter plate survival model

The final experiments in chapters three and four both shared a common design element of maintaining post-exposure worms in individual wells of a microtiter plate, housed in initially sterile medium. The rationale for this design was to facilitate individual worm tracking via physical separation, and also to limit ongoing bacterial colonization. Our control experiment results in chapter four indicate that this design created new issues, due to a high level of mortality in control worms.

One potential mechanism behind this result is a behavioral response in starved worms to downregulate activity, and appear straighter than well-fed worms (Wu et al. 2018). Given our activity-based assignment of live/dead status, this behavioral response may have led to an erroneous inflation of mortality in our control experiment. In light of this potential issue, we recommend considering a worm-agitation step to confirm death, and/or using a DAPI filter to detect “blue-death” in worms (Coburn et al. 2013).

Although we worked hard to guard against potential contamination between wells, (rearing worms separately, use of antibiotic wash), we cannot discount the possibility

that there may have been *Pseudomonas aeruginosa* contamination between our microtiter wells. Spillover could have happened during robotic plate loading and image capture, though our tools (BioTek Biospa + Cytation) are designed to abate this. One way to assess contamination in future experiments would be to conduct *P. aeruginosa* CFU estimation from dead control worms.

It is also possible that other aspects of our experimental design led to excess mortality. The evidence for this is not strong however, as our plate-reader controlled for temperature, oxygen, and limited exposure of light (when housed in our adjoining BioSpa unit, worms are protected from ambient light). Similar microtiter methods report survival curves that are similar to worm rearing on live OP50 NGM plates, though with the required supplement of regular live OP50 (of a concentration of 100mg/mL) at least every 5 days (Solis and Petrascheck 2011).

It should be noted, that even relatively small environmental shifts can alter observed survival dynamics. Stroustrup et al (2016) show that even small changes in temperature early in adulthood can demonstrably shift the observed survival distribution. Standard methods to arrest worm movement for handling also seem to induce detectable (if weak) sources of additional mortality (Manjarrez and Mailler 2020). Measuring mortality is ultimately a balancing act between maximizing observations and reducing additional background mortality.

For future work, we propose the periodic supplement of additional sources of nutrition to the buffer medium, for example heat-killed OP50. Though this could have the additional

effect of displacing live pathogen inside the host's gut, the payoff in buffering against starvation-induced changes in behavior would potentially be worthwhile.

Roadmap for future research

The research outlined in this thesis opens up several directions for future research. A first methodological step is to further tune the protocols laid out in chapter four to more effectively mortality in our controls. At present, we have a significant signature of infection, with the survival curve left-shifted following pathogen exposure (Figure 4.1). Yet we also have substantial estimated mortality, which limits our ability to parse the mapping of infection-induced mortality onto pathogen dynamics. To improve our interpretation of such mortality dynamics, we propose monitoring mortality using validated tools to measure mortality, such as using blue fluorescence as a proxy for death (Coburn et al. 2013). In principle, the observed signal is so strong that it makes distinguishing the time of death easy to ascertain, although images must be taken with sufficient frequency.

A second methodological avenue would be to explore alternate models of non-constant mortality, beyond the Gompertz model. Other studies have reported more complex, multi-modal distributions of time to death (Zhao et al. 2017), which is also hinted in our chapter three analysis of time to death (Figure 3.9B). These more complex patterns motivate the pursuit of alternate phenomenological and mechanistic models. From a mechanistic perspective, the incorporation of heterogeneity in host states is one potential avenue to address multi-modal death kinetics.

Third, the experimental approach presented in chapter four opens up a platform to assess the impact of ecological parameters governing pathogen exposure, such as the period of exposure, and/or the density of pathogen on the exposure plate. Manipulating these parameters will allow for examination of important ecological aspects of pathogen transmission, for example identifying and characterizing the role of threshold inoculum densities / exposure times in governing the fate and dynamics of infection.

Fourth, our imaging platform (chapter three) offers the potential to leverage pathogen virulence factor reporter constructs in tandem with our destructive sampling of pathogen burden (chapter four). While chapter three highlighted the technical limitations in my hands of using fluorescence data as a quantitative tool, fluorescence reporters can still provide valuable information on the timing of gene expression change. Of particular interest is the quorum-sensing (QS) control of virulence factors in *P. aeruginosa*. QS has been described as a 'stealth mode' of pathogen attack, where pathogens hold back their weaponry until a specific pathogen density as achieved (Williams et al. 2000). By using QS reporter strains in our experimental platform we will be able to directly test and quantify these ideas.

Fifth, our work opens the potential to study coupled infection and mortality dynamics beyond lab reference strains of pathogen and host. Both *C. elegans* and *P. aeruginosa* are model organisms, opening a tremendous body of genetic tools and mutants to the study of the 'dynamics of death' by infection. From the host perspective, profiling infections in immune mutants is of particular interest, for example the classical long-lived *daf-2*

mutants that exhibit enhanced anti-bacterial defenses when compared to wild-type worms (Garsin et al. 2001; Millet and Ewbank 2004; Foster, McEwan, and Pukkila-Worley 2020)

Appendices

Appendix 2, supplemental figures and tables for chapter two

Table A2.1. Summary of papers used for structured literature review and analysis.

Experiment	Pathogen	Strain	Host	Host strain	N	Time points	Duration (days)	notes
Chamillos2008_a	R. oryzae		Fruit fly		25	12	4	
Chamillos2008_b	C. bertholletiae		Fruit fly		25	12	2	
Chao2010	C. albicans		Zebrafish		20	4	2.08	
Day2012_a	S. aureus	LAC	C. elegans		30	7	1.91	
Day2012_b	S. aureus	RN6390	C. elegans		30	7	5.79	
deSouza2019_a	C. striatum	MDR1987	C. elegans		60	4	4	
deSouza2019_b	C. striatum	MDS1961	C. elegans		60	4	4	
deSouza2019_c	C. striatum	MDR2369	C. elegans		60	4	3	
deSouza2019_d	C. striatum	MDS1954	C. elegans		60	4	4	
Kim2015	S. agalactiae	COH1	Zebrafish		24	4	3	
Kong2014_a	S. aureus		C. elegans		60	6	4.03	liquid media
Kong2014_b	S. aureus		C. elegans		120	7	5	solid media
Lutter2008_a	P. aeruginosa	PAO1	Fruit fly		30	14	14	fed
Lutter2008_b	P. aeruginosa	PA14	Fruit fly		30	14	14	fed
Lutter2008_c	P. aeruginosa	PAK	Fruit fly		30	14	14	fed
Lutter2008_d	P. aeruginosa	PAO1	Fruit fly		30	24	1.5	nick
Lutter2008_e	P. aeruginosa	PA14	Fruit fly		30	24	1.5	nick
Lutter2008_f	P. aeruginosa	PAK	Fruit fly		30	24	1.5	nick
Lutter2008_g	P. aeruginosa	PA103	Fruit fly		30	24	1.5	nick
Ortega2017_a	C. albicans		C. elegans		20	5	5.04	
Ortega2017_b	C. krusei		C. elegans		20	5	5.04	
Ortega2017_c	C. orthopsliosis		C. elegans		20	5	5	
Ortega2017_d	C. parasliosis		C. elegans		20	5	5	
Ortega2017_e	C. metasliosis		C. elegans		20	5	5	
Ortega2017_f	C. dubliniensis		C. elegans		20	5	5	
Ortega2017_g	C. glabrata		C. elegans		20	5	5	
Vergunst2010_a	B.cenocepacia	K56-2	Zebrafish		20	6	2	
Vergunst2010_b	B. cepacia	CEP509	Zebrafish		20	6	5	

Table A2.2. Summary of exponential and Gompertz parameter fits.

	Gompertz					Exponential			
Extract_title	Term	Estimate	Term	Estimate	AICc	Term	Estimate	AICc	ΔAICc
Chamillos2008_a	a	0.07567	b	4.319497	-12.6469	λ	1.059159	-4.22649	8.420437
Chamillos2008_b	a	0.637393	b	1.672739	-9.66472	λ	1.426892	-6.50912	3.155595
Chao2010	a	0.273186	b	1.94841	-26.8097	λ	0.877433	-10.9358	15.87388
Day2012_a	a	0.005397	b	4.594713	-38.9331	λ	0.774906	4.526736	43.45985
Day2012_b	a	0.003484	b	4.055516	-13.7278	λ	0.491201	1.001166	14.729
deSouza2019_a	a	0.190243	b	0.574542	-7.21861	λ	0.436991	-3.54897	3.669641
deSouza2019_b	a	0.064217	b	2.040782	-20.9783	λ	0.636606	0.698175	21.67651
deSouza2019_c	a	0.163219	b	1.388197	-35.7911	λ	0.675208	0.721485	36.51263
deSouza2019_d	a	0.218963	b	0.939815	-14.0108	λ	0.620741	-3.81086	10.19993
Kim2015	a	0.022638	b	2.974698	-15.172	λ	0.609383	1.349629	16.52164
Kong2014_a	a	0.097353	b	0.806437	-8.58298	λ	0.365495	-0.60215	7.980832
Kong2014_b	a	0.0015	b	2.507278	-83.3951	λ	0.327189	4.290506	87.68557
Lutter2008_a	a	0.04466	b	0.258455	-61.6558	λ	0.141665	-16.3091	45.34668
Lutter2008_b	a	0.022626	b	0.405293	-41.0949	λ	0.142632	-7.78446	33.31039
Lutter2008_c	a	0.052066	b	0.173856	-30.5024	λ	0.117979	-16.7816	13.72079
Lutter2008_d	a	0.212839	b	4.543712	-141.87	λ	1.902075	-31.0324	110.8379
Lutter2008_e	a	0.134124	b	3.687845	-119.611	λ	1.181457	-12.6285	106.9829
Lutter2008_f	a	0.037365	b	6.325464	-107.549	λ	1.394889	-2.9441	104.6047
Lutter2008_g	a	0.060009	b	6.717605	-131.178	λ	1.768533	-16.0286	115.1494
Ortega2017_a	a	0.330169	b	0.463964	-27.4414	λ	0.586615	-11.1415	16.29983
Ortega2017_b	a	0.078691	b	0.746011	-11.1062	λ	0.3176	-0.99261	10.11363
Ortega2017_c	a	0.035687	b	0.967162	-9.80339	λ	0.269682	1.787793	11.59118
Ortega2017_d	a	0.033217	b	0.858857	-10.5259	λ	0.232608	0.990612	11.51654
Ortega2017_e	a	0.030915	b	0.942642	-11.7087	λ	0.246372	1.770934	13.47961
Ortega2017_f	a	0.015209	b	1.15861	-61.6502	λ	0.229815	0.073655	61.72386
Ortega2017_g	a	0.007788	b	1.235038	-32.6919	λ	0.187332	2.046451	34.73831
Vergunst2010_a	a	2.19E-05	b	7.216787	-78.7306	λ	0.752198	7.2233	85.95389
Vergunst2010_b	a	5.11E-07	b	8.257474	-51.2656	λ	0.402421	3.252331	54.51792

Figure A2.1 QQ-plots for exponential model fits.

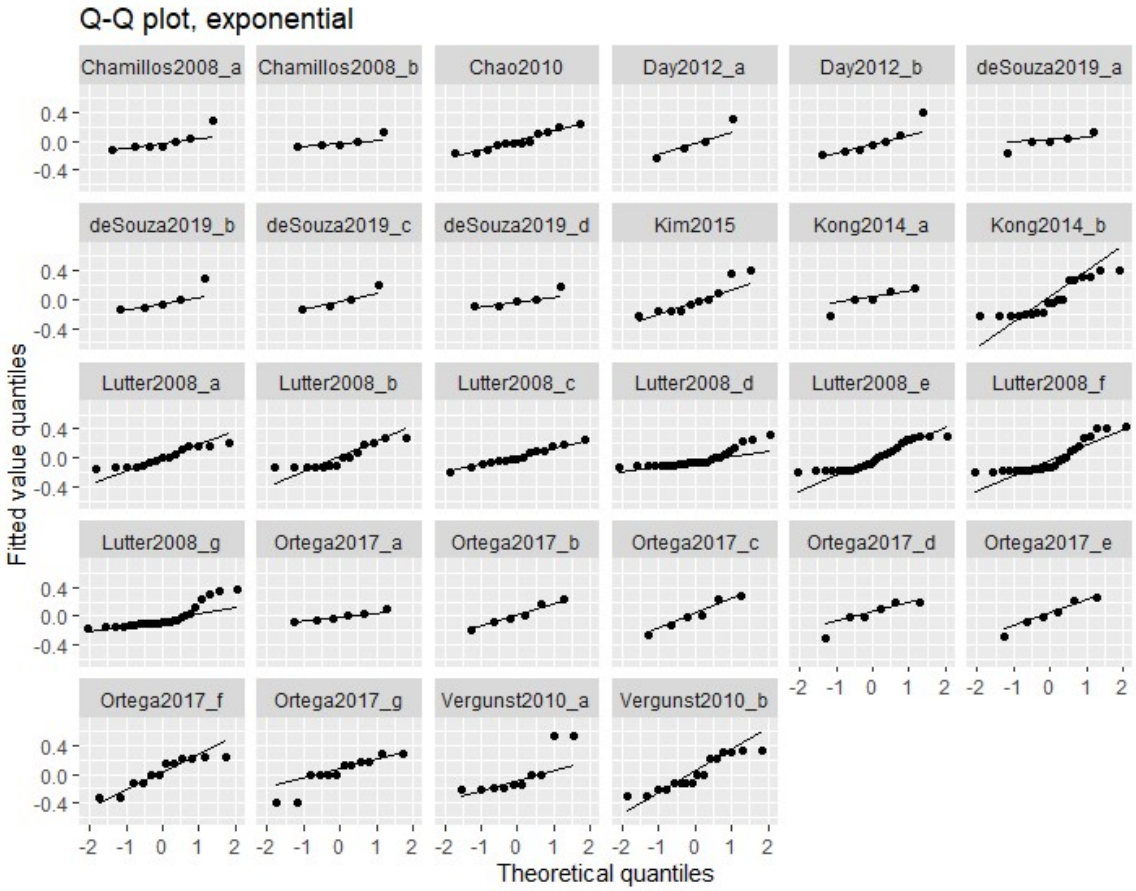

Figure A2.2 Plot of residuals for exponential model fits.

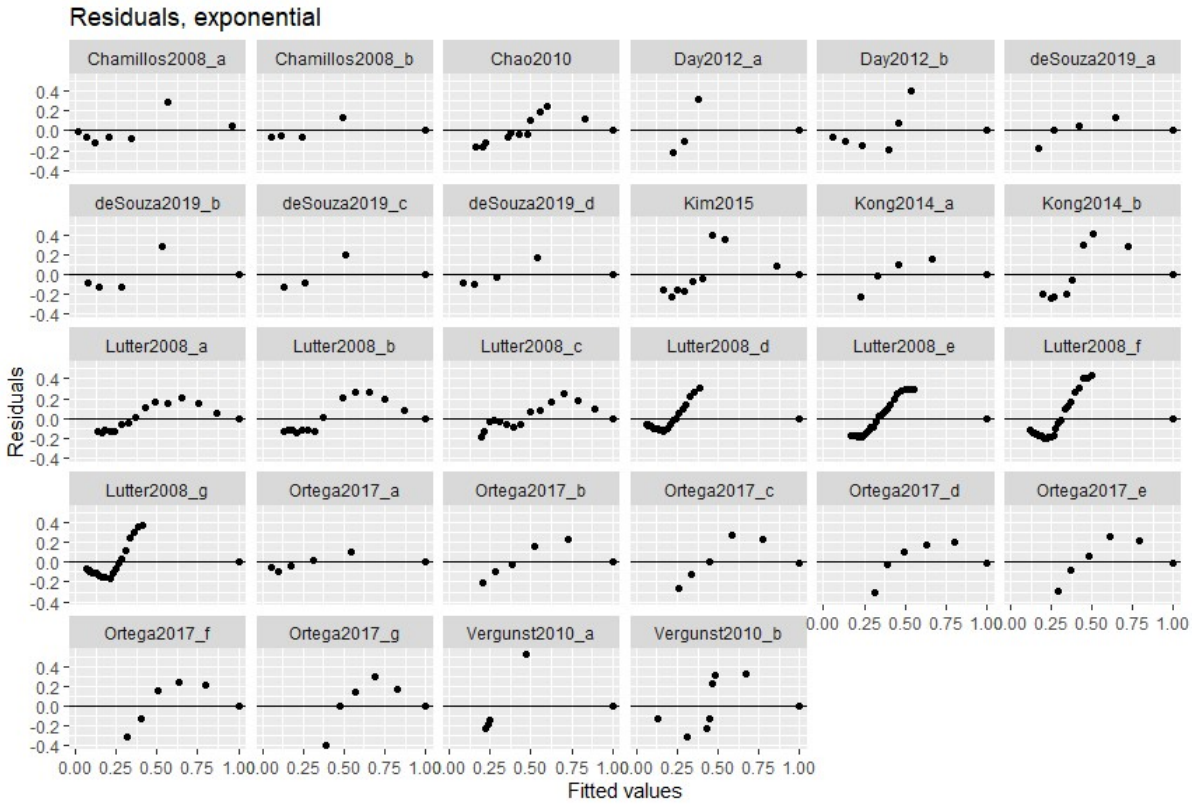

Figure A2.3 QQ-plot for Gompertz model fits.

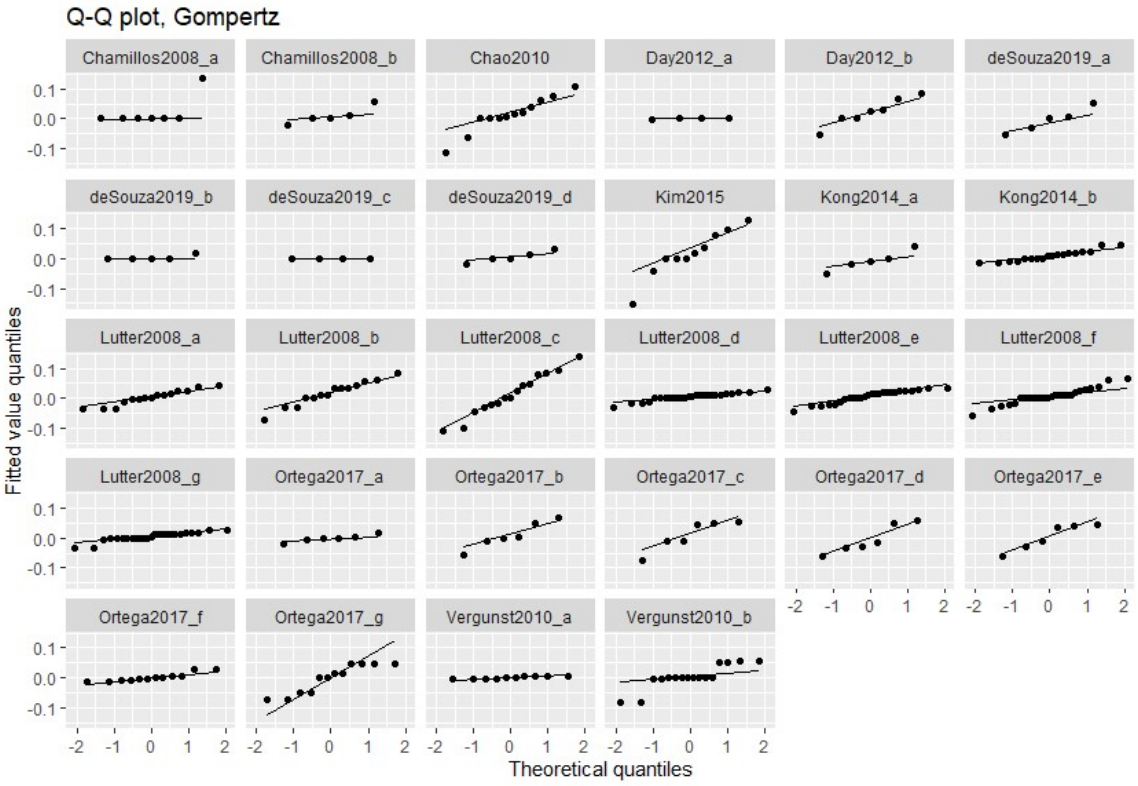

Figure A2.4 Plot of residuals for Gompertz model fits.

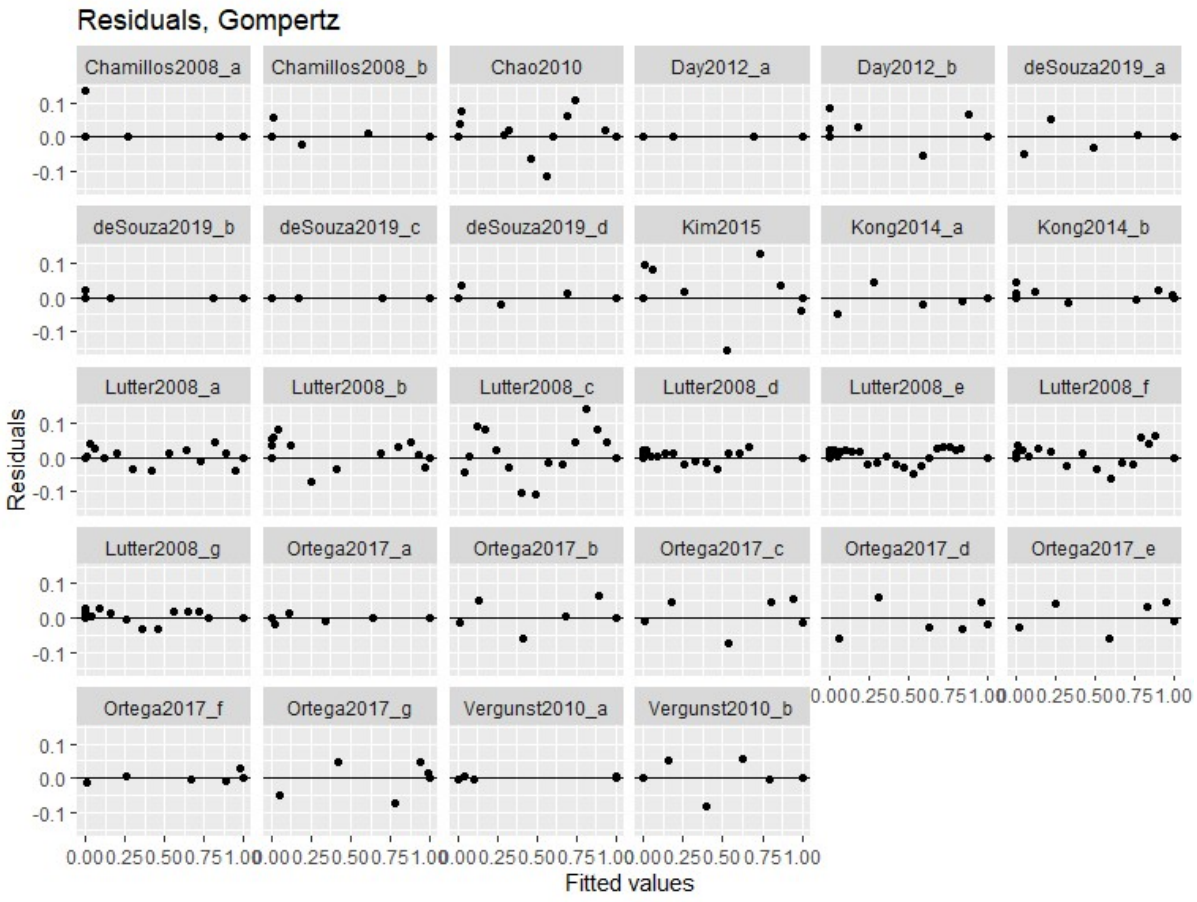

Appendix 4, supplemental tables for chapter four

Table A 4.1. Destructive sampling look-up table. At days 1 to 5 of the destructive sampling experiment, 36 worms were selected for CFU profiling, divided into multiple pools of live-only and dead-only worms. The following look up table was generated to produce a clear decision on how to partition the sample groups (last 6 columns), conditioned on the number of live and dead worms (first two columns).

Live	Dead		Live sample 1	Live sample 2	Live sample 3		Dead sample 1	Dead sample 2	Dead sample 3
36	0		12	12	12		0	0	0
35	1		12	12	11		1	0	0
34	2		12	11	11		2	0	0
33	3		11	11	11		3	0	0
32	4		11	11	10		4	0	0
31	5		11	10	10		5	0	0
30	6		10	10	10		6	0	0
29	7		10	10	9		7	0	0
28	8		10	10	8		8	0	0
27	9		10	10	7		9	0	0
26	10		13	13	0		10	0	0
25	11		13	12	0		11	0	0
24	12		12	12	0		12	0	0
23	13		12	11	0		13	0	0
22	14		11	11	0		7	7	0

21	15		11	10	0		8	7	0
20	16		10	10	0		8	8	0
19	17		10	9	0		9	8	0
18	18		9	9	0		9	9	0
17	19		9	8	0		10	9	0
16	20		8	8	0		10	10	0
15	21		8	7	0		11	10	0
14	22		7	7	0		11	11	0
13	23		13	0	0		12	11	0
12	24		12	0	0		12	12	0
11	25		11	0	0		13	12	0
10	26		10	0	0		13	13	0
9	27		9	0	0		10	10	7
8	28		8	0	0		10	10	8
7	29		7	0	0		10	10	9
6	30		6	0	0		10	10	10
5	31		5	0	0		11	10	10
4	32		4	0	0		11	11	10
3	33		3	0	0		11	11	11
2	34		2	0	0		12	11	11

1	35	1	0	0	12	12	11
0	36	0	0	0	12	12	12

A4.2 Statistical model fits used in text

Model 1: Linear model, pathogen growth ~ time

model_1<- lm(log_CFU ~ Time, data=df)

Coefficients:

	Estimate	SE	t value	p
(Intercept)	**3.00326**	**0.22066**	**13.61**	**3.25e-10**
Time	**0.28842**	**0.07017**	**4.11**	**0.000819**

Model 2: Linear model, pathogen growth ~ time, live worms only

library("dplyr")

df_2<- df %>% filter (status == 1)

model_2<- lm(logCFU ~ Time, data=df_2)

Coefficients:

	Estimate	SE	t value	p
(Intercept)	**3.12036**	**0.17201**	**18.140**	**5.56e-09**
Time	**0.13098**	**0.06927**	**1.891**	**0.0879**

Model 3: Generalized linear model, logit, Live/dead status ~ pathogen density

model_3<- glm(formula = status ~ log_CFU , family = "binomial", data = df)

Coefficients:

	Estimate	SE	z value	p
(Intercept)	**24.373**	**12.020**	**2.028**	**0.0426**
translog	**-6.026**	**3.054**	**-1.973**	**0.0485**

Model 4: Generalized linear mode, logit, Live/dead status ~ time

model_4<- glm(formula = status ~ Time , family = "binomial", data = df)

Coefficients:

	Estimate	SE	z value	p
(Intercept)	**3.5795**	**1.6328**	**2.192**	**0.0284**
Time	**-0.9473**	**0.4535**	**-2.089**	**0.0367**

Model 5: Generalized linear model, logit, live/dead status ~ time + log_CFU

model_5<- glm(formula = status ~ Time + log CFU , family = "binomial", data = df)

Coefficients:

	Estimate	SE	z value	p
(Intercept)	**26.6265**	**14.4258**	**1.846**	**0.0649 .**
Time	**0.3556**	**0.8480**	**0.419**	**0.6749**
translog	**-6.8933**	**4.0836**	**-1.688**	**0.0914 .**

Bibliography

Aaberge, Ingeborg S., Jan Eng, Gro Lermark, and Martinus Løvik. 1995. “Virulence of Streptococcus Pneumoniae in Mice: A Standardized Method for Preparation and Frozen Storage of the Experimental Bacterial Inoculum.” *Microbial Pathogenesis* 18 (2): 141–52. https://doi.org/10.1016/S0882-4010(95)90125-6.

Ahmed, Norus, Emanuel Heitlinger, Nicole Affinass, Anja A. Kühl, Natasa Xenophontos, Victor Hugo Jarquin, Jenny Jost, Svenja Steinfelder, and Susanne Hartmann. 2019. “A Novel Non-Invasive Method to Detect RELM Beta Transcript in Gut Barrier Related Changes During a Gastrointestinal Nematode Infection.” *Frontiers in Immunology* 10 (MAR): 445. https://doi.org/10.3389/fimmu.2019.00445.

Alizon, Samuel, and Minus van Baalen. 2005. “Emergence of a Convex Trade-off between Transmission and Virulence.” *The American Naturalist* 165 (6). https://doi.org/10.1086/430053.

Allen, Richard C., Luke McNally, Roman Popat, and Sam P. Brown. 2016. “Quorum Sensing Protects Bacterial Co-Operation from Exploitation by Cheats.” *ISME Journal* 10 (7): 1706–16. https://doi.org/10.1038/ismej.2015.232.

Allen, Richard C., Roman Popat, Stephen P. Diggle, and Sam P. Brown. 2014. “Targeting Virulence: Can We Make Evolution-Proof Drugs?” *Nature Reviews Microbiology*. Nature Publishing Group. https://doi.org/10.1038/nrmicro3232.

Anderson, Alexandra, and Rachel McMullan. 2018. “Neuronal and Non-Neuronal Signals Regulate Caernorhabditis Elegans Avoidance of Contaminated Food.” *Philosophical Transactions of the Royal Society B: Biological Sciences* 373 (1751). https://doi.org/10.1098/rstb.2017.0255.

Anderson, Roy M., and Robert M. May. 1979. “Population Biology of Infectious Diseases: Part I.” *Nature* 280 (5721): 361–67. https://doi.org/10.1038/280361a0.

Anderson, Roy M, and Robert M May. 1992. *Infectious Diseases of Humans: Dynamics and Control*. Oxford university press.

Angelo, Giana, and Marc R. Van Gilst. 2009. “Starvation Protects Germline Stem Cells and Extends Reproductive Longevity in C. Elegans.” *Science* 326 (5955): 954–58. https://doi.org/10.1126/SCIENCE.1178343.

Antia, R., B. R. Levin, and R. M. May. 1994. “Within-Host Population Dynamics and the Evolution and Maintenance of Microparasite Virulence.” *American Naturalist* 144 (3): 457–72. https://doi.org/10.1086/285686.

Armah, Henry B., Nana O. Wilson, Bismark Y. Sarfo, Michael D. Powell, Vincent C. Bond, Winston Anderson, Andrew A. Adjei, et al. 2007. “Cerebrospinal Fluid and Serum Biomarkers of Cerebral Malaria Mortality in Ghanaian Children.” *Malaria Journal* 6 (1): 147. https://doi.org/10.1186/1475-2875-6-147.

Austad, Steven N. 2005. “Diverse Aging Rates in Metazoans: Targets for Functional Genomics.” In *Mechanisms of Ageing and Development*, 126:43–49. Elsevier. https://doi.org/10.1016/j.mad.2004.09.022.

Bae, Taeok, Alison K. Banger, Adam Wallace, Elizabeth M. Glass, Fredrik Åslund, Olaf Schneewind, and Dominique M. Missiakas. 2004. “Staphylococcus Aureus Virulence Genes Identified by Bursa Aurealis Mutagenesis and Nematode Killing.” *Proceedings of the National Academy of Sciences of the United States of America* 101 (33): 12312–17. https://doi.org/10.1073/pnas.0404728101.

Barnes, Penelope D., Molly A. Bergman, Joan Mecsas, and Ralph R. Isberg. 2006.

"Yersinia Pseudotuberculosis Disseminates Directly from a Replicating Bacterial Pool in the Intestine." *Journal of Experimental Medicine* 203 (6): 1591–1601. https://doi.org/10.1084/jem.20060905.

Baugh, L Ryan, and Patrick J Hu. 2020. "Starvation Responses Throughout the Caenorhabditiselegans Life Cycle." *Genetics* 216 (4): 837–78. https://doi.org/10.1534/GENETICS.120.303565.

Beale, Elmus, Guigen Li, Man Wah Tan, and Kendra P. Rumbaugh. 2006. "Caenorhabditis Elegans Senses Bacterial Autoinducers." *Applied and Environmental Microbiology* 72 (7): 5135–37. https://doi.org/10.1128/AEM.00611-06.

Beanan, M.J., and S. Strome. 1992. "Characterization of a Germ-Line Proliferation Mutation in C. Elegans." *Development* 116 (3): 755–66. https://doi.org/10.1242/DEV.116.3.755.

Berg, Maureen, Ben Stenuit, Joshua Ho, Andrew Wang, Caitlin Parke, Matthew Knight, Lisa Alvarez-Cohen, and Michael Shapira. 2016. "Assembly of the Caenorhabditis Elegans Gut Microbiota from Diverse Soil Microbial Environments." *ISME Journal* 10 (8): 1998–2009. https://doi.org/10.1038/ismej.2015.253.

Biancalani, Tommaso, and Je↵ Gore. n.d. "Disentangling Bacterial Invasiveness from Lethality in an Experimental Host-Pathogen System (Supplementary Material: Theoretical Model)."

Biancalani, Tommaso, and Jeff Gore. 2019. "Disentangling Bacterial Invasiveness from Lethality in an Experimental Host-pathogen System." *Molecular Systems Biology* 15 (6). https://doi.org/10.15252/msb.20188707.

Blevins, Steve M., and Michael S. Bronze. 2010. “Robert Koch and the ‘golden Age’ of Bacteriology.” *International Journal of Infectious Diseases*. Elsevier. https://doi.org/10.1016/j.ijid.2009.12.003.

Boiko, O. G., Yu A. Labas, and A. V. Gordeeva. 2011. “An Outline of the Phylogenetic History of Metazoan Aging Phenomenon (to the Study of Creating a Common Metazoa Aging Theory).” *Advances in Gerontology* 1 (2): 122–29. https://doi.org/10.1134/S2079057011020044.

Borges, Diego C., Natalia M. Araújo, Cristina R. Cardoso, and Javier E. Lazo Chica. 2013. “Different Parasite Inocula Determine the Modulation of the Immune Response and Outcome of Experimental *Trypanosoma Cruzi* Infection.” *Immunology* 138 (2): 145–56. https://doi.org/10.1111/imm.12022.

Bradley, Derek, and Gerhard Roth. 2007. “Adaptive Thresholding Using the Integral Image.” *Journal of Graphics Tools* 12 (2): 13–21. https://doi.org/10.1080/2151237x.2007.10129236.

Brown, Sam P., Daniel M. Cornforth, and Nicole Mideo. 2012. “Evolution of Virulence in Opportunistic Pathogens: Generalism, Plasticity, and Control.” *Trends in Microbiology*. Elsevier. https://doi.org/10.1016/j.tim.2012.04.005.

Buppan, Pattakorn, Chaturong Putaporntip, Urassaya Pattanawong, Sunee Seethamchai, and Somchai Jongwutiwes. 2010. “Comparative Detection of Plasmodium Vivax and Plasmodium Falciparum DNA in Saliva and Urine Samples from Symptomatic Malaria Patients in a Low Endemic Area.” *Malaria Journal* 9 (1): 1–7. https://doi.org/10.1186/1475-2875-9-72.

Calahorro, Fernando, and Manuel Ruiz-Rubio. 2011. “Caenorhabditis Elegans as an

Experimental Tool for the Study of Complex Neurological Diseases: Parkinson's Disease, Alzheimer's Disease and Autism Spectrum Disorder." *Invertebrate Neuroscience*. Invert Neurosci. https://doi.org/10.1007/s10158-011-0126-1.

Carpenter, Anne E, Thouis R Jones, Michael R Lamprecht, Colin Clarke, In Han Kang, Ola Friman, David A Guertin, et al. 2006. "CellProfiler: Image Analysis Software for Identifying and Quantifying Cell Phenotypes." *Genome Biology 2006 7:10* 7 (10): 1–11. https://doi.org/10.1186/GB-2006-7-10-R100.

Carvalho, Constança, Augusta Gaspar, Andrew Knight, and Luís Vicente. 2019. "Ethical and Scientific Pitfalls Concerning Laboratory Research with Non-Human Primates, and Possible Solutions." *Animals* 9 (1). https://doi.org/10.3390/ani9010012.

Chamilos, Georgios, Russell E. Lewis, Jianhua Hu, Lianchun Xiao, Tomasz Zal, Michel Gilliet, Georg Halder, and Dimitrios P. Kontoyiannis. 2008. "Drosophila Melanogaster as a Model Host to Dissect the Immunopathogenesis of Zygomycosis." *Proceedings of the National Academy of Sciences* 105 (27): 9367–72. https://doi.org/10.1073/PNAS.0709578105.

Chao, Chun Cheih, Po Chen Hsu, Chung Feng Jen, I. Hui Chen, Chieh Huei Wang, Hau Chien Chan, Pei Wen Tsai, et al. 2010. "Zebrafish as a Model Host for Candida Albicans Infection." *Infection and Immunity* 78 (6): 2512–21. https://doi.org/10.1128/IAI.01293-09.

Coburn, Cassandra, Erik Allman, Parag Mahanti, Alexandre Benedetto, Filipe Cabreiro, Zachary Pincus, Filip Matthijssens, et al. 2013. "Anthranilate Fluorescence Marks a Calcium-Propagated Necrotic Wave That Promotes Organismal Death in C. Elegans." *PLOS Biology* 11 (7): e1001613. https://doi.org/10.1371/JOURNAL.PBIO.1001613.

Cole, John J., Neil A. Robertson, Mohammed Iqbal Rather, John P. Thomson, Tony McBryan, Duncan Sproul, Tina Wang, et al. 2017. “Diverse Interventions That Extend Mouse Lifespan Suppress Shared Age-Associated Epigenetic Changes at Critical Gene Regulatory Regions.” *Genome Biology* 18 (1): 58. https://doi.org/10.1186/s13059-017-1185-3.

Conery, Annie L., Jonah Larkins-Ford, Frederick M. Ausubel, and Natalia V. Kirienko. 2014. “High-Throughput Screening for Novel Anti-Infectives Using a *C. Elegans* Pathogenesis Model.” *Current Protocols in Chemical Biology* 6 (1): 25–37. https://doi.org/10.1002/9780470559277.ch130160.

Cornforth, Daniel M., Roman Popat, Luke McNally, James Gurney, Thomas C. Scott-Phillips, Alasdair Ivens, Stephen P. Diggle, and Sam P. Brown. 2014. “Combinatorial Quorum Sensing Allows Bacteria to Resolve Their Social and Physical Environment.” *Proceedings of the National Academy of Sciences of the United States of America* 111 (11): 4280–84. https://doi.org/10.1073/pnas.1319175111.

Cross, Alan S. 2008. “What Is a Virulence Factor?” *Critical Care (London, England)*. BioMed Central. https://doi.org/10.1186/cc7127.

Darby, Creg. 2005. “Interactions with Microbial Pathogens.” *WormBook : The Online Review of C. Elegans Biology*. https://doi.org/10.1895/wormbook.1.21.1.

Darch, Sophie E., Stuart A. West, Klaus Winzer, and Stephen P. Diggle. 2012. “Density-Dependent Fitness Benefits in Quorum-Sensing Bacterial Populations.” *Proceedings of the National Academy of Sciences of the United States of America* 109 (21): 8259–63. https://doi.org/10.1073/pnas.1118131109.

Davies, Jane C. 2002. “Pseudomonas Aeruginosa in Cystic Fibrosis: Pathogenesis and Persistence.” *Paediatric Respiratory Reviews* 3 (2): 128–34. https://doi.org/10.1016/S1526-0550(02)00003-3.

Day, Shandra R., Christopher M. Moore, John R. Kundzins, and Costi D. Sifri. 2012. “Community-Associated and Healthcare-Associated Methicillin-Resistant Staphylococcus Aureus Virulence toward Caenorhabditis Elegans Compared.” *Virulence* 3 (7). https://doi.org/10.4161/viru.22120.

Decaestecker, Ellen, Sabrina Gaba, Joost a M Raeymaekers, Robby Stoks, Liesbeth Van Kerckhoven, Dieter Ebert, and Luc De Meester. 2007. “Host-Parasite ‘Red Queen’ Dynamics Archived in Pond Sediment.” *Nature* 450 (December): 870–73. https://doi.org/10.1038/nature06291.

Dickinson, Daniel J., and Bob Goldstein. 2016. “CRISPR-Based Methods for Caenorhabditis Elegans Genome Engineering.” *Genetics* 202 (3): 885–901. https://doi.org/10.1534/genetics.115.182162.

Diggle, Stephen P., and Marvin Whiteley. 2020. “Microbe Profile: Pseudomonas Aeruginosa: Opportunistic Pathogen and Lab Rat.” *Microbiology (United Kingdom)* 166 (1): 30–33. https://doi.org/10.1099/mic.0.000860.

Dionne, Marc S., and David S. Schneider. 2008. “Models of Infectious Diseases in the Fruit Fly Drosophila Melanogaster.” *DMM Disease Models and Mechanisms*. Company of Biologists. https://doi.org/10.1242/dmm.000307.

Dirksen, Philipp, Sarah Arnaud Marsh, Ines Braker, Nele Heitland, Sophia Wagner, Rania Nakad, Sebastian Mader, et al. 2016. “The Native Microbiome of the Nematode Caenorhabditis Elegans: Gateway to a New Host-Microbiome Model.”

BMC Biology 14 (1): 1–16. https://doi.org/10.1186/s12915-016-0258-1.

Ebert, Dieter. 2005. “Some Parasites of Daphnia.” In *Ecology, Epidemiology, and Evolution in Daphnia*. National Center for Biotechnology Information (US). https://www.ncbi.nlm.nih.gov/books/NBK2043/.

Ebert, Dieter.. 2008. “Host-Parasite Coevolution: Insights from the Daphnia-Parasite Model System.” *Current Opinion in Microbiology*. Elsevier Current Trends. https://doi.org/10.1016/j.mib.2008.05.012.

Economos, Angelos C. 1979. “A Non-Gompertzian Paradigm for Mortality Kinetics of Metazoan Animals and Failure Kinetics of Manufactured Products.” *AGE* 2 (3): 74–76. https://doi.org/10.1007/BF02432250.

El-Gohary, A., Ahmad Alshamrani, and Adel Naif Al-Otaibi. 2013. “The Generalized Gompertz Distribution.” *Applied Mathematical Modelling* 37 (1–2): 13–24. https://doi.org/10.1016/j.apm.2011.05.017.

Estes, Jacob D., Scott W. Wong, and Jason M. Brenchley. 2018. “Nonhuman Primate Models of Human Viral Infections.” *Nature Reviews Immunology*. Nature Publishing Group. https://doi.org/10.1038/s41577-018-0005-7.

Fink, Mitchell P. 2014. “Animal Models of Sepsis.” *Virulence*. Taylor and Francis Inc. https://doi.org/10.4161/viru.26083.

Foster, Kyle J., Deborah L. McEwan, and Read Pukkila-Worley. 2020. “Measurements of Innate Immune Function in C. Elegans.” In *Methods in Molecular Biology*, 2144:145–60. Humana Press Inc. https://doi.org/10.1007/978-1-0716-0592-9_13.

Frank, Steven A. 2009. “The Common Patterns of Nature.” *Journal of Evolutionary Biology* 22 (8): 1563–85.

Gammon, Don B. 2017. “Caenorhabditis Elegans as an Emerging Model for Virus-Host Interactions.” *Journal of Virology* 91 (23). https://doi.org/10.1128/jvi.00509-17.

Garsin, Danielle A, Jacinto M Villanueva, Jakob Begun, Dennis H Kim, Costi D Sifri, Stephen B Calderwood, Gary Ruvkun, and Frederick M Ausubel. 2001. “Long-Lived C. Elegans Daf-2 Mutants Are Resistant to Bacterial Pathogens.” *Annu. Rev. Genomics Hum. Genet*. Vol. 2. www.sciencemag.org/cgi/content/full/300/5627/1921/DC1Fig.S1TableS1www.sciencemag.org.

Gavrilov, Leonid A., and Natalia S. Gavrilova. 2019. “New Trend in Old-Age Mortality: Gompertzialization of Mortality Trajectory.” *Gerontology* 65 (5): 451–57. https://doi.org/10.1159/000500141.

Ghosh, Poulomi, and Saprativ P. Das. 2020. “Nonhuman Primate Model Use in Understanding Infectious Diseases.” In *Model Organisms for Microbial Pathogenesis, Biofilm Formation and Antimicrobial Drug Discovery*, 489–508. Springer Singapore. https://doi.org/10.1007/978-981-15-1695-5_25.

Gilchrist, Michael A., and Akira Sasaki. 2002. “Modeling Host-Parasite Coevolution: A Nested Approach Based on Mechanistic Models.” *Journal of Theoretical Biology* 218 (3): 289–308. https://doi.org/10.1006/jtbi.2002.3076.

Gog, Julia R., Lorenzo Pellis, James L.N. Wood, Angela R. McLean, Nimalan Arinaminpathy, and James O. Lloyd-Smith. 2015. “Seven Challenges in Modeling Pathogen Dynamics Within-Host and across Scales.” *Epidemics* 10 (March): 45–48. https://doi.org/10.1016/j.epidem.2014.09.009.

Goll, Johannes, Seesandra V. Rajagopala, Shen C. Shiau, Hank Wu, Brian T. Lamb,

and Peter Uetz. 2008. “MPIDB: The Microbial Protein Interaction Database.” *Bioinformatics* 24 (15): 1743–44. https://doi.org/10.1093/BIOINFORMATICS/BTN285.

Grant, Andrew J, Olivier Restif, Trevelyan J McKinley, Mark Sheppard, Duncan J Maskell, and Pietro Mastroeni. 2008. “Modelling Within-Host Spatiotemporal Dynamics of Invasive Bacterial Disease.” Edited by David A Relman. *PLoS Biology* 6 (4): e74. https://doi.org/10.1371/journal.pbio.0060074.

Grenfell, Bryan, and John Harwood. 1997. “(Meta) Population Dynamics of Infectious Diseases.” *Trends in Ecology and Evolution*. Elsevier Ltd. https://doi.org/10.1016/S0169-5347(97)01174-9.

Gross, Jeremy, Ian J. Passmore, Jade C.S. Chung, Olena Rzhepishevska, Madeleine Ramstedt, and Martin Welch. 2013. “Universal Soldier: Pseudomonas Aeruginosa - an Opportunistic Generalist.” *Frontiers in Biology*. Springer. https://doi.org/10.1007/s11515-013-1267-x.

Gurney, James, Léa Pradier, Joanne S Griffin, Claire Gougat-Barbera, Benjamin K Chan, Paul E Turner, Oliver Kaltz, and Michael E Hochberg. 2020. “Phage Steering of Antibiotic-Resistance Evolution in the Bacterial Pathogen, Pseudomonas Aeruginosa.” *Evolution, Medicine, and Public Health* 2020 (1): 148–57. https://doi.org/10.1093/emph/eoaa026.

Handel, Andreas, and Pejman Rohani. 2015. “Crossing the Scale from Within-Host Infection Dynamics to between-Host Transmission Fitness: A Discussion of Current Assumptions and Knowledge.” *Philosophical Transactions of the Royal Society B: Biological Sciences* 370 (1675). https://doi.org/10.1098/rstb.2014.0302.

Høiby, Niels, Oana Ciofu, and Thomas Bjarnsholt. 2010. “Pseudomonas Aeruginosa Biofilms in Cystic Fibrosis.” *Future Microbiology*. Future Medicine Ltd London, UK . https://doi.org/10.2217/fmb.10.125.

Horcajada, Juan P, Milagro Montero, Antonio Oliver, Luisa Sorlí, Sònia Luque, Silvia Gómez-Zorrilla, Natividad Benito, and Santiago Grau. 2019. “Epidemiology and Treatment of Multidrug-Resistant and Extensively Drug-Resistant Pseudomonas Aeruginosa Infections.” https://doi.org/10.1128/CMR.00031-19.

Hsiao, Ju-Ya, Chun-Yao Chen, Mei-Jun Yang, and Han-Chen Ho. 2013. “Live and Dead GFP-Tagged Bacteria Showed Indistinguishable Fluorescence in Caenorhabditis Elegans Gut §.” *Journal of Microbiology* 51 (3): 367–72. https://doi.org/10.1007/s12275-013-2589-8.

Kamada, Nobuhiko, Yun Gi Kim, Ho Pan Sham, Bruce A. Vallance, José L. Puente, Eric C. Martens, and Gabriel Núñez. 2012. “Regulated Virulence Controls the Ability of a Pathogen to Compete with the Gut Microbiota.” *Science* 336 (6086): 1325–29. https://doi.org/10.1126/science.1222195.

Kang, Chanhee, Young-jai You, and Leon Avery. 2007. “Dual Roles of Autophagy in the Survival of Caenorhabditis Elegans during Starvation.” *Genes & Development* 21 (17): 2161. https://doi.org/10.1101/GAD.1573107.

Kim, Brandon J., Bryan M. Hancock, Natasha Del Cid, Andres Bermudez, David Traver, and Kelly S. Doran. 2015. “Streptococcus Agalactiae Infection in Zebrafish Larvae.” *Microbial Pathogenesis* 79 (February): 57–60. https://doi.org/10.1016/j.micpath.2015.01.007.

Kimura, Koutarou D., Heidi A. Tissenbaum, Yanxia Liu, and Gary Ruvkun. 1997. “Daf-2,

an Insulin Receptor-like Gene That Regulates Longevity and Diapause in Caenorhabditis Elegans." *Science* 277 (5328): 942–46. https://doi.org/10.1126/science.277.5328.942.

Kirienko, Natalia V., Brent O. Cezairliyan, Frederick M. Ausubel, and Jennifer R. Powell. 2014. "Pseudomonas Aeruginosa PA14 Pathogenesis in Caenorhabditis Elegans." *Methods in Molecular Biology* 1149: 653–69. https://doi.org/10.1007/978-1-4939-0473-0_50.

Kochanek, Kenneth D, Sherry L Murphy, Jiaquan Xu, and Elizabeth Arias. 2019. "National Vital Statistics Reports Volume 68, Number 9 June 24, 2019 Deaths: Final Data for 2017." https://www.cdc.gov/nchs/products/index.htm.

Kong, Cin, Wageeh A. Yehye, Noorsaadah Abd Rahman, Man Wah Tan, and Sheila Nathan. 2014. "Discovery of Potential Anti-Infectives against Staphylococcus Aureus Using a Caenorhabditis Elegans Infection Model." *BMC Complementary and Alternative Medicine* 14 (1): 1–17. https://doi.org/10.1186/1472-6882-14-4.

Kumar, Anand, Daniel Roberts, Kenneth E. Wood, Bruce Light, Joseph E. Parrillo, Satendra Sharma, Robert Suppes, et al. 2006. "Duration of Hypotension before Initiation of Effective Antimicrobial Therapy Is the Critical Determinant of Survival in Human Septic Shock." *Critical Care Medicine* 34 (6): 1589–96. https://doi.org/10.1097/01.CCM.0000217961.75225.E9.

Kurz, C. Léopold, and Jonathan J. Ewbank. 2000. "Caenorhabditis Elegans for the Study of Host-Pathogen Interactions." *Trends in Microbiology*. Elsevier Current Trends. https://doi.org/10.1016/S0966-842X(99)01691-1.

Kurz, C Léopold, Sophie Chauvet, Emmanuel Andrès, Marianne Aurouze, Isabelle

Vallet, Gérard P F Michel, Mitch Uh, et al. 2003. “Virulence Factors of the Human Opportunistic Pathogen Serratia Marcescens Identified by in Vivo Screening.” *The EMBO Journal* 22 (7): 1451–60. https://doi.org/10.1093/emboj/cdg159.

LaBauve, Annette E., and Matthew J. Wargo. 2012. “Growth and Laboratory Maintenance of Pseudomonas Aeruginosa.” *Current Protocols in Microbiology* 0 6 (SUPPL.25): Unit. https://doi.org/10.1002/9780471729259.mc06e01s25.

Le, Kim N., Mei Zhan, Yongmin Cho, Jason Wan, Dhaval S. Patel, and Hang Lu. 2020. “An Automated Platform to Monitor Long-Term Behavior and Healthspan in Caenorhabditis Elegans under Precise Environmental Control.” *Communications Biology* 3 (1): 1–13. https://doi.org/10.1038/s42003-020-1013-2.

Leevy, W. Matthew, Nathan Serazin, and Bradley D. Smith. 2007. “Optical Imaging of Bacterial Infection Models.” *Drug Discovery Today: Disease Models*. NIH Public Access. https://doi.org/10.1016/j.ddmod.2007.07.001.

Lewis, Anthony J., Christopher W. Seymour, and Matthew R. Rosengart. 2016. “Current Murine Models of Sepsis.” *Surgical Infections* 17 (4): 385–93. https://doi.org/10.1089/sur.2016.021.

Lindberg, HM, KA McKean, T Caraco, and IN Wang. 2018. “Within-Host Dynamics and Random Duration of Pathogen Infection: Implications for between-Host Transmission.” *Journal of Theoretical Biology* 446 (June): 137–48. https://doi.org/10.1016/J.JTBI.2018.01.030.

Lipsitch, M, and E R Moxon. 1997. “Virulence and Transmissibility of Pathogens: What Is the Relationship?” *Trends in Microbiology* 5 (1): 31–37. https://doi.org/10.1016/S0966-842X(97)81772-6.

Lister, Philip D., Daniel J. Wolter, and Nancy D. Hanson. 2009. “Antibacterial-Resistant Pseudomonas Aeruginosa: Clinical Impact and Complex Regulation of Chromosomally Encoded Resistance Mechanisms.” *Clinical Microbiology Reviews*. American Society for Microbiology (ASM). https://doi.org/10.1128/CMR.00040-09.

Liu, Bo, Dandan Zheng, Qi Jin, Lihong Chen, and Jian Yang. 2019. “VFDB 2019: A Comparative Pathogenomic Platform with an Interactive Web Interface.” *Nucleic Acids Research* 47 (D1): D687–92. https://doi.org/10.1093/NAR/GKY1080.

Lutter, Erika I, Monica M P Faria, Harvey R Rabin, and Douglas G Storey. 2008. “Pseudomonas Aeruginosa Cystic Fibrosis Isolates from Individual Patients Demonstrate a Range of Levels of Lethality in Two Drosophila Melanogaster Infection Models.” *INFECTION AND IMMUNITY* 76 (5): 1877–88. https://doi.org/10.1128/IAI.01165-07.

Magalhaes Filho, C. Daniel De, Brian Henriquez, Nicole E. Seah, Ronald M. Evans, Louis R. Lapierre, and Andrew Dillin. 2018. “Visible Light Reduces C. Elegans Longevity.” *Nature Communications* 9 (1). https://doi.org/10.1038/s41467-018-02934-5.

Mahajan-Miklos, Shalina, Man Wah Tan, Laurence G. Rahme, and Frederick M. Ausubel. 1999. “Molecular Mechanisms of Bacterial Virulence Elucidated Using a Pseudomonas Aeruginosa-Caenorhabditis Elegans Pathogenesis Model.” *Cell* 96 (1): 47–56. https://doi.org/10.1016/S0092-8674(00)80958-7.

Mallo, Gustavo V., C.Léopold Kurz, Carole Couillault, Nathalie Pujol, Samuel Granjeaud, Yuji Kohara, and Jonathan J. Ewbank. 2002. “Inducible Antibacterial Defense System in C. Elegans.” *Current Biology* 12 (14): 1209–14. https://doi.org/10.1016/S0960-9822(02)00928-4.

Manjarrez, Jacob R., and Roger Mailler. 2020. “Stress and Timing Associated with Caenorhabditis Elegans Immobilization Methods.” *Heliyon* 6 (7). https://doi.org/10.1016/J.HELIYON.2020.E04263.

Markaki, Maria, and Nektarios Tavernarakis. 2020. “Caenorhabditis Elegans as a Model System for Human Diseases.” *Current Opinion in Biotechnology*. Elsevier Ltd. https://doi.org/10.1016/j.copbio.2019.12.011.

Martin, Natalia, Jogender Singh, and Alejandro Aballay. 2017. “Natural Genetic Variation in the Caenorhabditis Elegans Response to Pseudomonas Aeruginosa.” https://doi.org/10.1534/g3.117.039057.

McElreath, Richard. 2018. “Statistical Rethinking : A Bayesian Course with Examples in R and Stan.” *Statistical Rethinking: A Bayesian Course with Examples in R and Stan*, January, 1–469. https://doi.org/10.1201/9781315372495.

Mideo, Nicole, Samuel Alizon, and Troy Day. 2008. “Linking Within- and between-Host Dynamics in the Evolutionary Epidemiology of Infectious Diseases.” *Trends in Ecology and Evolution*. Elsevier Current Trends. https://doi.org/10.1016/j.tree.2008.05.009.

Millet, Anne CM, and Jonathan J Ewbank. 2004. “Immunity in Caenorhabditis Elegans.” *Current Opinion in Immunology* 16 (1): 4–9. https://doi.org/10.1016/j.coi.2003.11.005.

Missov, Trifon I., Adam Lenart, Laszlo Nemeth, Vladimir Canudas-Romo, and James W. Vaupel. 2015. “The Gompertz Force of Mortality in Terms of the Modal Age at Death.” *Demographic Research* 32 (1): 1031–48. https://doi.org/10.4054/DemRes.2015.32.36.

Mohan, Vijayarani, S Vijayarani, and Mrs M Vinupriya. 2013. “Performance Analysis of Canny and Sobel Edge Detection Algorithms in Image Mining Privacy Preserving Data Mining View Project Performance Analysis of Canny and Sobel Edge Detection Algorithms in Image Mining.” *Article in International Journal of Innovative Research in Computer and Communication Engineering* 3297. www.ijircce.com.

Moradali, M. Fata, Shirin Ghods, and Bernd H. A. Rehm. 2017. “Pseudomonas Aeruginosa Lifestyle: A Paradigm for Adaptation, Survival, and Persistence.” *Frontiers in Cellular and Infection Microbiology* 0 (FEB): 39. https://doi.org/10.3389/FCIMB.2017.00039.

Nehme, Nadine T., Samuel Liégeois, Beatrix Kele, Philippe Giammarinaro, Elizabeth Pradel, Jules A. Hoffmann, Jonathan J. Ewbank, and Dominique Ferrandon. 2007. “A Model of Bacterial Intestinal Infections in Drosophila Melanogaster.” *PLoS Pathogens* 3 (11): 1694–1709. https://doi.org/10.1371/journal.ppat.0030173.

Nelson, George E., Tracy Pondo, Karrie Ann Toews, Monica M. Farley, Mary Lou Lindegren, Ruth Lynfield, Deborah Aragon, et al. 2016. “Epidemiology of Invasive Group a Streptococcal Infections in the United States, 2005-2012.” *Clinical Infectious Diseases*. Oxford University Press. https://doi.org/10.1093/cid/ciw248.

Ohlsen, Knut, and Tobias Hertlein. 2018. “Towards Clinical Application of Non-Invasive Imaging to Detect Bacterial Infections.” *Virulence*. Taylor and Francis Inc. https://doi.org/10.1080/21505594.2018.1425072.

Ortega-Riveros, Marcelo, Iker De-la-Pinta, Cristina Marcos-Arias, Guillermo Ezpeleta, Guillermo Quindós, and Elena Eraso. 2017. “Usefulness of the Non-Conventional Caenorhabditis Elegans Model to Assess Candida Virulence.” *Mycopathologia* 182 (9–10): 785–95. https://doi.org/10.1007/s11046-017-0142-8.

Palominos, M Fernanda, and Andrea Calixto. 2020. “Quantification of Bacteria Residing in Caenorhabditis Elegans Intestine.” https://doi.org/10.21769/BioProtoc.3605.

Pasteur, M. 1881. “An Address on Vaccination in Relation to Chicken Cholera and Splenic Fever.” *British Medical Journal* 2 (1076): 283–84. https://doi.org/10.1136/bmj.2.1076.283.

Pearce, Neil, and Debbie A Lawlor. 2016. “Causal Inference—so Much More than Statistics.” *International Journal of Epidemiology* 45 (6): 1895–1903. https://doi.org/10.1093/IJE/DYW328.

Pearl, Judea. 2009. *Causality*. Cambridge university press.

Pereira, Thais Cristine, Patrícia Pimentel de Barros, Luciana Ruano de Oliveira Fugisaki, Rodnei Dennis Rossoni, Felipe de Camargo Ribeiro, Raquel Teles de Menezes, Juliana Campos Junqueira, and Liliana Scorzoni. 2018. “Recent Advances in the Use of Galleria Mellonella Model to Study Immune Responses against Human Pathogens.” *Journal of Fungi*. MDPI AG. https://doi.org/10.3390/jof4040128.

Petralia, Ronald S., Mark P. Mattson, and Pamela J. Yao. 2014. “Aging and Longevity in the Simplest Animals and the Quest for Immortality.” *Ageing Research Reviews*. Elsevier Ireland Ltd. https://doi.org/10.1016/j.arr.2014.05.003.

Pletzer, Daniel, Sarah C. Mansour, Kelli Wuerth, Negin Rahanjam, and Robert E.W. Hancock. 2017. “New Mouse Model for Chronic Infections by Gram-Negative Bacteria Enabling the Study of Anti-Infective Efficacy and Host-Microbe Interactions.” *MBio* 8 (1). https://doi.org/10.1128/mBio.00140-17.

Poulin, R., and C. Combes. 1999. “The Concept of Virulence: Interpretations and Implications.” *Parasitology Today*. https://doi.org/10.1016/S0169-4758(99)01554-9.

Preston, D L, and P Johnson. 2010. “Ecological Consequences of Parasitism | Learn Science at Scitable.” *Nature Education Knowledge*. Vol. 1. http://www.nature.com/scitable/knowledge/library/ecological-consequences-of-parasitism-13255694.

Pullan, Rachel L., Jennifer L. Smith, Rashmi Jasrasaria, and Simon J. Brooker. 2014. “Global Numbers of Infection and Disease Burden of Soil Transmitted Helminth Infections in 2010.” *Parasites and Vectors* 7 (1): 37. https://doi.org/10.1186/1756-3305-7-37.

R Development Core Team. 2020. R: A Language and Environment for Statistical Computing, issued 2020. https://www.r-project.org/.

Redfield, Rosemary J. 2002. “Is Quorum Sensing a Side Effect of Diffusion Sensing?” *Trends in Microbiology*. Elsevier Current Trends. https://doi.org/10.1016/S0966-842X(02)02400-9.

Rohatgi, Ankit. 2021. “Webplotdigitizer: Version 4.5.” https://automeris.io/WebPlotDigitizer.

Ross-Gillespie, Adin, Michael Weigert, Sam P. Brown, and Rolf Kümmerli. 2014. “Gallium-Mediated Siderophore Quenching as an Evolutionarily Robust Antibacterial Treatment.” *Evolution, Medicine and Public Health* 2014 (1): 18–29. https://doi.org/10.1093/emph/eou003.

Roussel, Nicolas, Jeff Sprenger, Susan J Tappan, and Jack R Glaser. 2014. “ Robust Tracking and Quantification of C. Elegans Body Shape and Locomotion through Coiling, Entanglement, and Omega Bends .” *Worm* 3 (4): e982437. https://doi.org/10.4161/21624054.2014.982437.

Ruiz-Díez, Beatriz, Patricia Sánchez, Fernando Baquero, José L. Martínez, and Alfonso Navas. 2003. “Differential Interactions within the Caenorhabditis Elegans - Pseudomonas Aeruginosa Pathogenesis Model.” *Journal of Theoretical Biology* 225 (4): 469–76. https://doi.org/10.1016/S0022-5193(03)00288-1.

Rumbaugh, Kendra P., Urvish Trivedi, Chase Watters, Maxwell N. Burton-Chellew, Stephen P. Diggle, and Stuart A. West. 2012. “Kin Selection, Quorum Sensing and Virulence in Pathogenic Bacteria.” *Proceedings of the Royal Society B: Biological Sciences* 279 (1742): 3584–88. https://doi.org/10.1098/rspb.2012.0843.

Sami, Husam, Hussain Sattar Abood, Noor Ridha Kadhim, and Hussam Sami Awayid. 2019. “The First International Scientific Conference of Health and Medical Specialties……15-16.” https://www.researchgate.net/publication/335777432.

Samuel, Buck S., Holli Rowedder, Christian Braendle, Marie Anne Félix, and Gary Ruvkun. 2016. “Caenorhabditis Elegans Responses to Bacteria from Its Natural Habitats.” *Proceedings of the National Academy of Sciences of the United States of America* 113 (27): E3941–49. https://doi.org/10.1073/pnas.1607183113.

Sarkar, Sanjay, and Mark T. Heise. 2019. “Mouse Models as Resources for Studying Infectious Diseases.” *Clinical Therapeutics* 41 (10): 1912–22. https://doi.org/10.1016/j.clinthera.2019.08.010.

Sasson, Isaac. 2021. “Age and COVID-19 Mortality: A Comparison of Gompertz Doubling Time across Countries and Causes of Death.” *Demographic Research* 44 (16): 379–96. https://doi.org/10.4054/DemRes.2021.44.16.

Sauer, Brian, and Tyler J VanderWeele. 2013. “Use of Directed Acyclic Graphs.” https://www.ncbi.nlm.nih.gov/books/NBK126189/.

Sayers, Samantha, Li Li, Edison Ong, Shunzhou Deng, Guanghua Fu, Yu Lin, Brian Yang, et al. 2019. “Victors: A Web-Based Knowledge Base of Virulence Factors in Human and Animal Pathogens.” *Nucleic Acids Research* 47 (D1): D693–700. https://doi.org/10.1093/NAR/GKY999.

Schuster, Martin, and E. Peter Greenberg. 2006. “A Network of Networks: Quorum-Sensing Gene Regulation in Pseudomonas Aeruginosa.” *International Journal of Medical Microbiology*. Elsevier GmbH. https://doi.org/10.1016/j.ijmm.2006.01.036.

Seventer, Jean Maguire van, and Natasha S. Hochberg. 2016. “Principles of Infectious Diseases: Transmission, Diagnosis, Prevention, and Control.” In *International Encyclopedia of Public Health*, 22–39. Elsevier Inc. https://doi.org/10.1016/B978-0-12-803678-5.00516-6.

Shaner, Gregory, Erik L. Stromberg, George H. Lacy, Ken R. Barker, and Thomas P. Pirone. 1992. “Nomenclature and Concepts of Pathogenicity and Virulence.” *Annual Review of Phytopathology* 30 (1): 47–66. https://doi.org/10.1146/annurev.py.30.090192.000403.

Smith, David L., Katherine E. Battle, Simon I. Hay, Christopher M. Barker, Thomas W. Scott, and F. Ellis McKenzie. 2012. “Ross, Macdonald, and a Theory for the Dynamics and Control of Mosquito-Transmitted Pathogens.” *PLoS Pathogens*. Public Library of Science. https://doi.org/10.1371/journal.ppat.1002588.

Solis, Gregory M., and Michael Petrascheck. 2011. “Measuring Caenorhabditis Elegans Life Span in 96 Well Microtiter Plates.” *Journal of Visualized Experiments : JoVE*, no. 49: 2496. https://doi.org/10.3791/2496.

Souza, Cassius de, Liliane Simpson-Louredo, Higor Franceschi Mota, Yuri Vieira Faria,

Fellipe de Oliveira Cabral, Sabrina dos Santos Colodette, Maria E.Freire Castro Canellas, et al. 2019. “Virulence Potential of Corynebacterium Striatum towards Caenorhabditis Elegans.” *Antonie van Leeuwenhoek, International Journal of General and Molecular Microbiology* 112 (9): 1331–40. https://doi.org/10.1007/s10482-019-01265-9.

Stephens, Robin, Richard L. Culleton, and Tracey J. Lamb. 2012. “The Contribution of Plasmodium Chabaudi to Our Understanding of Malaria.” *Trends in Parasitology*. Elsevier Current Trends. https://doi.org/10.1016/j.pt.2011.10.006.

Stiernagle, Theresa. 2006. “Maintenance of C. Elegans.” *WormBook : The Online Review of C. Elegans Biology*. https://doi.org/10.1895/wormbook.1.101.1.

Stroustrup, Nicholas, Winston E Anthony, Zachary M Nash, Vivek Gowda, Adam Gomez, Isaac F López-Moyado, Javier Apfeld, and Walter Fontana. 2016. “The Temporal Scaling of Caenorhabditis Elegans Ageing.” *Nature* 530 (7588): 103–7. https://doi.org/10.1038/nature16550.

Stroustrup, Nicholas, Bryne E. Ulmschneider, Zachary M. Nash, Isaac F. López-Moyado, Javier Apfeld, and Walter Fontana. 2013. “The Caenorhabditis Elegans Lifespan Machine.” *Nature Methods* 10 (7): 665–70. https://doi.org/10.1038/nmeth.2475.

Swift, Jonathan. 1773. *On Poetry: A Rhapsody*.

Tan, M.-W., S. Mahajan-Miklos, and F. M. Ausubel. 1999. “Killing of Caenorhabditis Elegans by Pseudomonas Aeruginosa Used to Model Mammalian Bacterial Pathogenesis.” *Proceedings of the National Academy of Sciences* 96 (2): 715–20. https://doi.org/10.1073/pnas.96.2.715.

Tan, Man Wah, Shalina Mahajan-Miklos, and Frederick M. Ausubel. 1999. “Killing of

Caenorhabditis Elegans by Pseudomonas Aeruginosa Used to Model Mammalian Bacterial Pathogenesis." *Proceedings of the National Academy of Sciences of the United States of America* 96 (2): 715–20. https://doi.org/10.1073/pnas.96.2.715.

Tekippe, Michael, and Alejandro Aballay. 2010. "C. Elegans Germline-Deficient Mutants Respond to Pathogen Infection Using Shared and Distinct Mechanisms." *PLoS ONE* 5 (7): 11777. https://doi.org/10.1371/journal.pone.0011777.

Thanos, Panayotis K., John Hamilton, Joseph R. O'Rourke, Anthony Napoli, Marcelo Febo, Nora D. Volkow, Kenneth Blum, and Mark Gold. 2016. "Dopamine D2 Gene Expression Interacts with Environmental Enrichment to Impact Lifespan and Behavior." *Oncotarget* 7 (15): 19111–23. https://doi.org/10.18632/oncotarget.8088.

Thomas, Rachael J., Karleigh A. Hamblin, Stuart J. Armstrong, Claudia M. Müller, Monika Bokori-Brown, Stan Goldman, Helen S. Atkins, and Richard W. Titball. 2013. "Galleria Mellonella as a Model System to Test the Pharmacokinetics and Efficacy of Antibiotics against Burkholderia Pseudomallei." *International Journal of Antimicrobial Agents* 41 (4): 330–36. https://doi.org/10.1016/j.ijantimicag.2012.12.009.

Truscott, J. E., H. C. Turner, S. H. Farrell, and R. M. Anderson. 2016. "Soil-Transmitted Helminths: Mathematical Models of Transmission, the Impact of Mass Drug Administration and Transmission Elimination Criteria." *Advances in Parasitology* 94 (January): 133–98. https://doi.org/10.1016/bs.apar.2016.08.002.

Vandenbroucke, Jan P., Alex Broadbent, and Neil Pearce. 2016. "Causality and Causal Inference in Epidemiology: The Need for a Pluralistic Approach." *International Journal of Epidemiology* 45 (6): 1776–86. https://doi.org/10.1093/IJE/DYV341.

Vega, Nicole M., and Jeff Gore. 2017. “Stochastic Assembly Produces Heterogeneous Communities in the Caenorhabditis Elegans Intestine.” *PLoS Biology* 15 (3). https://doi.org/10.1371/journal.pbio.2000633.

Vergunst, Annette C., Annemarie H. Meijer, Stephen A. Renshaw, and David O’Callaghan. 2010. “Burkholderia Cenocepacia Creates an Intramacrophage Replication Niche in Zebrafish Embryos, Followed by Bacterial Dissemination and Establishment of Systemic Infection.” *Infection and Immunity* 78 (4): 1495. https://doi.org/10.1128/IAI.00743-09.

Vogel, Alexander J., Seth Harris, Nathan Marsteller, Shirley A. Condon, and Deborah M. Brown. 2014. “Early Cytokine Dysregulation and Viral Replication Are Associated with Mortality during Lethal Influenza Infection.” *Viral Immunology* 27 (5): 214–24. https://doi.org/10.1089/vim.2013.0095.

Wang, Nancy, Richard Strugnell, Odilia Wijburg, and Thomas Brodnicki. 2011. “Measuring Bacterial Load and Immune Responses in Mice Infected with Listeria Monocytogenes.” *Journal of Visualized Experiments : JoVE*, no. 54: 3076. https://doi.org/10.3791/3076.

Wang, Xin, Wenpeng Gu, Haiyan Qiu, Shengli Xia, Han Zheng, Yuchun Xiao, Junrong Liang, and Huaiqi Jing. 2013. “Comparison of the Cytokine Immune Response to Pathogenic Yersinia Enterocolitica Bioserotype 1B/O:8 and 2/O:9 in Susceptible BALB/C and Resistant C57BL/6 Mice.” *Molecular Immunology* 55 (3–4): 365–71. https://doi.org/10.1016/j.molimm.2013.03.017.

Way, Albert Sabin. 2017. “Timing of Early Antibiotics and Hospital Mortality in Sepsis,” 1–29. https://doi.org/10.2527/tas2016.0001.

White, Alexander G., Na Fu, W. Matthew Leevy, Jung Jae Lee, Michael A. Blasco, and Bradley D. Smith. 2010. “Optical Imaging of Bacterial Infection in Living Mice Using Deep-Red Fluorescent Squaraine Rotaxane Probes.” *Bioconjugate Chemistry* 21 (7): 1297–1304. https://doi.org/10.1021/bc1000998.

Wilder, Cara N., Stephen P. Diggle, and Martin Schuster. 2011. “Cooperation and Cheating in Pseudomonas Aeruginosa: The Roles of the Las, Rhl and Pqs Quorum-Sensing Systems.” *ISME Journal* 5 (8): 1332–43. https://doi.org/10.1038/ismej.2011.13.

Williams, Paul, Miguel Camara, Andrea Hardman, Simon Swift, Deborah Milton, Victoria J. Hope, Klaus Winzer, Barrie Middleton, David I. Pritchard, and Barrie W. Bycroft. 2000. “Quorum Sensing and the Population-Dependent Control of Virulence.” Edited by H. Smith, C. J. Dorman, G. Dougan, D. W. Holden, G. Dougan, and P. Williams. *Philosophical Transactions of the Royal Society of London. Series B: Biological Sciences* 355 (1397): 667–80. https://doi.org/10.1098/rstb.2000.0607.

Wollein Waldetoft, Kristofer, and Lars Råberg. 2014. “To Harm or Not to Harm? On the Evolution and Expression of Virulence in Group A Streptococci.” *Trends in Microbiology*. Elsevier Current Trends. https://doi.org/10.1016/j.tim.2013.10.006.

Wu, Jong Wuu, Wen Liang Hung, and Chih Hui Tsai. 2004. “Estimation of Parameters of the Gompertz Distribution Using the Least Squares Method.” *Applied Mathematics and Computation* 158 (1): 133–47. https://doi.org/10.1016/j.amc.2003.08.086.

Wu, Yin, Florentin Masurat, Jasmin Preis, and Henrik Bringmann. 2018. “Sleep Counteracts Aging Phenotypes to Survive Starvation-Induced Developmental Arrest in C. Elegans.” *Current Biology* 28 (22): 3610-3624.e8. https://doi.org/10.1016/J.CUB.2018.10.009.

Yang, Ching Chung. 2006. “Image Enhancement by Modified Contrast-Stretching Manipulation.” *Optics and Laser Technology* 38 (3): 196–201. https://doi.org/10.1016/j.optlastec.2004.11.009.

Zaborin, Alexander, Kathleen Romanowski, Svetlana Gerdes, Christopher Holbrook, Francois Lepine, Jason Long, Valeriy Poroyko, et al. 2009. “Red Death in Caenorhabditis Elegans Caused by Pseudomonas Aeruginosa PAO1.” *Proceedings of the National Academy of Sciences of the United States of America* 106 (15): 6327–32. https://doi.org/10.1073/pnas.0813199106.

Zelmer, Derek A. 1998. “An Evolutionary Definition of Parasitism.” *International Journal for Parasitology*. Elsevier Ltd. https://doi.org/10.1016/S0020-7519(97)00199-9.

Zhang, David, Scott T. Micek, and Marin H. Kollef. 2015. “Time to Appropriate Antibiotic Therapy Is an Independent Determinant of Postinfection ICU and Hospital Lengths of Stay in Patients with Sepsis.” *Critical Care Medicine* 43 (10): 2133–40. https://doi.org/10.1097/CCM.0000000000001140.

Zhang, Fan, Maureen Berg, Katja Dierking, Marie-Anne Félix, Michael Shapira, Buck S. Samuel, and Hinrich Schulenburg. 2017. “Caenorhabditis Elegans as a Model for Microbiome Research.” *Frontiers in Microbiology* 8 (MAR): 485. https://doi.org/10.3389/fmicb.2017.00485.

Zimmermann, Johannes, Nancy Obeng, Wentao Yang, Barbara Pees, Carola Petersen, Silvio Waschina, Kohar A. Kissoyan, et al. 2020. “The Functional Repertoire Contained within the Native Microbiota of the Model Nematode Caenorhabditis Elegans.” *ISME Journal* 14 (1): 26–38. https://doi.org/10.1038/s41396-019-0504-y.